1-1-2011

Flexural Creep Effects On Permanent Wood Foundation Made Of Structural Insulated Foam-Timber Panels

Mahmoud Shaaban Sayed Ahmed
Ryerson University

FLEXURAL CREEP EFFECTS ON PERMANENT WOOD FOUNDATION MADE OF STRUCTURAL INSULATED FOAM-TIMBER PANELS

By

Mahmoud Shaaban SAYED AHMED

B.Sc. Civil Engineering,

Construction and Building Department, High Institute of Engineering,

Egypt, 2000

A Thesis

Presented to Ryerson University

In partial fulfillment of the

Requirement for the degree of

Master of Applied Science

In the program of

Civil Engineering

Toronto, Ontario, Canada, 2011

AUTHOR'S DECLARATION

I hereby declare that I am the sole author of the thesis.

I authorize Ryerson University to lend this document to other institutions or individuals for the purpose of scholarly research.

Mahmoud SAYED AHMED

I further authorize Ryerson University to reproduce the document by photocopying or by other means, in total or part, at the request of other institutions or individuals for the purpose of scholarly research.

Mahmoud SAYED AHMED

BORROWERS

Ryerson University requires the signature of all persons using or photocopying this thesis.

Please Sign below, and give address and date.

Name	Signature	Address	Date

ABSTRACT

FLEXURAL CREEP EFFECTS ON PERMANENT WOOD FOUNDATION MADE OF STRUCTURAL INSULATED FOAM-TIMBER PANELS

Mahmoud Shaaban SAYED AHMED

M.A.Sc. Civil Engineering

Civil Engineering Department

Ryerson University

Toronto, Ontario, Canada, 2011

A Permanent Wood Foundation (PWF) is a panel composed of expanded polystyrene insulation and preserved stud cores laminated between oriented-strand boards and preserved plywood. This thesis presents the experimental testing on selected PWFs' sizes to investigate their long-term creep behavior under sustained soil pressure. The long-term creep tests were performed over eight months, followed by loading the tested panels to destruction to determine their axial compressive strength. The ultimate load test results showed that the structural qualification of PWF is "as good as" the structural capacity of the conventional wood-frame buildings. The obtained experimental ultimate compressive resistance and flexural resistance, along with the developed long-term creep deflection of the wall under lateral soil pressure can be used in the available Canadian Wood Council (CWC) force-moment interaction equation to establish design tables of such wall panels under gravity loading and soil pressure.

Keywords: Sandwich wall panels, permanent wood foundation, structural insulated panel, creep, compressive strength, flexural resistance, strength interaction equation, characteristic value.

ACKNOWLEDGEMENTS

The author would like to thank Dr. Khaled Sennah for all his continuous support. The author would also like to thank Mr. Nidal Jaalouk & Mr. Mohamad Aldardari, the Civil Engineering Technicians, for their valuable supports and directions in the structural laboratory The research support from Thermapan Structural Insulated Panels Inc of Fort Erie, Ontario, Canada, The Ontario Centres of Excellence (OCE) funding program and Ryerson School of Graduate Studies is greatly appreciated. Finally, the author would like to thank his family in Egypt; father, mother, wife and the kids, for their patience and encouragement.

Mahmoud SAYED AHMED

TABLE OF CONTENTS

LIST OF TABLES

LIST OF FIGURES

`

LIST OF SYMBOLS

A	Cross-sectional area
A_v	Shear area
b	Specimen width
b_g	Stud thickness, mm
b_f	Width of flange, mm
B_{at}	Axial stiffness of tension flange for OSB, N/mm
B_{ac}	Axial stiffness of compression flange for plywood, N/mm
c	Core depth
C_t	Creep Coefficient
c_t	Distance from neutral axis to tension face, mm
c_c	Distance from neutral axis to tension compression, mm
D	Dead load
d	Depth of stud
d	Distance between neutral axis of faces (c + f for equal facing thicknesses)
D	Flexural rigidity, or bending stiffness (D = EI)
e	Eccentricity = thickness/6
E	Young's modulus
E_s I	Bending stiffness taken from CWC Joist Selection Tables
f	Facing thickness
G	Shear modulus
H	Backfill height
h	Total panel thickness

h_c Flange thickness under compression, mm

h_t Flange thickness under tension, mm

I Second moment of area of the entire section about its centroid

K Constant to calibrate the long-term effects of dead load and live load

K_e, K_k The elastic modulus (E) represented as spring

K_s Service condition

L Beam span

L Live load

m_k Characteristic value

M_f Maximum factored bending moment

M_r Factored bending moment resistance

P Total applied load

P_f Factored axial load on stud

P_r Factored compressive resistance parallel to grain taken from CWC Stud Wall

q Lateral load

Q Shear force at the section

R_{fT} Inward reaction at top of panel, N

R_{fb} Inward reaction at bottom of panel, N

S First moment of area of that part of the section

S Specified snow load

S_y Standard deviation

t Time

t Thickness

T Temperature in Celsius

$\tilde{y}$ Mean value

V Shear stiffness

w_f Factored loading

x Location of maximum bending moment due to lateral load

X Distance from the reaction in shear zone of beam

z Distance from the neutral axis of the sandwich

σ_c Normal core stress

σ_f Normal facing stress

σ_{fc} Face failure in compression

σ_{ft} Face failure in tension

σ_e Stress equivalency

ε Strain

τ Shear stress

υ Poisson's ratio

$\boldsymbol{\eta_v = \eta_k}$ The viscosity represented as dashpot

θ Relative humidity in %

Δ Deflection

Δ_o Instantaneous deflection

Δ_B Deflection at mid-span of the sandwich panel due to bending

Δ_S Deflection at mid-span of the sandwich panel due to shear

LIST OF ABBREVIATION

ACI American Concrete Institute

AF&PA American Forest & Paper Association

ANSI American National Standards Institute

ASCE American Society for Civil Engineers

APA American Plywood Association

ASTM American Society for Testing Materials

B.S. British Standards

BW# Basement Wall Specimen Name and Number

CFS Cold Formed Steel

CSA Canadian Standard Association

CCMC Canadian Construction Materials Commission

CWC Canadian Wood Council

EFP Equivalent fluid pressure

EMC Equilibrium Moisture Content

EPS Expanded polystyrene

FPL Forest Products Laboratory

F.S. Factor of Safety

GFRP Glass fibre reinforced polymers

HSS Hollow Steel Structures

ICC-ES International Code Council – Evaluation Service

I.D Instantaneous Deflection

IPC Insulated Precast Concrete

IRD Instantaneous recovery deflection

L.M. Levenberg-Marquart Algorithm

LVDT Linear Variable Displacement Transducer

M.D. Maximum Deflection

M.S. Margin of Safety

NBCC National Building Code of Canada

NDS National Design Specification for Wood

NLGA National Lumber Grading Authority

NRC National Research Council Canada

OBC Ontario Building Code

OSB Oriented Strand Board

PD Permanent Deflection

PWF Permanent Wood Foundation

SIP Structural Insulated Panel

SLS Standard Linear Solid Model

S-P-F Spruce-Pine-Fur

SSE Summation of Squares of Errors

SW Sandwich structures

SWMT Sandwich Membrane Theory

TCS Test Control Software

ULC Underwriters Laboratories of Canada

CHAPTER I

INTRODUCTION

1.1 GENERAL

The structural insulated panel (SIP) is an engineered composite product composed of an insulating foam core sandwiched to provide the insulation and rigidity, and two face-skin materials to provide durability and strength The skin material may take the form of oriented strand board (OSB), traded plywood, fibre-cement board, and sheet metal. The SIP can be compared, structurally, to an I-beam; the foam core acts as the web, while the facings are analogous to the I-beam's flanges as shown in Fig. 1.1. In case of flexural loading, all of the elements of a SIP are stressed; the skins are in tension and compression, while the core resists shear and buckling. Under axial concentric in-plane loading, the facings of a SIP act as slender columns, and the core stabilizes the facings and resists forces that may cause local bucking of the facings. However, in the conventional stud wall system shown in Fig. 1.2, the studs transfer the load from the roof and floor down to the foundation, while the foam is installed between studs to provide insulation. SIPs are usually available in a thickness ranging from 100 to 350 mm, depending on climate conditions. These panels can be used in industrial, commercial and residential construction as lading. However, their significant use is walls, floors and roofs in low-rise residential, commercial and industrial buildings is shown in Fig. 1.3. The energy saving insulation, design capabilities, cost effectiveness, speed of construction and exceptional strength make SIPs the future material for high performance buildings (Said, 2006; Shaw, accessed 2011; RSMeans, 2007).

SIPs can also be used as permanent wood foundation for basement envelope systems that can replace the traditional plain concrete basement wall to save the operating cost i.e. heat, (Swinton, 2005). Figure 1.4 shows view of such SIP wall on which OSB sheets are used as axial and flexural load carrying element on the interior face, while treated plywood boards are used in the exterior wall exposed to earth. Figure 1.5 shows of the use of SIP in erecting basement walls in low-rise buildings. While Fig. 1.6 shows a schematic diagram of the basement wall construction using SIPs. In such a case, SIPs are placed vertically beside each other and connected together using a wood-spline joint incorporating timber stud nailed to the sides of the adjacent SIP faces.

1.2 THE PROBLEM

The developed structural insulated sandwich timber panels comprise insulated foam glued between two OSB boards. To determine the structural adequacy of the level of adhesion between the foam and the OSB boards and the level of composite action between them, it is felt necessary to conduct experimental testing to-collapse on the developed structural insulated sandwich timber panels. Clause 8.6 of the Canadian Standard for Engineering Design of Wood, CAN/CSA-O86.01, (2001) specifies the effective stiffness, bending resistance and shear resistance of stressed-skin panels shown in Fig. 1.7. These stressed skin-panels have continuous or splice longitudinal web members and continuous or spliced panel flanges on one or both panel faces, with the flanges glued to the web members. These strength equations are not applicable to SIPs since they do not address the adequacy of the foam as the main shear carrying element near the supports and the connector between the facings at the maximum moment location. Also, CAN/CSA-O86.01 specifies expressions for the effects of combined axial and bending on the

timber stud walls and posts which are applicable to SIPs. However, the available CAN/CSA-O86.01 compressive resistance equations for studs and posts cannot be applied to SIPs as a result of their structural performance at failure. The technical guide of Canadian Construction Materials Commission (CCMC) and National Research Council Canada (NRC) for stressed skin panels (with lumber 1200 mm o.c. and EPS core) for walls and roof, formed the basis for the experimental testing conducted in this thesis for flexure, axial eccentric and axial concentric, with the ultimate goal of providing enough technical data for strength and serviceability of the developed structural insulated sandwich timber panels. With this database, design tables can be established. CAN/CSA-S406, Construction of Preserved Wood Foundations, (1992) allows the use of permanent wood foundation (PWF) which is referred to in Part 9 of the National Building Code of Canada (2005) and in provincial building codes as applied to buildings not exceeding 557 m^2 (about 6000 ft^2) in building area and not more than two storeys high. Building that exceed these limits must be designed according to Standard CSA O86.01, Engineering Design on Wood, which is referenced in Part 4 of the NBCC. The PWFs are load-bearing wood-frame system designed as foundation for light frame construction. They are built using lumber and plywood, pressure-treated with approved water-borne wood preservatives. Design information for PWFs made of lumber studs is available which it is as yet unavailable for SIPs. Clause 4.1.1.4 of the 2006 Ontario Building Code (2006) specifies that buildings and their structural members shall be designed by one of the following methods:

(a) standard design procedures and practices provided by Part 4 of this code and any standards and specifications referred to in this code, except in cases of conflict the provisions of the building code shall govern, or

(b) one of the following three bases of design,

(i) analysis based on generally established theory,

(ii) evaluation of a given full-scale structure or a prototype by a loading tester, or

(iii) studies of model analogues,

provided the design is carried out by a person qualified in the specific method applied and provided the design ensures a level of safety and performance at least equivalent to that provided for or implicit in the design carried out by the methods referred to in Clause (a) above. PWF shown in Fig. 1.8 is subjected to gravity loaded associated with lateral soil pressure. To use the available CWC axial force-moment interaction equation for PWF design, experimental testing to-collapse is needed for the behavior of the wall under axial compressive loading as well as soil pressure. In addition, the soil pressure would cause short-term and long-term creep lateral deflection of the wall that would decrease the wall capacity. Information on the long-term creep behavior of the wall under sustained triangular loading, simulating soil pressure, is as yet unavailable.

1.3 THE OBJECTIVES

The main objectives of this research work can be stated as follow:

1. To contribute to the efficient design of structural insulated sandwich timber panels as permanent wood foundation by developing experimentally calibrated models capable of predicting their structural response when subjected to sustained flexural loading.
2. Testing to collapse the tested SIPs to investigate their ultimate load carrying capacities in both flexural and shear that would lead to design tables for SIP use as permanent wood foundation.

1.4 THE SCOPE

The scope of this study includes:

1- Conducting literature review on previous work and codes of practice related to structural behaviour of the stressed-skinned sandwich timber panels when subjected to Equivalent Fluid Pressure (EFP) and transverse loading.

2- Carrying out experiments on 6 actual-size PWF-SIP panels according to ASTM Standards to determine their flexural-creep performance.

3- Carrying out experiments to-collapse on 6 actual-size PWF-SIP panels according to ASTM Standard to determine their ultimate strength for axial compression and flexure.

4- Develop expressions for the long-term deflection of the studied panels under sustained soil pressure.

5- Provide research information on the use of the CWC axial force-bending interaction equation to design such panels as permanent wood foundation.

1.5 THE CONTENTS AND THE ARRANGEMENT OF THE THESIS

Chapter II of this thesis summarizes the literature review on sandwich panels and related Codes and Standards. Chapter III explain the experimental program conducted on selected SIP sizes. Chapter IV summarizes the experimental findings. Chapter V presents the procedure for the development of the long-term flexural creep deflection equations and guidelines on the use of the CWC axial force-moment interaction equation on the design of PWF made of SIPs. Chapter VI presents the conclusion of this research work and the recommendation for the future research. Figure 1.9 shows the thesis structure and research activities flow chart.

CHAPTER II

LITERATURE REVIEW

2.1 GENERAL

Structural insulated panel (SIP), shown in Fig. 2.1, consists of two layers of oriented strand board (OSB) with foam core made of expanded polystyrene foam (EPS), extruded polystyrene foam (XPS) or polyurethane foam. Structural Insulated Panels (SIPs) are prefabricated insulated structural elements for use in building walls, ceilings, floors and roofs. The Environmental Protection Agency (EPA) estimates that the average U.S. home releases 22,000 lbs of carbon dioxide (CO_2) into the atmosphere each year. This is twice the amount of the average vehicle. By reducing the amount of energy used for heating and cooling, SIPs can significantly reduce emissions produced by our homes and commercial buildings. Building with SIPs is better because it is more comfortable, stronger & safer, lightweight, faster to construct, more resource efficient, healthier living environment, save money, wave of the future, greater energy savings, straighter walls and more design friendly. A basic SIPs panel is made from Orientated Strand Board (OSB) facing boards with a Polyurethane core. SIPs can be used to construct the floor, walls and roof of a building enabling uniform detailing at interfaces providing continuity of insulation and minimal air leakage. The literature review summarized in this chapter includes (i) History of SIPs; (ii) Types of Structural insulated sandwich panels; (iii) Structural analysis and design of Sandwich panels; and (vi) Permanent Wood Foundation.

2.2 HISTORY OF SIPs

SIPs are environmentally friendly and ecologically sound. SIPs are the innovative building construction method of the twenty first century allowing the rapid deployment of buildings for domestic and commercial use. SIPs are structural insulated panels used to construct buildings. In the past, a significant amount of research was conducted to predict the behaviour of sandwich panels. However, only very few researchers have undertaken experimental studies to investigate the accuracy of design of timber sandwich panels. Building panels come in many configurations, known variously as foam-core panels, stressed-skin panels, nail-base panels, sandwich panels, and curtain-wall panels, among others. Many of these building panels are non-structural, while some have no insulation. And the term "panelized construction" can also include prefabricated stud walls and other configurations associated with the modular industry.

The SIPs have been used extensively in the USA and Canada over the past 50 years but the historical development of the theory of sandwich panels shows that a very few papers have been published which deal with the bending and buckling of sandwich panels with cores which are rigid enough to make a significant contribution to the bending stiffness of the panel, yet flexible enough to permit significant shear deformations (Allen, 1969).

- 1935- The concept of a structural insulated panel began as the Forest Products Lab (FPL) builds the first in a series of experimental SIP houses in Madison, WI.
- 1947- FPL builds the Experimental Sandwich building, which is tested and monitored for 31 years. The structure is still in use today.
- 1952- Alden P. Dow, one of the Wright's students, builds SIP homes in Midland, MI.
- 1958- NAHB builds demonstration research homes with SIPs.

- 1959- Koppers Corp. starts SIP plant in Detroit.
- 1962- American Plywood Association (APA) Lab Report # 193 on Sandwich Panels published.
- 1967- APA Lab Report # 193 first appears in the Model Building Code- UBC.
- 1969- APA Supplement Four on Sandwich Panels is released and rigid foam insulating products became readily available resulted in the production of structural insulated panels as we know them today.
- 1970- USDA Forest Service Research Paper FPL 144, Long-time Performance of Sandwich Panels in Forest Product Laboratory Experimental Unit, is published.
- 1973- Oil embargo- fuel prices soar.
- 1981- Oriented Strand Board (OSB) manufacturing begins.
- 1990- Group of SIP manufacturers form the Foam Core Panel Association (name later changed to Structural Insulated Panel Association (SIPA).
- 1991- SIP market study published. Spotted oil habitat threat reduces old growth timber availability.
- 1994- SIPA Strategic Long Range Plan developed. OSB oversupply brings OSB prices down.
- 1995- 1997- Industry production increases by 50% per year.
- 1962- present- The American Society for testing Materials (ASTM) standard defines a testing protocol to document the strength and stiffness properties under the following load applications:

(1) Creep; (2) Axial Loads; (3) Racking and diaphragm Loads; (4) Uplift Loads; (5) concentrated Loading; (6) combined Loading; (7) Impact loading; and (8) Transverse Loads.

2.3 COMMON TYPES OF STRUCTURAL INSULATED SANDWICH PANELS

2.3.1 Steel-Foam Panels

Light Weight Steel Frame Panels are an open type of Structural Insulated Sandwich panels, on which insulation is located on the external side of the frame to overcome the risk of cold bridging. Protection against corrosion of the mild steel panels is provided by galvanizing. Lightweight steel frame and the dry assembling method have the advantage of high load bearing capacity, placed at the external surface. Mild steel panels are protected by galvanizing. They are composed of thin C, U or Z-shaped cold formed steel (CFS) sections, as shown in Fig. 2.2. The thickness of the sheet varies between 0.6 to 2.5 mm for a maximum mass per unit of length 0.075kN/m. Other type of steel sandwich panels, shown in Fig. 2.3, is made of dense core of EPS (expanded polystyrene) sandwiched between two exterior layers of galvanized steel, resulting in a solid one-piece that provides structural framing, insulation, and exterior sheathing. The 1.2-m wide interlocking panels are strong, and easy to handle. The technique of sandwiching a foam core between casings has been used in refrigeration technology for decades. Many screen room additions and carports have been built using these panels.

2.3.2 Fiber Cement Faced Structural Insulated Panels

SIPs are engineered laminated panels with solid foam cores and structural sheathing on each side. The most common types of sheathing or skins materials are oriented strand board

(OSB) and plywood. Cement Faced Structural Insulated Panels can be used for below grade applications, as foundation or basement walls, and above grade applications, as floors. Some manufacturers produce cementitious SIPs with typically manufactured fiber cellulose reinforced cement boards for inside and outside skins. Fiber cellulose reinforced cement boards eliminate the need for gypsum drywall for fire resistance and can be taped and finished on the interior surface. The exterior surface is painted or coated with a vinyl or synthetic stucco permanent finish. OSB can be used instead of cellulose reinforced cement board for Fiber Cement Faced Structural Insulated Panels to accept brick veneer wall ties, to accept nailing of siding and for stucco applications. Cementitious SIP spans are up to 5 m, load-bearing walls up to four stories and roof panels up to 6 m spans. Cementitious SIPs are fastened together with power-driven screws through the inner and outer skins into either cement board or wood splines. Cementitious SIP is as energy efficient as OSB SIP and has similar connection details those of OSB-sheathed panels. Cementitious SIPs typically last longer and require less maintenance than other types of SIPs panels. Cementitious SIP has higher strength, higher fire rating, higher rot and vermin resistance, higher resistance to moisture absorption and lighter in weight than OSB SIP. Cementitious SIP is air tight as it has continuous air barrier with very low air leak, fully insulated with uniform insulation coverage and thermal bridge panels. Cementitious SIP has finishes as smooth finish, stucco, vinyl siding, brick or stone which can be installed. Figure 2.4 shows schematic diagrams of the SIP made of fiber cement (Novak, 2009).

2.3.3 Precast Concrete Sandwich Panel

Concrete panels have been in use for more than 50 years. Precast concrete sandwich panels are made with two reinforced slabs of high strength concrete. The space between concrete

slabs is filled with a sound attenuating foam barrier. To make precast concrete sandwich panels, a first concrete slab is formed having embedded in it one end of connectors which extend from it's surface in two directions with the path between the two containing only thermally insulative material. A layer insulative material is positioned adjacent to a central portion of said connectors to form a solid layer and a second layer of concrete is cast so as to receive the upper ends of said connectors. The connectors provide resistance to shear in at least two directions and include insulative high tensile strength members extending in more than one direction between the concrete slabs. The face shells of sandwich panel's main functions are providing protection to the insulation and meeting the immediate demands of handling and imposed loads. The face shells of sandwich panels must continue to give satisfactory performance under long time service. The structural concrete shells of the sandwich panels were reinforced with welded wire fabric should confirm to ASTM A82-62T, "Cold Drawn Steel wire for concrete reinforcement." They are available with a perfectly smooth face, ready for paint. Provisions are made for electrical boxes and conduits in the panel at the factory. The conduit is stubbed out above the ceiling line for connection by the electricians in the field. There is no need to install furring strips and drywall on either side of the demising wall. The precast concrete, as shown in Fig. 2.5a, has benefits as a cladding material. It has strength and solidity, recalling traditional concepts of enclosure, yet is a modern prefabricated product with all the advantages of quality control, 'just-in-time' site delivery, fast installation and extreme durability. In most cases, precast panels are cast using a mix that will simulate the appearance and texture of natural stone, generally known as reconstructed or cast stone. Panels may also be faced with brick slips, natural stone or terracotta tiles. Most precast concrete cladding systems comprise single layers of factory-manufactured precast concrete that are installed on a building, providing a weather-resistant

external finish. Standard sandwich panels, with two layers of precast with insulation between, are a well-established product. The insulating materials were commercially available rigid board stock or batting: one foamed polyurethane plastic, two foamed polystyrene plastics, one glass fiber, one foamed glass and one autoclaved cellular concrete. Brick clad concrete masonry panels, as shown in Fig. 2.5b, have a service life greater than 60 years. The two layers are connected by proprietary stainless steel connectors, typically consisting of wind and shear connectors. The latter are strategically positioned orthogonally to achieve suitable suspension of the outer leaf. The system provides structural integrity as it does not rely on insulation for load transference. Various insulation types can be used, including mineral fibre insulation materials. In order to optimise the cladding system, the inner leaf of the sandwich panel may be used as a load-bearing structural element to support floor units. This provides further efficiencies for the construction process and minimises the need to co-ordinate different trades. Exposure conditions may cause temperature and moisture differentials is sandwich construction and these conditions may have a more pronounced effect on the satisfactory long time structural behaviour than do the imposed loads.

IPC (Insulated Precast Concrete) system, shown in Fig. 2.6, is insulated concrete sandwich wall system. It is composed from a 50-mm thick layer of extruded polystyrene insulation sandwiched between one 100-mm thick and one 50-mm layer of concrete. The three layers are held together by high-strength, patented, fibre-composite connectors.

2.3.4 Plywood Sandwich Panels

Plywood serves as an ideal facing material for the sandwich panels. Plywood Sandwich Panel has high strength and light weight. In addition, it is easily finished, dimensionally stable, and

easily repaired if damaged. Polystyrene foams, and paper honey combs can be used as core material in the Plywood Sandwich Panel after considering the resistance of the core material to shearing forces, to heat and vapour transmission, to degradation by heat, age, and moisture; and compatibility with glues. Cross-section of plywood sandwich panel is shown in Fig. 2.7.

2.3.5 FRP Sandwich Panels

Traditional foam-core sandwich construction exhibits low transverse stiffness, susceptibility to in-plane shear, face-to-core debonding and buckling instability. The 3-D FRP sandwich panels consists of, glass fiber reinforced polymer (GFRP) laminates and foam core sandwich where top and bottom skin GFRP layers are connected together with through-thickness fibre as shown in Fig. 2.8. The panels are fabricated using pultrusion and the through thickness fibres are injected during the pultrusion process. The width of the panels can vary from 1.8 m to 2.6 m while the panel thickness can be fabricated with a total thickness up to 100 mm (Hassan et al., 2003).

2.4 STRUCTURAL ANALYSIS AND DESIGN OF SANDWICH PANELS

Sandwich panel is consisting of two relatively thin faces and a foamed plastic core. The structural performance of the sandwich panels depends on the two faces and the core acting together as a composite element, and this raises unique design problems, not all of which may be fully understood by those responsible for their manufacture, design, and use. Sandwich panels have flexible cores, therefore their behaviour is more complex than that of the plain plates and it is important to understand the numerous failure modes of sandwich panels so that appropriate

design criteria can be developed. In addition to face buckling, the other possible modes of failure are as follows:

• Failure of fasteners;

• crushing of the sandwich panel at a point of support or line load;

• yielding of metal face in tension;

• shear of the core, including shear bond failure;

• Failure of the sandwich panel at a point of connection; and

• Blistering.

The expected service life of all the structural panel systems is in excess of 60 years. The fully profiled sandwich panels are susceptible to local buckling effects under compression, bending, or their combinations. Few research has been carried out in Europe and USA to investigate the behaviour and design of sandwich panels for different failure conditions. In Canada, the choice of faces and cores is not infinite; face materials may be available in relatively few gauges or standard thicknesses; core materials are restricted in the choice of thickness and density. Since the plate elements of the profiled sandwich panels are supported by foam core, their local buckling behaviour is significantly better than that of plate elements without foam core. Buckling of the panels may occur at a stress level lower than the yield stress of steel, but the panels, particularly those with low b/t ratios, will have considerable post-buckling strength. Such local buckling and post-buckling phenomena are very important in the design of sandwich panels. The process of trial and error is often the most effective method of designing sandwich panels. Design methods should be as precise as the final analysis or check calculation and should indicate roughly where the process of trial and error should begin. The practical usage of

sandwich panels as cladding of buildings has increased dramatically in recent years. This has stimulated increased activity in research and development as a result of which most technical problems associated with this form of construction have been solved but still a lot of research needed to be done on:

• The influence of the shear flexibility of the core on the global behaviour.

• The influence of the core in restraining local buckling of the faces.

• The variability of core material properties.

• The influence of temperature-induced stresses has to be considered as structural sandwich panels have low thermal capacity, poor fire resistance with rigid plastic foam cores and it may deform when one side of faceplate is exposed to intense heat.

• Creep under sustained load with rigid foam cores.

• The influence of deflections.

The basic concept of a sandwich panel is that the face plates carry the bending stresses and the core carries the shear stresses. As a sandwich with thick faces and a weak core is an inefficient sandwich because the faces are working as two independent elements, one short cut is to ignore completely any effects due to the thickness of the faces. For identification and comparison for core material properties, density, shear strength, shear modulus and compression modulus have to be determined by tests for each panel type produced. Classical methods of analysis solutions have only been derived for a few simple cases of greatest practical significance. An early contribution to the subject was made by Chong and Hartsock (1972, 1974), Chong (1986). A useful approximate solution for panels which have either one or both faces profiled has been given by Wolfel (1978). He made the usual assumption that the applied

load is shared between two separate load-carrying systems -- namely, the sandwich part, which includes the influence of core shear; and the flange part, which merely involves bending of the flanges. He then made the further assumption that these two systems are quite independent, except that their deflections coincide at some critical point, usually at the mid-span. This method is worth describing in a little more detail because, as well as yielding equations of practical value. It also provides a valuable insight into the way in which sandwich panels behave. If the bending stiffness of the faces is neglected, the sandwich panel carries load as a consequence of axial forces in the flanges and a shear force in the core. When irregular loading or support conditions arise, it becomes necessary to resort to numerical methods of analysis. Jungbluth and Berner (1986) have described a finite difference approach which appears to be the favoured method in Germany. An alternative numerical method, related to the finite element solution, has been given by Schwartze (1984). Yet another technique has been developed in the US in which thin faces are modelled by finite shell strips and relatively weak cores by finite prisms (Cheung, 1986a,b). However, for general purposes, it is believed that the conventional finite element method offers the best approach. In many applications, the finite element method is approximate and it is necessary to use a large number of elements in order to obtain accurate solutions. For three-layered sandwich beams, the solutions are exact and the minimum number of elements necessary to model the problem will give a precise solution. The general solution for the bending of panels with profiled faces was first given by Davies (1986), who then extended it to panels subject to combined axial load and bending, giving solutions for panels with both flat and profiled faces (Davies, 1987). As the former is a special case of the latter, there is little point in omitting the axial load terms when programming the method.

2.4.1 Historical Development of Sandwich Theory

In recent years, sandwich panels are increasingly used in building structures particularly as roof and wall cladding systems. They are also being used as internal walls and ceilings. Because of their good thermal properties, they have been used in cold-storage buildings. Sandwich (SW) structures are three-layer high performance lightweight structures (Wiedemann, 1996; Stamm and Witte, 1974; Plantema, 1966), consisting of a soft core which is covered by stiff skin layers. They are characterized by both excellent bending stiffness and low weight. However, due to their comparatively high shear flexibility, the global behaviour concerning deflection and buckling is described by a shear flexible theory (Mindlin, 1951; Reissner, 1945), where only the membrane stresses in the thin skin layers are considered, whereas the in-plane stresses appearing in the core are neglected. This theory is known as the Sandwich Membrane Theory (SWMT), which has proven to be reliable for a long time. Past research (Davies and Hakmi, 1992, 1991) has investigated the local buckling behaviour and developed modified effective width rules for the plate elements in sandwich panels. For an at least approximate description of both global structural behaviour of SW and local phenomena, the SWMT must be extended. For this purpose (Kuhhorn, 1993, Kuhhorn, 1991; Kuhhorn and Schoop, 1992) presented a thickness flexible, geometrically nonlinear SW-shell theory using seven kinematic degrees of freedom. This theory is able to solve the problems mentioned above with sufficient accuracy if the local perturbations considered are characterized by wavelengths which are not too short (numerical investigations show that this theory is applicable for wrinkling problems characterized by half waves longer than 0.8-times of the core thickness). This extended theory includes the independent bending stiffness of each skin separately. Also a linear thickness stretch distribution over the height of the core is taken into account whereas the core in-plane stresses

remain unconsidered. Due to the increasing interest in the use of structural sandwich panels, a good deal of research has continued in recent years (Davies, 1993). Research and development of sandwich panels with profiled faces began only in late 1960s (Chong and Hartsock, 1993). These rules can be applied successfully for plate elements with low width to thickness ratios (b/t), but their applicability to slender plates is questionable. In sandwich panel construction, the b/t ratio can be as large as 600 (Mahendran and Jeevaharan, 1999). To investigate the applicability of current design rules for slender plates with such large b/t ratios, a detailed investigation into the local buckling behaviour of profiled sandwich panels was conducted using extensive series of laboratory experiments on 50 foam supported steel plates. The static behaviour and strength of sandwich panels is based on the composite action of the three structural layers, namely the two faces and the core (Davies, 2001). For design purposes, such local buckling and post buckling problems are treated by utilizing the concept of effective width principles.

Figure 2.9 shows a typical longitudinal and cross-section in a sandwich beam made of a foam core and two facings (i.e. OSB boards). There remains the considerable problem of the sandwich panel with an anti-plane core, one which posses no stiffness in X-Y plane and in which the shear stresses τ_{zx},τ_{yz} are constant throughout the depth (i.e. they are independent of Z). Such panels differ from ordinary homogeneous plates in that the bending deformations may be enhanced by the existence of non-zero shear strains (ε_{zx}, ε_{yz}) in the core and of direct strains ε_z in the core, perpendicular to the faces. The shear strain and the direct strain in the core are also directly associated with the possibility of short wavelength instability of the faces (wrinkling). This problem has been the subject of two main methods of analysis, which may be referred to for convenience as the general and the selective methods. In the general methods, equations are

setup to define the equilibrium of the separate faces and of the core and to prescribe the necessary continuity between the faces and the core. The result is a set of differential equations which may be solved in particular cases for the transverse deformation of the panel, the flattening of the core and other equations of interest. In the selective method, which has been the basis of this being named (again for convenience) as the bending problem and the wrinkling problem. In the bending problem, it is convenient to assume that the core is not only anti-plane, but also indefinitely stiff in the z- direction. This excludes the flattening of the core and wrinkling instability, but it does permit the assessment of the effect of core shear deformation on the deflections and stresses in the panel. In the wrinkling problem, the true elastic properties of the core are taken into account but the task is simplified by permitting the middle planes of the faces to deflect in the z- direction only, not in their own planes.

2.4.1.1 The General Method

The general method has been investigated by Reissner (1950) in relation to isotropic panels with very thin faces. It has been concluded that the effect of core flexibility in the z-direction is less important than the effect of core shear deformation in the transverse planes. A relatively simple differential equation for the transverse displacement has been driven by neglecting the effect of direct transverse core strains. A very similar equation to Reissner's equation has been driven by Eringen (1951) where the geometrical thickness of the equal faces was neglected, and their local bending stiffnesses and also the bending stiffness of the core was included. By the assumption that the vertical and horizontal displacements in the core are directly proportional to z-direction, the inclusion of the latter is contradicted to some extent. A much more recent analysis conducted by Heath (1960) also included a very similar equation, but

for a sandwich with an orthotropic core. Heath's analysis was based on earlier work by Hemp (1948) and is apparently independent of Reissner's work (1950).

Raville (1955a,b) applied the general method to the problem of a simply-supported rectangular panel with uniform transverse load and with thin faces. The three displacements of points in the orthotropic anti-plane core are expressed as polynomials in z, but the complexity of the analysis again makes it necessary to revert to the simplifying assumption of infinite core stiffness in the z-direction. For practical purposes the general method is evidently intractable when applied to sandwich panels, but more success has been achieved in relation to sandwich struts and beams. The early works of Williams et al (1941) and Cox and Riddell (1945, 1949) fall into this category. The first of these deals with a sandwich strut with thick faces and an isotropic core (with an extension for orthotropic cores) and the analysis is used to form a link between the extreme cases of wrinkling instability (no longitudinal displacement of the faces during buckling) and of overall Euler-type instability, modified for shear deformations in the core (no direct core strains in the z-direction). A very thorough analysis of the behaviour of struts with isotropic faces and cores has been outlined by Goodier (1946) and Goodier and Neou (1951).

2.4.1.2 The Selective Method

Selective method; bending problem

Most of published work on sandwich panels refers to the selective method and, in particular, to the bending problem, in which core strains in the z-direction is neglected. The assumption that the core is weak in the xy-plane leads in any case to the conclusions that the core

makes no contribution to the flexural rigidity of the sandwich, that the core shear stresses in zx and yz planes, are independent of z and that a straight line drawn in the unloaded core normal to the faces remains straight after deformation, but is no longer normal to the faces. These assumptions (core weak in xy-plane, stiff in z-direction) allow the displacements of the panel to be expressed in terms of only three variables, one of which is the transverse displacement. The other two variables are a matter of choice. Figure 2.10 shows a summary of this method of analysis in case of flexural stresses as well as shear stresses.

Selective Method; wrinkling problem

The literature of the wrinkling problem is less extensive than that of the bending problem. As mentioned earlier, wrinkling is characterized by its short waves involving bending of the skins and compression or elongation of the core material in the transverse direction. This type of local failure occurs when the core thickness is such that the overall buckling is not likely to happen. The problem of symmetrical wrinkling of sandwich panels was studied by many investigators with the first major paper by Gough et al. (1940). It contains an examination of the stability of a straight strut stabilized in various ways by an isotropic elastic medium. Some of the cases considered are directly applicable to the compression faces of sandwich beams and to the anti-symmetrical wrinkling of sandwich struts which it may be referred to it as a “skew ripple”. An analysis of the same kind was made by Hoff and Mautner (1945) for symmetrical wrinkling of sandwich struts. In all these studies, a linear distribution of the transverse displacement through the core was considered, and the faces were treated as plates on elastic foundation. The analytic solution for the symmetrical wrinkling stress can be obtained by using an elasticity approach. The assumptions commonly accepted for this type of analysis are: The in-plane

stresses in the core are neglected. That is, with X-Y axes in the plane of a sandwich plate, and Z-axis perpendicular to it: in which normal, shear stresses and subscript denoting the core. Thus, the relevant deformations in the core are in the transverse direction and shear deformations in XZ and YZ planes. The wrinkling consists of a plane deformation. Thus, if a sandwich panel is compressed in X- direction, the lateral deflection is independent of y. The core can be treated as a semi-infinite medium in which the displacement decreases exponentially with maximum value at the interface with the skin. Since the faces are thin in comparison with the core thickness, the deflection of each face is identified with the displacement of the core at its surface. The effect of Poisson's ratio of the core material is neglected.

Taking into consideration the mechanical behaviour of sandwich panel, SIP failure modes under static loading includes (Straalen et al., 2010): (i) failure of the face (yielding or fracture); (ii) wrinkling and dimpling of the face; (iii) shear failure of the core material; (iv) shear crimping of the core material (instability phenomenon); (v) overall buckling (and interaction effects with local failure models); (vi) delimitation of the interface between the core and the face; (vii) long-term creep; and (viii) overall and local deflections. All these failure modes are shown in Fig. 2.10.

2.4.1.3 Flexural Stresses in Sandwich Panels

A number of researchers have studied the failure modes of sandwich structures in flexure (Zenkert et al., 2002; Thomsen, 1995; Yoshii, 1992; Triantafillou and Gibson, 1987). Triantafillou and Gibson studied failure modes of sandwich beams with aluminum face sheets and a rigid polyurethane foam core. Failure maps for various core densities and span-to-depth

ratios were constructed for face yielding face wrinkling, core yield in shear, and core yield in tension and compression. Based on similar failure equations, a weight optimum design of composite sandwich structures was proposed by Yoshii (1992). A summary of design approaches to sandwich construction may be found in a book published by Zenkert (1997) while information on cellular solids is available elsewhere (Gibson and Ashby, 1988). Under flexure a sandwich beam exhibits various failure modes depending on the state of stress and the materials used. The flexural rigidity for the sandwich panel is highly affected the failure mode. It can be defined as the sum of the flexural rigidities of the faces and the core measured about the neutral axis of the sandwich cross-section, Allen (1969). The potential failure modes together with the corresponding simplistic failure criteria are summarized below:

1. Face failure in tension or compression: $-\sigma_{fc} \leq \sigma_f \leq \sigma_{ft}$
2. Face wrinkling due to compression: $\sigma_f \leq 0.5(E_f E_c G_c)^{1/3}$
3. Core failure in shear: $\tau_c \leq \tau_{cs}$
4. Core failure in tension or compression: $-\sigma_{cc} \leq \sigma_c \leq \sigma_{ct}$
5. Face/core interface failure: $\tau_i \leq \tau_{is}$

In the above equations σ = in-plane normal stress, τ = out-of-plane shear stress, E = Young's modulus, G = shear modulus, sub f = face, sub c = core, sub i = interface, sub fc = face compressive strength, sub ft = face tensile strength, sub cs = core shear strength, and sub is = interface shear strength. In case of localized loading, face/core indentation is an additional failure mode.

Ordinary bending theory is used to define the normal stresses in the faces and the core by adapting the composite nature of the cross section, defining the appropriate form of the flexural

rigidity, D, of the composite section. The stresses in the faces and the core, shown in Fig. 2.10, have been defined by Allen (1969) as follows:

$$\sigma_f = \frac{M\, z\, E_f}{D} \qquad \text{for } c/2 \leq z \geq h/2 \tag{2.1}$$

$$\sigma_c = \frac{M\, z\, E_c}{D} \qquad \text{for } -c/2 \leq z \geq h/2 \tag{2.2}$$

Where: h = specimen height

c = core thickness

E_f = modulus of elasticity of the facing material

E_c = modulus of elasticity of the core material

D = sandwich flexural rigidity (Equation 2.3)

σ_c = normal core stress

σ_f = normal facing stress

M = bending moment

z = distance from the neutral axis of the sandwich

The flexural rigidity is commonly referred to as D and can be defined as the sum of the flexural rigidities of the faces and the core measured about the neutral axis of the sandwich cross-section. Allen (1969) has defined the flexural rigidity for a narrow sandwich beam (transverse stresses in the y direction are assumed to be zero) as follows.

$$D = E_f \frac{bf^3}{6} + E_f \frac{bfd^2}{2} + E_c \frac{bc^3}{12} \tag{2.3}$$

Where: E_f = modulus of elasticity of the facing material

E_c = modulus of elasticity of core material

D = sandwich flexural rigidity (D = EI)

b = specimen width

c = core thickness

f = facing thickness

d = distance between neutral axis of faces (c + f for equal facing thicknesses)

On the right hand side of the equation, the first term may be neglected in comparison with the second if:

$$d / f > 5.77 \quad (2.4)$$

If this condition is fulfilled, the local bending stiffness of the faces (bending about their own separate centroidal axes) makes a negligible contribution of the flexural rigidity of the sandwich. The third term may be neglected in comparison with the second if

$$\frac{E_f f d^2}{E_c c^2} > 16.7 \quad (2.5)$$

If this condition is fulfilled, the bending stiffness of the core is negligible.

2.4.1.4 Shear Stresses in Sandwich Panels

The form of the shear stress (τ) for a point located at distance z from the neutral axis of a homogenous beam can be easily derived by ordinary bending theory and appears in many basics text books as follows.

$$\tau = \frac{QS}{Ib} \quad (2.6)$$

Where Q = shear force at the section

I = second moment of area of the entire section about its centroid

b = width at given depth in section ($b = z_1$)

S = first moment of area of that part of the section where $z>z_1$

For a sandwich beam, the moduli of elasticity of the component parts are accounted for by representing the sum of the products of S and E in Equation 2.7; the profile of the shear stress through the depth is defined in Equation 2.8 (Allen, 1969).

$$\tau = \frac{QS}{Db} \sum(SE) \tag{2.7}$$

$$\tau\,(z) = \frac{Q}{D}\left[E_f \frac{fd}{2} + \frac{E_c}{2}\left(\frac{c^2}{4} - z^2\right)\right] \tag{2.8}$$

Allen (1969) shows that Equation 2.8 may be simplified if the sandwich has a relatively weak core and if the flexural rigidity of faces about axis of faces is small (i.e. Equation 2.4 is satisfied). For sandwich cross-section with relatively stiff faces and weak core, it is common to assume the shear stress of the faces is negligible. Therefore, Equation 2.6, which defines the shear stress through the depth of the core, reduces to Equation 2.9.

$$\tau = \frac{Q}{bd} \tag{2.9}$$

The normal and shear stress profiles of a sandwich beam are given in Fig. 2.11 where the maximum facing stress at the outer fiber is obtained by using z = h/2 in Equation 2.1, the minimum facing stress at the interface of the core is obtained by using z = c/2, and maximum shear stress in the core as given in Equation 2.9. Figure 2.11 presents a chart for sandwich panel selection based on material modulus and density (Jochen Pflug et al., 2008), while Figs. 2.12 and 2.13 shows procedure and coordinate systems for layered analysis of composite material section, respectively (Reddy, 2004).

2.4.1.5 Elastic Deflection Analysis of Sandwich Panels

The plywood Design Specification Supplement, entitled "Design and Fabrication of plywood Sandwich Panels" (APA, 1990) simplifies the total elastic mid-span deflection (Δ_T) for the uniformly loaded-simply supported sandwich beam with relatively thin and stiff faces, and thick weak cores. It is simplified to the sum of bending and shear deflection as follows:

$$\Delta_T = \Delta_B + \Delta_S \tag{2.10}$$

Where: Δ_B = deflection at mid-span of the sandwich panel due to bending

Δ_S = deflection at mid-span of the sandwich panel due to shear

The form of the elastic bending deflection for a simply-supported homogeneous beam of uniform cross-section in quarter-point loading, as follow:

$$\Delta_B = \frac{11\ P\ L^3}{384\ EI} \tag{2.11}$$

Where: P = total applied load

L = beam span

E = modulus of elasticity of the beam material

I = moment of inertia of the uniform cross-section

EI = flexural rigidity

By applying the boundary conditions for the simply-supported quarter point load beam ($w_2 = 0$ at $x = 0$, the maximum shear deflection (at $x = L/4$) associated with the shear deformation of the sandwich loaded at quarter points is defined by the following equation:

$$\Delta_s = w_{2max} = \frac{PL}{8\ AG} \tag{2.12}$$

Where A = bd^2 /c and AG is referred to as the shear stiffness

P = total applied load

L = beam span

G = core shear modulus

X = distance from the reaction in shear zone of beam

w_2 = displacement at x

Thus, the total sandwich beam deflection reflecting the bending and shear component is defined in by the following equation:

$$\Delta_S = \frac{11\ P\ L^3}{384\ D} + \frac{PL}{8\ AG} \tag{2.13a}$$

2.4.1.6 Deflection Criteria for Sandwich Panels Subjected to Bending and Axial Loading

For Preserved Wood Foundation shown in Fig 1.7, the wall can be treated as a beam of 1 m width subjected to eccentric axial gravity loading and triangle load simulating soil pressure. Considering the wall with simply-supported ends, the short-term lateral deflection of the wall can be obtained from the following equation

$$\Delta_{Short-term} = \Delta_{Bending} + \Delta_{Shear} - \Delta_{Ecc\ @\ mid-span} \tag{2.14}$$

Where

$$\Delta_{Bending} = \frac{q\ L^2}{360} . \frac{x}{D} \left\{7 - 10\ \frac{x^2}{L^2} + 3\frac{x^4}{L^4}\right\} \tag{2.15}$$

$$\Delta_{Shear} = \frac{Q}{AG} = \frac{Q}{V} = \frac{qLx}{6V}\left[1 - \frac{x^2}{L^2}\right] \tag{2.16}$$

Where V is the shear stiffness as AG, A is the core cross-section in shear, G is core shear rigidity, Q is the first moment of area about the neutral axes of the section. Since the deflection is calculated at the serviceability limit state, q should equal the specified soil pressure of 4.7 kN/m^2 per meter depth of the wall. L and x are variables shown in Figures 1.7 and 1.8.

The Flexural Rigidity "D = EI" for dissimilar face to be taken as (equation 2.17), where the suffix 1 and 2 refer to the upper and lower faces respectively:

$$D = \frac{b\, d^2 E_1 E_2 t_1 t_2}{E_1 t_1 + E_2 t_2} + \frac{b}{12}\left(E_1\, t_1^3 + E_2\, t_2^3\right) \qquad (2.17)$$

Where

d = the distance between the centre lines of the upper and lower faces

b = the beam width

t = thickness of the face

E = modulus of elasticity for the face material

V is shear stiffness, and G is the shear modulus of the core to be taken as:

$$G = \frac{E}{2\,(1+\upsilon)} \qquad (2.18)$$

Where E is the modulus of elasticity, υ is the Poisson's ratio

The third term in Equation 2.14 results from the t/6 eccentricity of the gravity load at the top of the wall and it can be neglected since it produces lateral deflection of the wall towards the soil, opposite to the major lateral deflection from soil pressure.

2.4.1.7 Long-term Deflection Analysis of Sandwich Panels

In 1996, ASTM included creep loading as an official protocol addressing SIP performance. At this point engineers and designers need validated techniques to define SIP creep performance to consumers and code officials. The National Design Specification for Wood, NDS, (NFPA, 1991) provided convenient method (equation 2.19) for calculating total deflections for structural wood products subject to long term loading:

$$\Delta_{Total} = K\,(\Delta_{long\ term}) + \Delta_{short\ term} \qquad (2.19)$$

Where $\Delta_{long\ term}$ = immediate deflection under dead load +long-term portion of live loads

K = constant to calibrate the long-term effects of dead load and live load

$\Delta_{short\ term}$ = deflections under short-term portions of design load

The long-term deflection constant, K, ranges in magnitude from 1.5 for seasoned lumber and glue laminate timbers, and; up to 2 for green lumber. There is a great need in the SIP industry to develop a similar relationship for long-term SIP behavior. This creep behavior can be defined by experimental testing. Figure 2.15 shows a schematic diagram of creep behavior of a typical material. The first region shows the instantaneous deflection-time relationship as the member reaches its immediate deflection. The next region defines primary creep where deflection increases at a decreasing rate. The secondary creep region shows the deflection increasing at a nearly constant rate and finally, the tertiary creep region ending in failure. Alternatively, if the structure is unloaded before the onset of the tertiary stage, the deflection is immediately reduced; the elastic deflection will be fully recovered for viscoelastic material and the structure continues to recover its creep deflection.

The creep behavior of wood on wood (OSB faced solid-sawn wood stud core) panels has been researched by Wong et al. (1988) for three months load duration. Davis (1987) summarized research predicting the influence of creep on urethane and EPS core metal faced panels for ten year load duration. Huang and Gibson (1990) reported results on the creep of metal faced urethane core panels. Other work by Huang and Gibson (1991) defined creep parameters for polyurethane foam cores from shear creep tests as recommended by ASTM-C273-61. Taylor (1996) conducted a series of creep testing on OSB/foam structural insulated panels to measure the three month mid-span creep deflections due to sustained loading at the quarter points. Four manufacturers were included in the experimental plan (two EPS core SIP manufacturers and two urethane core SIP manufacturers). The SPS designates the expanded polystyrene core type. The results suggested the use of a fractional deflection factor, K, for the calibration of long-term deflection as 1.5 for EPS core and 2.0 for urethane core for cumulative deflection duration up to three months in the NDS long-term equation.

The ratio of creep to elastic strain is of a great interest to designers. It is defined as Creep Coefficient and denoted by $C_{(t)}$. The American Concrete Institute Standard (ACI 318-2008) states that the effect of creep and shrinkage deflection shall be multiplied by the initial deflection by the creep factor.

$$\boldsymbol{C_{(t)} = \frac{Creep\ plus\ Shrinkage\ Strains}{Elastic\ Strain} \leq 2.0} \qquad (2.20a)$$

And it is taken as 2.0 for 5 years or more;

1.4 for 12 months;

1.2 for 6 months; and

1.0 for 3 months.

For the Structural Insulated Panels the deflection under long-term loading must be limited, the total deflection, including creep effects shall be calculated as followed in the SIP Design Guide (NTA, 2009). Where K_{cr} is the fractional creep (Δ_f/Δ_i = 1 + C_t), equals to 4.0 for SIP loaded with lateral earth pressure. Table 2.2 shows different values for K_{cr} versus different type of loading used in connection with equation 2.20b.

$$\Delta_T = \sum K_{cr}\, \Delta_i \tag{2.20b}$$

Creep is the deformation under sustained load over time as shown in Fig. 2.16a. It is also time-dependent parameter which can be quantified as creep compliance (known as specific creep) and relative creep (known as creep coefficient); both parameters are function of temperature, and moisture in case of wood, Fig. 2.16b. The creep rate is increased by the increase of the temperature and/or humidity. Initial strain due to the loading is the major difference for creep for different panel sizes, it obeys the basic model of Hooke's law ($\sigma = E\varepsilon$). Creep is defined in ACI 209R-92 (ACI, 2008), *Predication of Creep, Shrinkage, and Temperature Effects in Concrete Structures*, as a constant stress under conditions of steady relative humidity and temperature, assuming the strain at loading (nominal elastic strain) as the instantaneous strain at any time. In wood Creep includes three distinct types of behaviour, which are difficult to separate because they can all operate simultaneously. These are time-dependent (viscoelastic) creep, mechano-sorptive (moisture-change) creep, and the pseudo-creep and recovery that have been ascribed to differential swelling and shrinkage (Hunt, 1999).

Creep-strain response for wood-based structure is viscoelastic, where represented by elastic spring and viscous dashpot. Viscous flow to ideal fluid requires rate of strain with respect to time

be proportional to the applied stress, obeying Newton's law, while plastic deformation is due irreversible changes of position, where strain does not change when the stress is removed.

$$\sigma \propto \frac{\boldsymbol{d\varepsilon}}{\boldsymbol{dt}} = \eta \frac{d\varepsilon}{dt} \tag{2.21}$$

$$\varepsilon = \frac{\boldsymbol{\sigma t}}{\eta} \tag{2.22}$$

Where E is the modulus of elasticity, σ is the stress, ε is the strain, η is viscosity and t is the time.

Rheological models (Wu, Q., 2009) are illustrated by Kelvin-Voigt (solid) and Maxwell (fluid). Maxwell body is a dashpot and spring in series, while Kelvin-Voigt body is a dashpot and spring in parallel. Maxwell and Kelvin-Voigt are special cases of Kelvin. Kelvin body is determined by Inverse Laplace Transform through the following relation, the two parameters K_e and η_v can be determined by the using of Marquart-Levenberg algorithm (Least Squares Regression) in connection with experimental data (Betten, 2008).

$$\varepsilon_b(t) = \frac{\sigma_o}{K_e}\left[1 - \exp\left(-t/\eta_v\right)\right] \tag{2.23}$$

Where σ is the stress, t is the time, K_e = E is the elastic modulus, η_v is the viscosity

For long-term creep, Maxwell model's dashpot strain will scale linearly, and by time the spring strain contributes less. Maxwell model is not well used to discuss the creep behaviour. Kelvin-Voigt model (Thomson, 1865; and Voigt, 1892) shortly called Kelvin consists of one linear spring (Hooke) and one linear dashpot (Newton), connected in parallel, also known as the three element model and the standard linear solid model (SLS) (Wineman and Rajagopal, 2001).

The model assumes full recovery after stress removing, due to the negative stress exerted by the spring. The model is limited and used for short term and primary creep deflection. The three element / parameter model is Kelvin body model in series with dashpot to study the effect of elastic, viscous flow and the retarded elastic. It is called Burger Model (Burgers, 1935). Fridley et al. (1992) developed the four element model to predict the effect of load and environment. It is the four element model with spring to enhance the model from linear to non-linear model. Figure 2.17 presents schematic diagrams of such models, while Table 2.1 summarizes the developed models and equations.

2.5 PREVIOUS EXPERIMENTAL WORK ON SIPs

Few authors conducted research work on the structural behavior related to sandwich panels. Among them, Liu and Zhao (2007) studied the effect of soft honeycomb core on the flexural vibration of sandwich panel using low order and high order shear deformation models. Aviles and Carlsson (2007) conducted experimental study of the in-plane compressive failure of sandwich panels consisting of glass/epoxy face sheets over a range of PVC foam cores, and a balsa wood core containing one or two circular or square interfacial debonds. In most specimens, failure occurred by local buckling of the debonded face sheet followed by rapid debond growth towards the panel edges, perpendicular to the applied load. Meyer-Piening (2006) dealt with the linear static and buckling analysis of an asymmetric square sandwich plate with orthotropic stiffness properties in the face layers. Gupta and Woldesenbet (2005) and Gupta et al. (2002) studied experimentally and theoretically the behavior of sandwich-structured composites containing syntactic foam as core material under three-point bending loading conditions. They presented a method of analysis for syntactic foams and the sandwich structures containing syntactic foam as core material. Olsson (2002) suggested an engineering method to predict the

impact response and damage of flat sandwich panels. The approach accounts for local core crushing, delamination and large face sheet deflections. Yoon et al. (2002) studied experimentally the non-linear behavior of sandwich panels made of thermoplastic foam core and carbon/epoxy fabric faces. The experimental data were compared with the predicted results from a proposed analytical method and the finite-element analysis. Tham et al. (1982) studied, using the finite-prism-strip modeling, the flexural and axial compressive behavior of the prefabricated architectural sandwich panels made of foam-in-place rigid urethane cores and light-gauge cold-formed metal facing. A similar study was recently conducted elsewhere but with plain concrete core (Hossain and Wright, 2004a,b).

The use of the terms long beam flexure and short beam flexure when addressing sandwich panel testing is very essential, as the former is used to determine face-sheet, i.e. the surface layers of the sandwich panel, properties and the latter to determine core shear properties. Such a distinction is logical since we know that, for a given applied loading, the flexural stresses (tensile and compressive) in the face-sheets increase as beam length increases, but the shear stresses in the core do not. That is, long beams produce high bending stresses while short span lengths do not. Most recently, Sennah et al. (2009, 2008) and Butt (2008) performed experimental studies on the static flexural and flexural-creep performance of SIPs for roofs and floors in residential construction. The experimental program included testing 52 panels of different thickness and span length under increasing static loading to-collapse. The results proved that the tested SIPs are as good as the conventional timber joist system specified in part 9 of the NBBC, with respect to strength and serviceability. Zarghooni (2009) studies the flexural creep of selected SIP sizes under sustained gravity loading. Mohamed (2009) texted few SIP

panels under compressive axial loading to develop design tables for the required served span of joists in single and two-storey residential construction. This research needs to be extended to permanent wood foundation made of SIPs.

2.6 PERMANENT WOOD FOUNDATION

The permanent wood foundation (PWF), shown in Fig. 1.7, is a complete wood frame foundation (load-bearing walls) for low-rise, residential, industrial, commercial and other types of buildings (CSA, 1997). All lumber and plywood in PWF is pressure treated with water-borne preservatives. Nails and straps must be corrosion resistant. The walls are designed to resist soil pressure loads in addition to the normal vertical loads from roofs, floors and top walls. Improved moisture control methods around and beneath the foundation result in comfortable, dry living space below grade. The foundation is placed on a granular drainage layer which extends 300 mm beyond the footings. Porous backfill is brought up to within 300 mm of finished grade and the remaining space filled with less permeable or native soil sloped away from the house. The porous drainage material directs ground water to below the basement, thus preventing hydrostatic pressure and leaks in the basement walls or floors. A sump is provided, in accordance with the building code, and is drained by mechanical or gravity means. No drainage (weeping) tile is needed around the footings as this may impede the flow of water. The granular drainage layer can accommodate a large influx of water during peak storm conditions. It also provides a large surface area for water to percolate into the subsoil. Caulking between all wall panels and between the walls and the footings, and a moisture barrier applied to the outside of the walls provide additional protection against moisture. The result is a dry basement that can be easily insulated and finished for maximum comfort and energy conservation. PWF has many

other advantages including (i) increased living space since drywall can be attached to the foundation wall studs, (ii) rapid construction, whether framed on site or prefabricated off-site, and (iii) buildable during winter times using minimal measures around the footings to protect them from freezing. CAN/CSA-S406, *Construction of Preserved Wood Foundations*, (CSA, 1992) allows the use of permanent wood foundation (PWF) which is referred to in Part 9 of the National Building Code of Canada (2005) and in provincial building codes. It describes the required materials and methods of construction of permanent wood foundations made of lumber studs. While more design information is available in the CSA book "Permanent Wood Foundation (CSA, 1997). Design information of PWF made of SIPs is as yet unavailable.

Clause 5.5.12 of CAN/CSA O86-2001 (CWC, 2001) specifies that PWF stud wall must be braced by the floor structure at the top and the bottom, with no surcharge at the ground level, as shown in Figures 1.7 and 1.8. Also it was specified that the stud wall has to satisfy the interaction equation

$$\frac{M_f + P_f \Delta}{M_f} + \left(\frac{P_f}{P_r}\right)^2 \leq 1.0 \qquad (2.24)$$

Where; M_f = maximum factored bending moment

$$M_f = \frac{w_f H^2}{6L}\left[L - H + \frac{2}{3}\sqrt{\frac{H^3}{3L}}\right] \qquad (2.25)$$

W_f = factored loading (N/mm)

= 1.5 x specified lateral soil pressure (kN/m^2) x stud spacing (m)

P_f = factored axial load on stud (kN)

P_r = factored compressive resistance parallel to grain taken from CWC Stud Wall Selection table (K_D = 1.0) (kN).

M_r = factored bending moment resistance taken from CWC Joist Selection Tables, and modified for permanent load duration (K_D = 0.65) (kN.m)

M_f = maximum factored moment due to lateral load, N.mm

Δ = deflection due to lateral load, mm

K_D = factor of 0.65 applies to the calculation of M_r and a K_D factor of 1.0 applies to the calculation of P_r.

a = variable length as shown in figure 5.9, equal to zero for slab floor system

H, L, x = variables shown in Figs. 1.7, 1.8 and 5.9.

The deflection used to estimate the secondary moment $P_f \Delta$ can be calculated by the following equation

$$\Delta = \frac{w_f (L-x)}{360\ EI\ LH} K_\Delta \tag{2.26}$$

Where

$$K_\Delta = [\ 10\ H^2(H-3a)(2L-x)x - 3(H-a)^5 + K_2] \tag{2.27}$$

$$K_2 = \frac{3L}{L-x}\ (H-a-x)^5 \qquad \text{when} \quad x \leq H\text{-}a \tag{2.28}$$

$K_2 = 0$ when $X > H\text{-}a$

$$x = H - \sqrt{\frac{H^3}{3L}} \tag{2.29}$$

$E_s I$ = bending stiffness taken from CWC Joist Selection Tables ($kN.m^2$)

L, H, x, a are variables shown in figures 1.7, 1.8 and 5.9

The PWF made of stud walls should have a maximum deflection under specified loads less than or equal to the deflection limit of span/300. This maximum deflection may be calculated using the given formula with x = 0.45L for triangular loading. Also, the PWF should

have a factored shear resistance, V_r, greater than or equal to the factored shear force, V_f, which can be calculated from the following equation.

$$V_f = \frac{w_f H}{2}\left[\frac{H}{3L} - \left(\frac{H-d}{H}\right)^2\right] \quad (2.30)$$

Where d = depth of stud (m)

H, L = variables shown in figures 1.7, and 1.8

w_f = factored loading (N/mm)

= 1.5 x specified lateral soil pressure (kN/m^2) x stud spacing (m)

The factored shear resistance, V_r, can be obtained from the CWC Joist Selection Table. The tabulated values must be modified for permanent load duration. Typically, the lateral loads on wood foundation wall are based on well-drained soil having an equivalent fluid pressure of 4.7 kN/m^2 per meter of depth, as permitted by the National Building Code of Canada (NBCC) for the average stable soils in Part 9 buildings. Where the lateral soil load is treated as a dead load.

2.7 US ACCEPTANCE CRITERIA FOR SANDWICH PANELS

International Code Council – Evaluation Service (ICC-ES) Acceptance Criteria (AC04) for Sandwich Panels requires that load-bearing shall support an axial loading applied on eccentricity of 1/6 of the panel thickness to the interior or towards the weaker facing material of an interior panel. ICC-ES states that the ultimate axial compressive load to be divided by a factor of safety (usually a factor of 3 is used) to determine the allowable axial load. The resultant normal stresses on the core and face do not have the same linear relationship, and found to be constant throughout each by the following equation.

$$\sigma_c = \frac{E_c.P}{A_c.E_c + A_f.E_f} \tag{2.31}$$

$$\sigma_f = \frac{E_f.P}{A_c.E_c + A_f.E_f} \tag{2.32}$$

Where A_c and A_f are the core area and the flange area, respectively, E_c and E_f are the modulus of elasticity of the foam and the faces, respectively.

The skin faces resist higher level of normal stress than the core (foam). That is why the skin faces fail due to axial compressive load. APA Plywood Design Specification Supplement 4 – *Design & Fabrication of Plywood Sandwich Panels*, (APA, 1990) specifies the following design equations.

The panel compression strength under axial loading must satisfy Equation 2.33, otherwise the strut becomes unstable when the axial thrust is equal to P_e.

$$P \leq P_e \text{ where } P_e = C_e \,.\, F_c \,.\, A_f \tag{2.33}$$

The eccentric load factor considering the minimum eccentricity equal to not less than t/6 ($e \geq t/6$)

$$C_e = \frac{1}{1 + \frac{e.y_c}{r^2}\sec\left[\frac{12L}{2r}\sqrt{\frac{3P}{A_f.E_b}}\right] + \frac{3\,P.e.y_c}{2A_v\,.G.I}} \tag{2.34}$$

The critical global buckling load for a pinned-pinned column under axial loading

$$P \leq P_{cr} \text{ where}$$

$$P_{cr} = \frac{\pi^2 E_b I}{3\,(12L)^2\left[1 + \frac{\pi^2 E_b I}{\frac{\pi^2 E_b I}{(12L)^2 A_v G}}\right]} \tag{2.35}$$

Where;

A_f = Area of face,

A_v = Shear Area of panel for symmetric panel,

C_e = Eccentric load factor,

E_b = SIP modulus of elasticity under transverse bending (psi),

F_c = Allowable facing compressive stress (psi),

G = SIP shear modulus (psi),

I = SIP moment of inertia (in^4/ft),

L = Span length (ft),

P = Applied axial or concentrated load (lb/ft),

P_{cr} = Allowable axial load (lb/ft),

r = radius of gyration (in),

y_c = Distance from centroid to the extreme compression fiber (in).

CHAPTER III

EXPERIMENTAL STUDY

3.1 GENARAL

The Structural insulated foam-timber panels (SIPs) are produced in standard sizes of 1.2 m wide and different lengths ranging from 2.43 to 4.90 m. SIPs can be used in used for many different applications, such as interior and exterior walls, roofs, floors, foundations, timber frame, additions, and renovations.

Thermapan SIPs (Thermapan, 2007) are composed of thick layer of expanded polystyrene insulation (EPS) board laminated between two sheets of oriented strand board (OSB), as shown in Figs. 3.1 and 3.2. The facing of these developed panels is made of two faces of Oriented Strand Board (OSB), 11 mm (7/16") thickness, holding a foam core for floor and wall construction. SIP floors and walls are installed by placing the panels side by side as shown in Fig. 3.3. The joint between the panels in the span direction can be a lumber-spline connection. In case of lumber-spline joint, a recess in formed along the longitudinal edges of the foam during manufacturing. After placing the panel over the wall, a sawn lumber is inserted in the recess along the panel length. Then, the adjacent panel slides over the sawn lumber, followed by nailing the OSB facings to the solid lumber.

The experimental research program aimed to develop a better understanding of the structural behaviour of these timber sandwich panels at service and ultimate loading conditions when they act as basement walls in residential construction. This chapter summarizes the

geometrical and material properties of the tested panels, the different setups for the tests, and the test procedure.

3.2 GEOMETERIC DESCRIPTION OF PANELS

The tested panels were divided into 5 groups based on the size of the panel and the test type. Table 3.1 summarize the geometric characteristics of the tested panels. All panels were manufactured for basement wall construction with 1.2 m wide. To allow for the construction of preserved wood foundation, the interior facing was made of 11 mm (7/16") OSB sheets, while the exterior facing exposed to soil was made of 15.5 mm (5/8") Canadian softwood plywood. The height of each panel in groups I, III and V was 3.048 m (10'), with a total thickness of 260.35 mm (10 ¼"). While the height of panels in groups II and IV was 2.743 m (9') with a total thickness of 209.35 mm (8 ¼"). For the sake of testing walls with lumber spline connection, a panel segment of 1200 mm width, with lumber spline connection at its mid-width as shown in Fig. 3.2, was considered in this study. In this panel, the sandwich core is made of two adjacent strips of expanded polystyrene foam 541 mm wide each with vertical preserved Spruce-Pine-Fur stud (lumber-spline) to connect the panel segments using nails. Such studs are made of 38x234 mm or 38x184 mm lumber for panel group I and group II, respectively. Two top preserved lumber plates and one bottom lumber plate, with same configuration as that used in the lumber spline connection, are mechanically connected using nails to the panel facings at their top and bottom ends to provide means for supporting elements on the top and bottom of the wall.

3.3 MATERIAL PROPERTIES

The interior face of SIPs used as permanent wood foundation as produced by Thermapan Inc. are oriented strand board (OSB) manufactured and grade stamped as per APA (1990). The OSB board fabricate panels had 1R24/2F16/W24 panel mark with 11 mm thickness construction sheathing. The material properties for OBS boards are specified as follows:

Modulus of elasticity: 800,000 psi (5515 MPa) in the span direction

225,000 psi (1551 MPa) in the direction normal to the span direction

Modulus of rupture: 4200 psi (28.955 MPa) in the span direction

1800 psi (12.409 MPa) in the direction normal to the span direction

However, material characteristics as specified in the OSB Design Manual (2004) for the 1R24/2F16/W24 panel are as follows:

Bending resistance, M_r = 228 N.mm/mm

Bending stiffness, EI = 730,000 $N.mm^2/mm$

Axial stiffness, EA = 38,000 N/mm

Axial tensile resistance, T_r = 57 N/mm

Axial compressive resistance, P_r = 67 N/mm

Shear through thickness resistance, V_r = 44 N/mm

Shear through thickness rigidity, G = 11,000 N/mm

To allow for the construction of preserved wood foundation the panel exterior facing exposed to soil was made of 15.5 mm (5/8") Canadian softwood plywood (CSP). CSP has 5 plies and demonstrates the following characteristics:

Bending resistance = 520 N.mm/mm if the applied force is in the direction of face grain

Bending resistance = 280 N.mm/mm if the applied force is normal to the direction of face grain

Bending stiffness, EI = 2000,000 $N.mm^2/mm$ if the applied force is in the direction of face grain

Bending stiffness, EI = 630,000 $N.mm^2/mm$ if applied force is normal to direction of face grain

Axial stiffness, EA = 71,000 N/mm if the applied force is in the direction of face grain

Axial stiffness, EA = 47,000 N/mm if the applied force is normal to the direction of face grain

Axial tensile resistance, T_r = 110 N/mm if the applied force is in the direction of face grain

Axial tensile resistance, T_r = 71 N/mm if the applied force is normal to direction of face grain

Axial tensile resistance, P_r = 120 N/mm if the applied force is in the direction of face grain

Axial tensile resistance, P_r = 79 N/mm if the applied force is normal to direction of face grain

Shear through thickness resistance, V_r = 38 N/mm

Shear through thickness rigidity, G = 7,100 N/mm

These values are based on dry service conditions and standard-term duration of load.

The expanded polystyrene (EPS) core type 1 has been used to fabricate the panels. The priority density demonstrates a load failure of 25 psi when tested as per ASTM C297. The expanded polystyrene (EPS) core material must meet the standard CAN/ULC-S701 and ASTM C578 Type 1 to demonstrate the following characteristics:

Nominal density	1.0 lbs/ft^3 (16 kg/m^3)
Flexural strength:	25 psi (172 kPa)
Tensile strength:	15 psi (103 kPa)
Compressive strength:	10 psi (70 kPa)
Shear strength:	12 psi (83 kPa)
Shear modulus:	400 psi (2758 kPa)

The off-white one-part polyurethane structural adhesive used to connect the foam to the facings proved to meet the following standards (Thermapan, 2007):

ICBO Acceptance Criteria for Sandwich Panel Adhesive (AC05)

ASTM D7446-09: Standard Specification for SIP Adhesives for Laminated OSB to Rigid Cellular Polystryne Thermal Insulation Core Materials

ANSI/APA PRS-610.1: Standard for Performance-Rated SIP in Wall Application

ASTM D-2294: 7 Day High Temperature Creep Test

ASTM C-297: Tension Test of Flat Sandwich Construction in a Flatwise Plane

ASTM D-1877: Resistance of Adhesive to Cyclic Laboratory Aging Conditions

ASTM D-905: Block Shear Test Using Plywood

ASTM D-1002: Strength Properties of Adhesive Bonds in Shear by Tension Loading

The used Spruce-Pine-Fur (S-P-F) lumber with grade number 2 has been used as lumber-spline connection in the core of the panel. Lumber grading and specification should be in accordance with the National Lumber Grading Authority (NLGA) standard grading rules for Canadian Lumber and identified by the grade stamp of an association or independent grading agency in accordance with the provisions of CSA Standard CAN/CSA-O141. The material properties for S-P-F are specified in CSA-O86.01 as follows:

Bending at extreme fibre, f_b = 11.8 MPa

Longitudinal shear, f_v = 1.0 MPa

Compression parallel to the grain, f_c = 11.5 MPa

Compression perpendicular to the grain, f_{cp} = 5.3 MPa

Tension parallel to the grain, f_t	= 5.5 MPa
Modulus of elasticity, E	= 9500 MPa
Shear modulus, G	= 0.065 E

For all panels, 2"x0.095" diameter, hot-dipped galvanized, gun nails at 8" spacing with ¾" minimum edge distance to connect the OSB sheet and plywood plate to the foam splines and limber splines. Also, this nail arrangement was used to connect the panel facings to the lumber studs at the top and bottom of the walls. The used nails are to conform to CAN/CSA B111 "Wire Nails, Spikes and Staples".

3.4 EXPERIMENTAL TEST METHODS

In 2007, the National Research Council Canada (NRC) prepared a technical guide (IRC, 2007) that describe the technical requirements and performance criteria for the assessment of stressed skin panels (with lumber 1200 mm o.c. and EPS core) for walls and roofs for the purpose of obtaining a CCMC (Canadian Construction Materials Commission) evaluation report. The requirements and criteria referenced in this guide were developed to evaluate the performance of stressed skin panels for walls and roofs with respect to their performance as an alternative solution established with respect to Part 4, Structural Design, and Part 9, Housing and Small Buildings, of the National Building Code of Canada (NBCC, 2005). The Technical Guide focuses on the structural qualification of stressed skin composite panels as being "as good as" the structural capacity of the conventional wood-frame buildings. A successful evaluation conforming to this Technical Guide will result in a published CCMC Evaluation Report that is applicable only to products bearing the proper identification number of CCMC's evaluation

number. This NRC/IRC/CCMC Technical Guide specifies test methods for SIPs similar to those specified in ASTM E72-02, *Standard Test Methods for Conducting Strength Tests of Panels for Building Construction*, (ASTM, 2002) as well as ICC AC04, *Acceptance Criteria for Sandwich Panels*, (2004). It should be noted that ICC AC04 acceptance criteria is based on ASTM E72 standard test methods. As such, bending qualification tests on the panels were conducted in accordance with the method described in the ASTM E72-02, *Transverse Load Test*. ASTM E72-02 specifies at least three identical specimens for each test. This condition is reflected in the tested panel groups shown in Table 3.1.

The structural behavior of structural insulated panels considered in this study for permanent wood foundation was examined under sustained loading simulating soil pressure. Also, such panels were examined under increasing axial compressive loading to-collapse. To gather enough research information for the analysis of the walls under combined axial and compressive loading, selected wall group V of 3.048 m height was considered to be tested under flexural loading. This is because research data on the flexural behavior of wall group IV of height 2.743 m was available elsewhere (Mohamed, 2009). The following subsections describe the test procedure and the structural qualification criteria for each test.

3.4.1 Long Term Creep Test

Flexure-creep is defined as deflection under constant load over period of time beyond the initial deformation due to the application of the load. ASTM C 480-62, *Standard Test Methods of for Flexural Creep of Sandwich Construction*, (1988) covers the determination of the creep rate of sandwich panels under constant flexural load. In case of flexural loading of floors and roofs, a

typical setup for this test consists of a simply-supported panel loaded by uniformly distributed loads along the panel. Thus, the SIPs are subjected to one-dimensional flexure thereby minimizing the influence of transverse stiffness on the study results. Specified flexure-creep load is applied and mid-span instantaneous deflection is recorded using dial gauges. The averaged measured mid-span deflection readings can then be used to develop the average deflection-time history for each tested specimen. Figure 3.14 schematically defines the immediate deflection (Δ_0) as the deflection at time t = 0 immediately after the application of the load. The final deflection Δ_f is defined as the deflection immediately before the removal of the load at the end of the test period. Figure 3.14 shows the definitions of critical points in deflection-time relationship for a typical creep curve as follows:

Δ_0 = immediate deflection after application of full load

Δ_i = Deflection at time t_i

Δ_f = Final deflection before removal of the sustained load

Δ_u = Deflection immediately after removal of load (unload)

Δ_{u24} = Deflection 24hours after removal of load

Δ_{u48} = Deflection 48 hours after removal of load

In case of test method for long-term creep of SIPs, the 2007 NRC/CCMC Technical Guide specified at least three panels to be tested to evaluate the design. Zarghooni (2009) used this guide to conduct long-term creep tests on selected SIP specimens under sustained flexural loading for floor and roof construction. He applied a 0.5 kPa dead load simulating the weight of superimposed finished roofing and ceiling materials, in addition to a live load of 1.9 kPa similar to the floor live load in residential construction.

In case of permanent wood foundation, shown in Fig. 1.8, the wall is subjected to a permanent soil pressure that would develop increasing lateral deflection on the wall with time. To determine the increase on wall lateral deflection due to creep effect, a typical setup for the flexural creep testing of simply-supported basement wall panel was designed to sustain a triangular loading. This triangular loading simulates the lateral soil pressure which is specified as an equivalent fluid pressure equal to 4.7 kN/m^2 per meter of wall depth as per National Building Code of Canada NBCC Article 9.15.2.4 for average stable soils (NBCC, 2005, CWC, 2005).

Two sets of panel sizes were considered in this testing with 3.048 and 2.74 m, respectively. Three identical panels of 1.22 m width for each group; BW1, BW2 and BW3 for the first group and BW4, BW5 and BW6 for the second group. Figure 3.6 shows a schematic diagram of one of these panels before loading. The panel was supported over two steel rollers of 25.4 mm diameter and 1220 mm length, with a 1220×150×12 mm steel plate between each supporting roller and the specimen. Also, similar steel plates were inserted between the steel rollers and 150 x150 x 13 HSS steel box beam that is in turn supported over two concrete cylinders of 150 mm diameter and 300 mm length. Figure 3.13 shows view of this steel support assembly.

Solid concrete bricks of 6.44 lbs and 200x100x60 mm side dimensions were used to apply triangular loading over the SIP specimens. Bricks were arranged in several layers and incremental piles to produce the intended soil pressure of 4.7 kN/m^2/m depth of wall. As such, panel group I of 3.048 m height was loaded with bricks of 20,563.20 N total weight (where w =

0.5x4.7x2.7^{2}x1.2 in kN/panel width) in a pattern shown in Fig. 3.4. While panel group II of 2.74 m height was loaded with bricks of 16,243.00 N total weight (where w = 0.5x4.7x2.4^{2}x1.2 in kN/panel width) as shown in Fig. 3.5. It should be noted that the length of the triangular loading was taken as 2700 mm for panel group I and 2400 mm for panel group II, leaving 300 mm length unloaded. This unloaded length represents the wall height between the ground level and the first floor level as indicated in Fig. 1.8. Figures 3.7 through 3.12 show views of the triangular loading over the tested panels.

Analogue dial indicators were placed at the maximum bending moment location which was calculated to be at 0.45 of the panel span. Figure 3.13 shows view of a tested specimen with the dial indicators located near the mid-span location. After taking initial readings, each panel was loaded with solid concrete blocks. Then, dial reading was recorded after 5 minutes of applying the loading. Then, deal readings were recorded every 30 minutes for 6 hours, followed by recording readings every day for 30 days and finally once per week till unloading time. Then, each panel was unloaded. After unloading, dial gauge reading was recorded for 48 hours. Also Humidity-Temperature sensors were placed near the panels and both humidity and temperature readings were recorded parallel to dial gauge readings.

3.4.2 Test method for SIP Panels under Axial Compressive Loading

The objective of this set of testing is to provide the experimental ultimate axial load that can be carried by the wall for further analysis of the wall under combined axial and lateral loading. For the purpose of structural qualifications of SIPs, the NRC/IRC/CCMC Technical Guide specifies test methods for SIPs which is similar to those specified in ASTM E72-02,

Standard Test Methods for Conducting Strength Tests of Panels for Building Construction, (ASTM, 2002) as well as ICC-ES AC04, *Acceptance Criteria for Sandwich Panels*, (2004). The ICC AC04 acceptance criteria are based on ASTM E72 standard test methods. The 2008 ANSI/APA PRS-610.1, *Standard for Performance-Rated Structural Insulated Panels in Wall Applications*, published by *APA–The Engineered Wood Association* in USA, provides similar structural qualification procedure and criteria for the performance-rated SIPs to those in ASTM E72-02 and ASTM E 1803-06, *Test Methods for Determining Structural Capacities of Insulated Panels*. ASTM E72-02 specifies at least three identical specimens for each test group. As such, Groups III and IV have been selected for tests under axial compressive loading for permanent wood foundation as shown in Table 3.1. It should be noted that panels in groups III and IV are those listed in groups I and II but after conducting the long-term flexural creep testing.

3.4.2.1 Axial Compressive Load Test setup

AC04 specifies that load bearing wall panels shall support an axial loading applied with an eccentricity on one-sixth the panel thickness to the interior or towards the weaker facing material of an interior panel. The test setup shall be capable of accommodating rotation of the test panel at the top of the wall due to out-of-plane deflection with the load applied throughout the duration of the test with the required eccentricity. AC04 also specifies that the test panel shall have wall sill and cap plate details with connections matching the proposed field installations. Axial loads shall be applied uniformly or at the anticipated spacing of the floor or roof framing. Figure 3.15 shows a schematic diagram of the proposed hinged-fixed condition of the wall imposed during testing. It should be noted that the wall was resting directly over the laboratory floor similar to the field condition. This type of end connection is assumed fixed (not allowed to

rotate), however, it is believed that it will behave as partially-fixed joint since physical means for complete fixed connection did not exist.

To prepare for the test, the wall panel aligned vertically and supported directly over the laboratory's floor or over an elevated precast concrete slab units. A uniformly distributed line load was applied on the top side over the 1220 mm width using a loading assembly. This loading assembly was composed of a 1220×350×12 mm steel base plate resting over the top side of the panel. A 125×125×12.7 mm HSS box beam of length 1220 mm was welded to the top side of the steel base plate to transfer the applied jacking load over the panel width. Two 70×70×9 mm steel angles of 1220 mm length were welded to the steel base plate, one on each side of the wall panel to stabilize the loading assembly during the test. The weight of the loading assembly was calculated as 1.25 kN. Figure 3.16 and 3.17 show schematic diagrams of the elevation and side view of the test setup for axial loading. In addition, Fig. 3.17 shows a schematics diagram of the loading assembly for the t/6 eccentric compressive loading, where t is the total thickness of the wall. Figure 3.18 shows view of the tested walls before testing, while Fig. 3.19 shows view of the top loading assembly on top of the wall.

3.4.2.2 Instrumentation for Axial Compressive Load Test

Two Linear Variable Displacement Transducers (LVDTs) were used to measure horizontal displacement at the mid-height of the panel as shown in Fig. 3.18. Each LVDT was located at 300 mm from the vertical free edge of the wall panels. Four potentiometers (POTs) were installed vertically over the four corners on the top side of the panels as shown in Fig. 3.19 to record axial shortening of the wall panel under load. The compressive load was applied

through a jacking load system with a universal flat load cell of 222 kN (50,000 Ib) capacity to measure the jacking load. During testing, the process for collecting and converting data captured by the LVDTs, POTs and load cell were done using a test control software (TCS) with SYSTEM 5000 data acquisition unit which was adjusted to sample the data at rate of 10 reading per second during the test. Figure 3.20 shows view of the data acquisition system and the pump used in the testing.

3.4.2.3 Axial Compression Load Test Procedure

ASTM E72 specifies that wall panels shall be loaded in increments to failure with deflections taken to obtain deflections and set characteristics. The test set-up was prepared for each test which included installing the POTs and LVDTs at the predetermined locations. For each panel, the jacking load was continuously at a slow rate. Visual inspection was continuously conducted during the test record any change in the structural integrity of the wall panel. Each test was terminated after the wall panel failure. Failure of the panel was considered when the recorded jacking load was not increasing or when the panel could not absorb more loads while recorded axial shortening was increasing by continuously pressing the pump handle. Mode of failure was recorded and test data was then used to draw the load-deflection and load-axial shortening relationships for each panel.

3.4.3 Test method for SIP Panels under Flexural Load

As it was mentioned earlier, the objective of this test was to establish the factored design flexural capacity of selected wall panels that would further be uses with the obtained factored design axial compressive load to apply the axial load-moment interaction equation for design.

This would determine either the factored axial load or factored bending moment that can safely be applied on the wall panels. Bending qualification tests on the panels were conducted as specified in the method described in the ASTM E72-02, *Transverse Load Test.* ASTM E72-02 specifies at least three identical specimens for each test group. To gather enough research information for the analysis of the walls under combined axial and compressive loading, selected wall group V of 3.048 m height was considered to be tested under flexural loading. This is because research data on the flexural behavior of wall group IV of height 2.743 m was available elsewhere (Mohamed, 2009).

3.4.3.1 Flexure Load Test setup

Each tested panel was supported over two 25.4 mm steel rollers at each side in the short direction. 1200×150×12 mm steel plates were inserted between the steel rollers and the supporting steel pedestal resting on the laboratory strong floor. Other similar-size steel plates were inserted between the supporting roller and the panel bottom facing. A 150×150×12.7 mm HSS beam of 2400 mm length used to transfer the applied jacking load to a 102×1020×6.4 mm HSS beam that was laid transversally over the top panel facing at the quarter points to spread the load over the panel width. Steel roller and plate assembly similar to that used to support the panel over the steel pedestals was used to support the 2400 mm length HSS beam over the two 1220 mm length HSS spread beams at the quarter points. The weight of this loading system is 2.0 kN. Figure 3.21 shows a schematic diagram of the test setup, while Fig. 3.22 shows view of the test setup of specimen BW4 before testing. Figure 3.23 shows views of the bearing plate assembly to transfer the applied load to the supporting elements.

3.4.3.2 Instrumentation for the Flexure Load Test

Mid-span deflection was measured using 4 Linear Variable Displacement Transducers (LVDTs). Two LVDTs were located at 25 mm from the panel free edges and other two LVDTs located at the third points of the panel width. The load was applied through a jacking load system with a universal flat load cell of 222 kN (50,000 Ib) capacity. During each test, the process for collecting and converting data captured by the LVDTs and load cell was done using a test control software (TCS) with a SYSTEM 5000 data acquisition unit which was adjusted to sample the data at rate of 10 reading per second during the loading test.

3.4.3.3 Flexure Load Test Procedure

Flexural tests were performed in the structures laboratory of Ryerson University. The test set-up was prepared for each test as explained earlier. For each panel, jacking load was applied in increments so that visual inspection could be performed to record any change in structural integrity of the sandwich panel. The tests were terminated after panel failure when the jacking load was not increasing while panel deflection was increasing by continuous pressing of the pump handle. At that stage, failure mode was observed and test data was then used to draw the load-deflection relationships for each panel.

CHAPTER IV

EXPERIMENTAL RESULTS

4.1 GENARAL

This chapter presents the experimental results of the tested panels for (i) long-term creep behavior, (ii) flexural behaviour and ultimate load carrying capacity, and (iii) axial compression behaviour. Structural qualification criteria for tested panels as set forth by test methods, codes and standards are discussed. These experimental findings will be used further in Chapter V to develop theoretical creep model to predict the long-term deflection of the basement along the life time of the building.

4.2. CODE REQUIREMENTS FOR THE STRUCTURAL QUALIFICATIONS OF THE PWFs

The Structural qualifications of the SIPs have been assessed based on:

1- The general design principles provided in CSA Standard CAN/CSA-O86.01, *Engineering Design of Wood*;

2- The evaluation criteria set forth in the NRC/CCMC Technical Guide which focuses on SIPs as being "as good as" the conventional wood-frame buildings with respect to strength and serviceability; and

3- CSA Standard CAN/CSA-S406-92, *Construction of Preserved Wood Foundations*, (1992) and the *National Building Code of Canada* (NBCC 2005).

Based on NBCC and CAN/CSA-S406, the following loads and load factors can be used to examine the structural adequacy of the panels for serviceability and ultimate limit states design:

Dead load factor = 1.25

Live load factor = 1.50

Dead load for roofs = 0.5 kPa

Dead load for floors = 0.47 kPa

Wall (with siding) = 0.32 kPa

Wall (with masonry veneer) = 1.94 kPa

Foundation wall = 0.27 kPa

Partitions = 0.20 kPa

The intensity of the triangular lateral soil pressure = 4.7 $kN/m^2/m.depth$

Live load for residential construction = 1.9 kPa

Snow load for residential construction = 1.9 kPa (for simplification of comparison in this thesis)

Deflection limit for serviceability (live load effect) = span / 180.

In case of roofs and floors, the deflection limit of span/360 is a serviceability limit condition which may be waived in case of industrial buildings, with span/180 as live load deflection limit when no roof ceiling is provided and with span/240 when ceilings other than plaster or gypsum are used (NBCC Part 9, 2005). The deflection limit of span/360 is intended to limit floor vibration and to avoid damage to structural elements or attached nonstructural elements. CAN/CSA-O86.01 specifies a span/180 deflection limit for wind columns and in case of floor and roofs subjected to total load (i.e. dead load + live load). In case of basement wall, the

soil pressure exists as long as the building exists. As such, the soil pressure can be considered as permanent load and the span/300 for wall deflection limit for total loads can be used to evaluate the serviceability limit state of such walls.

It should be noted that the specified snow load in buildings can be calculated using the following equation (NBCC, 2005).

$$S = I_s [C_b . S_s + S_r] \quad (4.1)$$

Where S is the specified snow load, C_b is the basic snow load of 0.6, S_s is the 1-in-50 year ground snow load in kPa, and S_r is the associated 1-in-50 year rain load in kPa. In addition, NBCC specifies that no case shall the specified snow load be less than 1 kPa. The building importance factor, I_s, is based on the building use and occupancy as stated in NBCC Table 4.1.6.2. In case of normal buildings, I_s is taken as 1.0 for ultimate limit state design and 0.9 for serviceability limit state design.

To determine the maximum load effect on building walls, NBCC specifies the following load combination scenarios using specified dead , snow, live and wind loads.

Load Case 1 $1.4 \times D$ (4.2)

Load Case 2 $1.25 \times D + 1.5 \times S + 0.5 \times L$ (4.3)

Load Case 3 $1.25 \times D + 0.5 \times S + 1.5 \times L$ (4.4)

Table 4.1 summarises these load combinations as set forth in NBCC. The superimposed earth pressure shall be increased to 1.5, except when the soil depth exceeds 1.2 m. In this case, the factor may be reduced to (1 + 0.6/h), but not less than 1.25, where h is the depth of soil, in meters, supported by the basement wall.

In case of wall design based on experimental findings, the deflection and ultimate load carrying capacity of each panel group are basically the average of those for the three panels in each panel group as per the acceptance criteria for SIPs set forth in ICC-ES AC04 (2004). The acceptance criteria states that of the results of one of the tested panel vary more than 15% from the average values of the three panels, one of the following two actions can be chosen: (i) the lowest test value may be used; or (ii) the average result based on a minimum of five tests may be used regardless of the variations. Moreover, the results from two tests could be used when the higher value does not exceed the lower value by more than 5% and the lower value is used with the required factors of safety. Factor of safety for ultimate load carrying capacity of SIPs is dependent on the followings: (i) consistency of materials, (ii) the range of test results, and (iii) the load-deformation characteristics of the panel. AC04 generally applies a factor of safety of 3 to the ultimate load based on the average of three tests which called in this research as panel group. However, for the case of the tested panels in this research, AC04 provides the following factors of safety applicable to uniform transverse loads:

F.S. = 3.0 for ultimate load at shear failure for all loading conditions.

F.S. = 2.5 for ultimate reaction at failure for all loading conditions

F.S. = 2.5 for ultimate load determined by bending (facing buckling) failure under allowable snow loads.

F.S. = 2 for ultimate load determined by bending (facing buckling) failure under allowable live loads up to 0.958 kPa (20 Lb per square foot).

In contrast to the factor of safety measure, shown in Eq. 4.5, the Margin of Safety (M.S., shown in Eq. 4.6) is other verification measure on which positive margin greater than or equal to zero satisfies the design requirement.

Factory of safety (F.S.) = Material Strength / Design load (4.5)

The Margin of safety (M.S.) = Failure Load / Design Load – 1 (4.6)

APA- The Engineered Wood Association specifies the general wall-unity equation, Equations 4.7, to check the compression-bending interaction in walls. It takes into effect the eccentric axial load and the transverse (bending) load obtained from the soil earth pressure for the panel to determine the design suitability at the allowable stress level. However, for Preserved Wood Foundation, CSA O86 specifies Equation 4.8 for compression-bending interaction at the ultimate limit states design. It states that the resistance to combined bending and axial load shall satisfy the appropriate interaction equation.

$$\frac{\textbf{Design Axial Load}}{\textbf{Allowable Axial Load}} + \frac{\textbf{Design Transverse Load}}{\textbf{Allowable Transverse Load}} \leq \mathbf{1} \quad (4.7)$$

$$\left(\frac{P_f}{P_r}\right)^2 + \frac{M_f + P_f\Delta}{M_f} \leq 1.0 \quad (4.8)$$

Equation 4.8 takes into account the transvers loads created from the transverse lateral load, its deflection, and the applied factored compressive force, P_f, taken at $\Delta = t/6$ where t is the total thickness of the wall. However, soil pressure causes transverse (flexural) deformation of the wall once backfill is added on the back of the wall. This transverse deflection increases with time due to such sustained load. As such, an additional applied factored moment would apply on the wall resulting from the multiplication of the applied factored compressive force and the long-term

creep deflection of the wall due to sustained soil pressure. This long term deflection can be determined by calculating the relative creep constant, C_t.

Relative creep, as shown in Equation 4.9, is the measuring unit for change in compliance during the test expressed in terms of the original compliance (BS, 1999; Dinwoodie, 2000).

$$\text{Relative Creep } (C_t) = \frac{\text{Deflection (t)} - \text{Initial Deflection } (t_o)}{\text{Initial Deflection } (t_o)} \text{ x } 100\% \qquad (4.9)$$

It should be noted that the direction for wall transverse deflection due the t/6 eccentricity of the gravity load is in opposite direction to that produced by soil pressure. As such, the net deflection should be used in Equation 4.8.

In case of wall panel axial load tests, AC04 specifies that wall panels shall support an axial loading applied with an eccentricity of 1/6 the panel thickness. Also, AC04 specifies that the factored design resisting axial load is determined from the experimental axial load at a net axial deformation of 3.18 mm (1/8") or the ultimate load divided by a factor of safety determined in accordance with those specified for transverse load testing mentioned above, whichever is lower.

4.3 LONG TERM CREEP RESULTS

4.3.1 Code Requirements for Long-term Creep Tests of SIPs

To determine the increase on wall lateral deflection due to creep effect, a typical setup for the flexural creep testing of simply-supported basement wall panel was designed to sustain a triangular loading as presented in Chapter III. This triangular loading simulates the lateral soil pressure which is specified as an equivalent fluid pressure equal to 4.7 kN/m^2 per meter of wall

depth as per NBCC Article 9.15.2.4 for average stable soils (NBCC 2005; CWC, 2005). To check for serviceability limit-state design criteria, Canadian Standard CSA/CAN O86.01, Clause A5.5.12.2, specifies that (i) studs for exterior foundation walls may be designed as members subjected to combined bending and axial compressive loading; and (ii) deflection due to lateral and axial loads should not exceed 1/300 of the unsupported height of the stud.

4.3.2 Instantaneous deflection results

The instantaneous deflections of the panels just after loading them with the triangular pressure were recorded. Table 4.2 summarizes these deflection values for each loaded panel. Results show the instantaneous deflections were 7.69, 8.023 and 8.39 mm for panels BW1, BW2 and BW3, respectively, for panel Group I. However, these values were 8.14, 7.24 and 8.715 mm for panels BW4, BW5 and BW6, respectively, for panel Group II. It can be observed that the deflection value for each panel is within 15% of the average deflection. As such, the deflection of each panel group was simply taken as the average of the deflection values of the three panels in each group. This resulted in wall short term deflection-to-span ratios as 1/379 and 1/341 for groups I and II, respectively. Those ratios are observed to be smaller than the deflection limit of span/300 specified in CAN/CSA-O86.01. As such the tested SIPs are qualified with respect to serviceability limit states requirements. It should be noted that in practice, the net instantaneous deflection of the wall is the difference between the lateral deflection due to soil pressure and the wall deflection to the t/6 gravity load eccentricity mentioned earlier in this chapter. This would make the deflection qualifications of SIPS more conservative compared to the limiting deflection value.

4.3.3 Temperature and Relative Humidity

Wood is anisotropic and hygroscopic organic material. It has three structural directions, namely: the radial, the tangential, and the longitudinal directions. It adsorbs and loss moisture from the surrounding air to be in equilibrium with the surrounding environment. The gain and loss of moisture content affect the increase and decrease of the creep rate for the studied panels as shown in the schematic diagram in Fig. 2.16. In addition to panel deflection, both the room temperature and relative humidity were recorded for each panel over time. It should be noted that panels BW1, BW2, BW4 and BW5 were at the same environment in the basement of the structures lab, while panels BW3 and BW6 were located in the same basement but in other spot separated by concrete wall from other locations. Figures 4.1 and 4.2 depict the change in the room temperature and relative humidity during creep test for such panels. It can be observed that the room temperature was between 22ºC and 25 ºC, while the relative humidity ranged between 20 to 70%. The increase in deflection with time for the tested panel groups I and II is shown in Figs. 4.3 and 4.4, respectively. It can be observed that the long-term creep deflection did not increase smoothly with time due to the cyclic change in temperature and relative humidity over time as will be discussed in Chapter 5.

4.3.4 Long term deflection results for SIP Group I

Three identical panels, BW1, BW2 and BW3 of 3.048 m length were tested for long-term creep performance over a period of 8 months. Chapter III discussed the test setup and test procedures for such panels. Figures 4.3a, 4.3b and 4.3c depict the deflection-time history for panels BW1, BW2 and BW3, respectively. Due to the triangular shape of soil pressure deflection was recorded at 0.45 of the panel span, as the expected location of the maximum deflection.

Figure 4.3a shows that the Instantaneous deflection (ID) for specimen BW1 was 7.69 mm, while the long-term maximum deflection (MD) after 241 days (5788 hours) was 10.995 mm, an increase of about 43%. After removing the triangular load, panel deflection was recorded over two days to determine the recovery deflection. Figure 4.3a shows that the Instantaneous recovery deflection (IRD) was 7.42 mm after removing the sustained loading, while permanent deflection (PD) was 2.73 after 48 hours from removing of sustained loading. This entails a 64.5% final creep recovery within 2 days of unloading.

Similar results were observed for panel BW2 as shown in Fig. 4.3b. It can be observed that the Instantaneous deflection was 8.02 mm, while the maximum deflection after 241 days was 11.28 mm, an increase of about 41%. It can also be observed the Instantaneous recovery deflection was 6.51 mm after removing the sustained loading, while the permanent deflection was 4.45 after 48 hours from removing of the sustained loading. This leads to a final creep recovery of 44.5% after 2 days of unloading. In case of specimen BW3, Fig. 4.3c shows that the Instantaneous deflection was 8.39 mm, while the maximum deflection after 241 days was 11.08 mm, an increase of about 32.1%. It can also be observed the iinstantaneous recovery deflection was 7.86 mm after removing the sustained loading, while the permanent deflection was 2.615 after 48 hours from removing of sustained loading. This makes the final creep recovery 68.8% to the measured deflection just before unloading. Figure 4.3d shows the deflection-time history for all tested identical panels in Group I for the sake of comparison.

Table 4.3 summarizes the deflection results obtained from the creep tests. It should be noted that the long term deflections values were within 15% of the average deflection value for

Group I. As such, the average deflection will be used further to determine the relative creep coefficient for ultimate limit state design. In general creep-deflection for group I can be summarized into ID of 8.03 mm, MD of 11.12 mm, relative creep of 38.6%.

4.3.5 Long term deflection results for SIP Group II

Three identical panels, BW4, BW5 and BW6 of 2.74 m length, were tested for long-term creep performance over a period of 8 months. Chapter III discussed the test setup and test procedures. Figures 4.4a, 4.4b and 4.4c show the deflection-time history recorded at 0.45 of the span length of specimens BW4, BW5 and BW6, respectively. It can be observed that the instantaneous deflection (ID) for panel BW4 was 8.140 mm, while the maximum deflection (MD) after 241 days (5788 hours) was 11.35 mm, an increase of about 39%. It can also be observed the Instantaneous recovery deflection (IRD) was 7.71 mm after removing the sustained loading, while permanent deflection (PD) was 3.31 after 48 hours from removing of sustained loading. This leads a final creep recovery of 59.3% after 2 days of unloading. For panel BW5, the instantaneous deflection was 7.24 mm, while the maximum deflection after 241 days was 10.02 mm, an increase of about 38%. It can also be observed the Instantaneous recovery deflection was 7.01 mm after removing the sustained loading, while permanent deflection was 2.34 after 48 hours from removing of sustained loading, leading to a final creep recovery of 67.7%. In case of panel BW6, the Instantaneous deflection was 8.72 mm, while the maximum deflection after 241 days was 11.12 mm, an increase of about 28%. It can also be observed the iinstantaneous recovery deflection was 8.31mm after removing the sustained loading, while permanent deflection was 2.14 after 48 hours from removing of sustained loading, leading to a final creep recovery of 75.5% to the original deflection.

Figure 4.3d shows the deflection-time history for all tested identical panels in Group I for the sake of comparison.

Figure 4.4d combined the deflection-time history of the tested panels, while Table 4.3 summarizes the deflection results obtained from the creep tests. It should be noted that the long term deflections values were within 15% of the average deflection value for Group I. As such, the average deflection will be used further to determine the relative creep coefficient for ultimate limit state design. Results for Group II show that the ID is 8.03 mm, the MD is 10.83 mm, and the relative creep is 35%.

4.4. RESULTS FROM ECCENTRIC COMPRESSION TESTS

4.4.1 General

After conducting the flexural creep tests on panel Groups I and II, these panels were further tested to-complete-collapse under eccentric axial compression with the applied load centred at t/6 from the panel centre line from the OSB side. These panels are designated Groups III and IV in the test matrix shown in Table 3.1. Discussions of the experimental results of such panels are presented in the following section.

4.4.2 Code Requirements for the eccentric compression test of SIPs

The acceptance criteria for SIPs as permanent wood foundation as set forth in ICC-ES AC04 (2009) is to test three identical panels from each size. Load-bearing wall panels shall support an axial loading applied with an eccentricity (off-centre) of one-sixth the panel thickness

(e = t/6) to the interior face of the wall. The test setup shall be capable of accommodating rotation of the test specimen at the top of the wall due to out-of-plane deflection with the load applied throughout the duration of the test with the required eccentricity.

AC04 specifies that the allowable axial load is determined from the axial load at a net axial deformation of 3.18 mm (0.125 inch) or the ultimate load divided by a factor of safety determined in accordance with AC04 Section 4.2.4, whichever is lower. In addition, loads transferred by fasteners shall not exceed established fastener values.

4.4.3 Results for the SIP panel Group III of 3.048 m height

Three identical panels forming Group III were tested to-complete-collapse under eccentric compressive loading. Each panel was 260.3 mm thickness, 1220 mm width and 3048 mm length. Figures 4.5 and 4.6 shows views of panel BW1 before and after loading. Figures 4.7 and 4.8 show that failure occurred due to crushing of OSB face at about 200 mm from the top of the panel. In addition, delamination of the OSB-foam interface at that location occurred. With respect to panel BW2, Figures 4.9 presents views of the tested panel before loading. While Figs. 4.10 through 4.13 depict panel deformation failure mode after testing. It can be observed that the panel deformed in flexure towards the OSB side. This led to fracture of the lumber-spline as well as the OSB facing near the mid-height of the panel. Also, it led to delamination at the OSB-foam interface between the panel footer and mid-height of the panel. Figure 4.11 shows complete separation of plywood face and foam from the OSB facing and the bottom plate footer. Panel BW3 failed in very similar fashion to panel BW1. Figures 4.14 and 4.15 show views of the tested panel before and after loading. Figure 4.16 show close-up view of the failure mode which is

crushing at in the OSB facing at about 200 mm from the top of the panel. Table 4.4 summarizes the recorded failure mode for each tested panel.

Figures 4.36, 4.37 and 4.38 depict the axial load-axial displacement history for panels BW1, BW2, and BW3, respectively. Given the general linear shape of such relationship between the applied load and corresponding axial shortening of the wall, it can be concluded that the failure was sudden, as observed during testing. Results show that the ultimate jacking load was 291.46, 341.83, 285.47 kN for panels BW1, BW2, BW3, respectively. It can be observed that the ultimate jacking load for panel BW2 is more than 15% difference with the average jacking load of the three panels, and per AC04, since the results vary more than 15% from the average of the three, the lower value is used as 285.47 kN, as presented in Table 4.5. Table 4.5 summarizes also the maximum axial and lateral displacement of each panel at failure. It shows that the average vertical displacement was 22.655, 34.85, and 23.255 mm, while the average lateral displacement was 4.665, 4.525, and 9.13 mm for the BW1, BW2 and BW3 respectively. It should be noted that Table 4.5 shows the axial load test results per panel width without including the weight of the loading system of 2 kN. Figure 4.42 shows the axial load-average axial displacement relationships for panels BW1, BW2 and BW3 for the sake of comparison. Also, Figs. 4.44, 4.45 and 4.46 depict the relationship between the applied gravity load and the associated lateral deflection of the wall at its mid-height for panels BW1, BW2 and BW3, respectively. No general trend is observed given the fact that the failure mode is somewhat different from one panel to the other as depicted from the combined Fig. 4.50 for the tested panels in Group III.

.

4.4.4 Results for the SIP panel Group IV of 2.74 m height

Group IV, made of three identical panels BW4, BW5 and BW6, were tested to-complete-collapse under eccentric compressive loading. Each panel was of 209.55 mm, 1220 mm width and 2743.2 mm length. Figures 4.17 and 4.18 show views of the tested panels before and after loading. Close-up views of the failure mode are presented in Fig. 4.19. The panel showed general flexural deformation before failure that was mainly due to OSB-foam delamination along more than two-third of the panel height starting from the bottom plate footer. Crushing of OSB facing at the junction with the bottom plate footer was observed as depicted in Fig. 4.19. With respect to panel BW5, Fig. 4.20 shows views of the panel before loadings. Close-up of the failure mode is shown in Fig. 4.21 which was due to OSB crushing at about 50 mm from the top of the panel. Figures 4.22 and 4.23 show views of panel BW6 before and after loading. While Fig. 4.24 shows close-up view for failure mode which was crushing of OSB face at the about 200 and 400 mm from the top of the wall, accompanied by OSB wrinkling. Table 4.4 summarizes the recorded failure mode for each tested panel.

Figures 4.39, 4.40 and 4.41 show that the ultimate jacking load was 173.69, 182.86 and 292.94 kN for panels BW4, BW5, BW6, respectively. It can be observed that the ultimate jacking load for panel BW6 is more than 15% difference with the average jacking load of the three panels, of the three panels, and per AC04, since the results vary more than 15% from the average of the three, the lower value is used as 173.69 kN, as presented in Table 4.5. Figure 4.43 shows the axial load-average axial displacement relationships for panels BW4, BW5 and BW6 for the sake of comparison. Table 4.5 summarizes also the maximum axial and lateral displacement of each panel at failure. It shows that the average vertical displacement was 20.33,

33.735, and 22.285 mm, while the average lateral displacement was 10.33, 13.45 and 10.74 mm for the BW4, BW5 and BW6 respectively. It should be noted that Table 4.5 shows the axial load test results per panel width without including the weight of the loading system of 2 kN. Figures 4.47, 4.48 and 4.49 depict the relationship between the applied gravity load and the associated lateral deflection of the wall at its mid-height for panels BW4, BW5 and BW6, respectively. No general trend is observed given the fact that the failure mode is somewhat different from one panel to the other as depicted from the combined Fig. 4.51 for the tested panels in Group IV.

4.5 RESULTS FROM FLEXURAL TESTS

4.5.1 General

Per Equation 4.7, the resisting moment of the panels should be determined to examine the panel for combined bending and axial compression. In this research, panel Group V, presented in Table 3.1, was tested under flexural loading. This panel group represented the 3.048 m panel length. Discussion of the experimental results of these flexural tests is presented in the following sections. It should be noted panel Group II or IV of 2.74 mm length was not tested here in flexure since its flexural test results were available elsewhere (Mohamed, 2009).

4.5.2 Code Requirements for the Flexural Test of SIPs

The flexural tests on the panels were conducted in accordance with the method described in the ASTM E72-02, *Standard Test Methods for Conducting Strength Tests of Panels for Building Construction*, (ASTM, 2002) as well as ICC AC04, *Acceptance Criteria for Sandwich Panels*, (2004), for the *Transverse Load Test* .

4.5.3 Results of flexural tests for panel Group V of 3.048 m length

Per Table 3.1, panel Group V consists of three identical panels of 3.048 m length. The panels were tested in flexure up-to-complete-collapse. Each panel was 260.3 mm thickness, 1,220 mm width and 3,048 mm length. Figure 4.25 shows view of panel BW1 before testing, while Figure 4.26 shows view of the permanent deformed shape of the panel after failure. It was observed that the failure mode of the panel was due to shear failure at the interface between the top plywood face and foam core as shown in Figure 4.27. A delamination (debonding) between the top foam-Plywood interface and the foam core at the support location going towards the quarter point of the panel suddenly occurred at failure. Noise was heard when approaching failure load and shear failure was abrupt causing a sudden drop in the applied jacking load as depicted in the flexural load-deflection history shown in Figure 4.52.

Panels BW2 and BW3 showed similar behaviour to panel BW1. Figures 4.28 and 4.29 show views of panel BW2 before and after loading, respectively. While, Figs. 4.29 and 4.30 show close-up views of the failure mode, which was mainly shear failure at the top facing-foam core interface between the support and the quarter point. Due to rotation at the support, nail tearing occurred at the support between the end plate and the panels facings as depicted in Fig. 4.31. Figures 4.32 and 4.33 shows views of the tested panel BW3 before and after loadings, while Figs. 4.34 and 4.35 shows close-up views of the shear failure at the interface between the top facing and the foam at the support location.

Figure 4.53 show the flexural load-deflection relationships for panel BW2 and BW3, respectively. General linear relationship between the applied load and the mid-span deflection

was observed. The absence of the nonlinear behaviour observed experimentally supports the sudden failure that occurred without warning. With respect to the ultimate load carrying of the tested panels, it was observed that the ultimate jacking load was 64.87, 56.20, 89.11 kN, for panels BW1, BW2 and BW3, respectively. One may observe that the ultimate jacking load for BW3 is far greater than those for panels BW1 and BW2. As per AC04, since the results vary more than 15% from the average of the three, the lower value is used as the average of the ultimate loads for the group as 56.20 kN, which will be used in further analysis in this thesis. It should be noted that Figure 4.54 shown a kink at an applied load of about 78 kN. Then, the panels continued to carry more loads till it failed at 89.11 kN. It is suspected that a the connection between the facings and the internal lumber studs was overcome and the lumber studs and the lumber spline joint started to attract more loads. Results from LVDTs Located at the mid-span location showed an average mid-span displacement of 27.17, 37.56 mm, and 49.99 mm, for panels BW1, BW2, BW3, respectively. Table 4.6 shows the flexural load results without including the weight of the loading system of 2 kN. Figure 4.58 shows the applied flexural load-average deflection relationship for the tested panels in this group for the sake of comparison.

4.5.4 Results of flexural tests for panel Group V of 2.74 m length

Mohamed (2009) tested three identical panels in flexure to-complete-collapse. Each panel was of 209.55 mm thickness, 1,220 mm width and 2,743.2 mm length. Figures 4.55, 4.56, 4.57 show the flexural load-deflection relationship for such panels that referred to in this thesis as BW4, BW5, BW6, respectively. With respect to the ultimate load carrying of the tested panels, it can be observed that the ultimate jacking load was 51.54, 49.77, and 50.99 kN for panels BW4, BW5 and BW6, respectively. While the average mid-span maximum deflection recorded at

failure was 26.22, 39.60, and 28.10 mm, for panels BW4, BW5, BW6, respectively. Table 4.6 shows the flexural load results without including the weight of the loading system of 2 kN. Figure 4.59 a combined applied load-average deflection history of such panels for the sake of comparison.

4.6 FULL AND PARTIAL COMPOSITE ACTION

PWF strut/beam under compression or flexural exhibits partial interaction slip occurring across the interface of its top to the top and bottom S-P-F plates due to the interface bond force that exceeds the interface bond strength. As a result, there would be a step change between the strain in sheeting faces and the stud in core. However the slip strain was assumed to be constant throughout the thickness of the strut which leads to a uniform slip at the ends (Oehlers, 1993). In which, if the maximum load or moment capacity was reached without the interface bond force exceeding the interface bond strength then the strut/beam exhibits full composite action or full interaction (Hossain and Wright, 2004a).

4.6.1 Compression Test

The major characteristics of the axial-transverse crushing responses under the compression load-displacement (P-δ) response for specimens of group I and II was initially nonlinear showing the effect of the partial composite action. Afterward it increases linearly to the maximum load as it behaves in its full composite action. In panels BW2, BW4, and BW5, the jacking load experienced a significant drop at a load level close to ¾ the failure load, subsequently the load recovered up at which value the band proceeded to broaden in essentially a steady-state manner up to failure as shows in Figs 4.37, 4.39, 4.40, respectively. Under eccentric

compression load, the faces merely behave as two independent beams or struts and the sandwich effect is lost.

4.6.2 Flexural Test

Sandwich panels in which the core can transfer between zero and 100 percent of the longitudinal shear required for a fully composite panel are said to be semi-composite panels. The PCI approach (PCI, 1997) for the semi-composite sandwich panel assumes that such panels behave both as a fully composite panel and a non-composite panel at different stages in the life of the panel. As seen in the Figs. 4.52 through 4.57, the flexural behaviour shows the initial fully composite action (horizontal shear transfer) due to the linear relation of the load-deflection diagrams. However the actual behaviour falls in between the full and partial composite actions, which indicates a semi-composite behaviour of the panel beyond the straight line portion of the diagram till failure.

CHAPTER V

PREDICTED CREEP MODELS OF SIPS AS PERMENANT WOOD FOUNDATION

5.1 GENERAL

This chapter investigates the applicability of existing flexural creep models on structural insulated panels used as permanent wood foundation in low-rise buildings, when subjected to soil pressure. Also, this chapter identifies the parameters to be used in the strength interaction equation 4.8 as stated in the design standard. The chapter investigates the applicability of available flexural creep models on the prediction of the creep deflection of SIP panels subjected to sustained soil pressure. Also, a discussion on the use of the strength interaction equation on the design of permanent wood foundation made from SIPs.

5.2 VISCOELASTIC LONG-TERM CREEP DEFLECTION

5.2.1 Short-term deflection

In the absence of experimental data when different panel length is used, the short-term (instantaneous) deflection for serviceability limit-state design criterian SIPs used as permanent wood foundation can be calculated based on the following equation.

$$\Delta_{short-term} = \Delta_{Bending} + \Delta_{Shear} - \Delta_{Ecc\ @\ mid-span} \quad (5.1)$$

Where $\Delta_{Bending}$ the deflection due to flexural deformation is, Δ_{Shear} is the deflection due to shear deformation and $\Delta_{Ecc\ @\ mid-span}$ is the deflection due to gravity load eccentricity of t/6.

Allen (1969) introduced Equations 5.2 and 5.3 to determine the flexural deflection and flexural rigidity of the wall, respectively, when subjected to triangular soil pressure allover its height.

$$\Delta_{Bending} = \frac{qL^3}{360}\frac{x}{D}\left[7 - 10\frac{x^2}{L^2} + 3\frac{x^4}{L^4}\right] \quad (5.2)$$

If the faces are not of the same material or of unequal thickness, the flexural stiffness, D = EI, can be calculated using the following equation (Allen, 1969; Diab, 2003).

$$D = \frac{b\,d^2 E_1 E_2 t_1 t_2}{E_1 t_1 + E_2 t_2} + \frac{b}{12}\left(E_1 t_1^3 + E_2 t_2^3\right) \quad (5.3)$$

Where the suffixes 1 and 2 refer to the upper and lower faces, respectively. In this equation, the contribution of the core to the flexural stiffness is negligible, and thus it was ignored.

CAN/CSA-O86-01 specifies the following equations 5.4.a through 5.4.d to calculate the flexural deflection for permanent wood foundation of the two configurations shown in Fig. 5.9 when the soil pressure extents from the soil ground surface down to the bottom of the wall.

$$\Delta_{Bending} = \frac{w_f\,(L-X)}{360\,E_S I\,LH} K_\Delta \quad (5.4.a)$$

$$K_\Delta = \left[10\,H^2\,(H-3a)(2L-x)x - 3(H-a)^5 + K_2\right] \quad (5.4.b)$$

$$K_2 = \frac{3L}{L-x}(H-a-x)^5 \quad (5.4.c)$$

$$x = H - a - H\sqrt{\frac{H-3a}{3L}} \quad (5.4.d)$$

CAN/CSA-O86.01 specifies that the deflection of stressed skin panels, shown in Fig. 1.7, shall be calculated using the effective stiffness, $(EI)_e$, determined in accordance with Clause 8.6.2,

multiplied by the panel geometry reduction factor, X_g, determined in accordance with Clause 8.6.3.2. The effective stiffness, called D also, is shown in Equation 5.5.

$$(EI)_e = (EI)_w K_{SE} + b_f (B_{at}\, y_t^2 + B_{ac}\, y_c^2) K_s \quad (5.5a)$$

$$(EI)_e = (EI)_w K_{SE} + b_f (B_{at}\, y_t^2) K_{s(OSB)} + b_f (B_{ac}\, y_c^2) K_{s(Ply)} \quad (5.5b)$$

Where B_{at}: axial stiffness of tension flange for OSB, N/mm

B_{ac}: axial stiffness of compression flange for plywood, N/mm

K_S: service condition factor for modulus of elasticity of OSB and plywood

K_{SE}: service condition factor for sawn lumber used as webs.

Since facings of stress-skinned panels can be formed of two materials (i.e. OSB and plywood), the neutral axis of the cross-section shown in Fig. 1.7 can be determined based on Equations 5.6 and 5.7 as follows.

$$Web = \sum E_w . A_w (h_t + 0.5\, h_w) K_{SE}$$

$$Flanges = b_f [B_{at} (0.5 h_t) + B_{ac} (h_t + h_w + 0.5\, h_c)] K_s \quad (5.6a)$$

$$Flanges = b_f [B_{at} (0.5 h_t) K_{s(OSB)} + B_{ac} (h_t + h_w + 0.5\, h_c) K_{s(Ply)}] \quad (5.6b)$$

$$c_t = \frac{\sum EA\, y}{\sum EA} = \frac{Web + Flanges}{E_w A_w + b_f (B_{at} + B_{ac}) K_s} \quad (5.7a)$$

$$c_t = \frac{\sum EA\, y}{\sum EA} = \frac{Web + Flanges}{E_w A_w + b_f B_{at} K_{s(OSB)} + b_f B_{ac} K_{s(Ply)}} \quad (5.7b)$$

Shear Deflection is the second parameter in the short-term deflection equation 5.1. It results from possible shear deformation of the foam core since it has small shear modulus compared to that of the OSB or plywood. This shear deflection can calculated as shown in Equation 5.8 for the loading case of triangular soil pressure shown in Fig. 5.9 (Allen, 1969).

$$\Delta_{Shear} = \frac{Q}{AG} = \frac{Q}{V} = \frac{w_f L x}{6 V} [1 - \frac{x^2}{L^2}] \quad (5.8)$$

Where V is the shear stiffness as AG, A is the foam cross-section in shear, and G is foam shear rigidity. Since the deflection is calculated at the serviceability limit state, it should equal the specified soil pressure of 4.7 kN/m^2 per meter depth of the wall.

Group I

By considering Equation 5.3.b, and using b = 1220 mm, d = 247.1 mm, E_1 = 2000 N/mm^2, E_2 = 3032.258 N/mm^2, t_1 = 11 mm, and t_2 = 15.5 mm, the flexural rigidity (D) of the sandwich panel of Group I is 1.118E+12 N.mm^2. Using Equations 5.4, the flexural deflection of the panel under soil pressure is 6.709 mm, with w_f = 14.992 N/mm (w_f = 2 x 20.5632 / 2.7432), L = 3048 mm, H = 2743.2 mm, x = 1371.6 mm, and a = 0. However, the shear deflection of the foam is calculated using 5.8 as 10.928 mm using a foam shear modulus of 2.758 N/mm^2, shear area of (1220 - 38) x (260.35 – 11 – 15.5) = 276410.7 mm^2. It can be observed that the total short term deflection due to flexural and shear deformation of SIPs without the effect of the lumber stud is 6.709 + 10.928 = 17.637 mm, which is far greater that the experimental deflection of 8.0343 mm. Given the presence of the shear stud at the lumber spline connection, the shear deflection of the lumber stud is calculated using Equation 5.8 as 1.518 mm. By inspection, one may notice that the total short term deflection for the facings and the lumber stud is 6.709 + 1.518 = 8.227 mm, which is greater that the experimental value (8.0343 mm) by 2.398 %. As such, one may consider the presence of lumber stud at the spline connection prevented the contribution of the foam in shear deformation of the core area.

By using Equation 5.5 specified in CSA-O86.01 for the flexural stiffness (EI) of stress-skinned panels shown in Fig. 1.7, the flexural stiffness of the SIP wall without the effect of the foam is 1.585E+12 N.mm^2. This value was calculated using B_{at} of 47000 N/mm, B_{ac} of 22000 N/mm, $K_{s(OSB)}$ of 1.0 for OSB, $K_{s(Ply)}$ and K_{se} of 0.85 for plywood and 0.94 for stud, respectively. It should be noted that $K_{s(Ply)}$ and K_{se} is taken as 0.85 and 0.94 for wet condition, since the lowest recorded relative humidity in the laboratory during the creep testing was more than 19%. One may observe that the flexural stiffness calculated using the Canadian Code equation is greater that the calculated value using Allen's equation 5.3b by 43.87%. The makes the CWC flexural deflection 4.732 mm instead of 6.709 mm calculated using Allen's equation. Also, the total deflection using CWC equation is 4.732 + 1.518 = 6.25 mm which is smaller than the recorded experimental deflection (8.0343 mm) by 22.2%.

Group II

Similar observations were drawn for panel group II as follows. By considering Equation 5.3.b, and using b = 1220 mm , d = 196.1 mm , E_1 = 2000 N/mm^2, E_2 = 3032.258 N/mm^2, t_1 = 11 mm, and t_2 = 15.5 mm, the flexural rigidity (D) of the sandwich panel of Group II is 0.7E+12 N.mm^2. Using Equations 5.4, the flexural deflection of the panel under soil pressure is 6.1163 mm, with w_f = 13.323 N/mm (w_f = 2 x 16.243 / 2.4384), L = 2743.2 mm, H = 2438.4 mm, x = 1234.44 mm, and a = 0. However, the shear deflection of the foam is calculated using 5.8 as 10.06 mm using a foam shear modulus of 2.758 N/mm2, shear area of (1220 – 38) x (209.35 – 11 – 15.5) = 216128.7 mm^2. It can be observed that the total short term deflection due to flexural and shear deformation of SIPs without the effect of the lumber stud is 6.1163 + 10.06 = 16.1763 mm, which is far greater that the experimental deflection of 8.03167 mm. Given the presence of

the shear stud at the lumber spline connection, the shear deflection of the lumber stud is calculated using Equation 5.8 as 1.398 mm. By inspection, one may notice that the total short term deflection for the facings and the lumber stud is 6.1163 + 1.398 = 7.5143 mm, which is less than the experimental value (8.03167 mm) by 6.44 %. As such, one may consider the presence of lumber stud at the spline connection prevented the contribution of the foam in shear deformation of the core area.

By using Equation 5.5 specified in CSA-O86.01 for the flexural stiffness (EI) of stress-skinned panels shown in Fig. 1.7, the flexural stiffness of the SIP wall without the effect of the foam is 0.8E+12 N.mm^2. This value was calculated using B_{at} of 47000 N/mm, B_{ac} of 22000 N/mm, $K_{s(OSB)}$ of 1.0 for OSB, $K_{s(Ply)}$ and K_{se} of 0.85 for plywood and 0.94 for stud respectively. It should be noted that $K_{s(Ply)}$ and K_{se} is taken as 0.85 and 0.94 for wet condition, since the lowest recorded relative humidity in the laboratory during the creep testing was more than 19%. One may observe that the flexural stiffness calculated using the Canadian Code equation is greater that the calculated value using Allen's equation 5.3b by 22.62%. That makes the CWC flexural deflection 4.98761 mm instead of 6.1163 mm calculated using Diab's equation. Also, the total deflection using CWC equation is 4.98761 + 1.398 = 6.386 mm which is smaller than the recorded experimental deflection (8.03167 mm) by 20.48%.

General comment on CWC service condition

Since the experimental study test was assumed to be in dry condition when applying Allen's equation, K_s and K_{se} in equation 5.5 were assumed to be 1.0 for the sake of better comparison of CWC equation with Allen's equation for the prediction of flexural stiffness. As such, the CWC flexural stiffness increases resulting in a reduction in the short term deflection.

For example, the flexural stiffness for groups I, and II become 1.806E+12 and 0.9185E+12 N.mm^2, respectively. This makes the predicted short term deflection due to flexure to be 5.67 mm instead of 4.15 mm for Group I and to be 4.69 mm instead of 6.09 mm for Group II. Still, Allen's expression proved to be more reliable that the CWC equation in predicting the flexural stiffness of the SIP panels.

5.2.2 Long-term deflection

In reference to Equation 2.19 in Chapter II, the total deflection is the summation of the short-term (instantaneous) deflection and the deflection due to creep effects. The latter is the product of the portion of load that would be sustained for a period of time times the relative creep constant. The following subsections discuss how to calculate this constant based on experimental data as well as the available creep models.

5.2.3 Forms of creep models

Linear viscoelastic materials are those in which the stress is directly proportional to the time-dependant strain. Models of parabolic form have been employed with good success to describe the primary and secondary creep deflection of wood and rigid foam materials, as well as the sandwich panels (Davies, 1987; Huang and Gibson, 1990, 1991; Gerhards, 1985; Hoyle et al., 1985). Typically called a power model, the full form is presented in Equation 5.12 as

$$\Delta_p(t) = \Delta_o + A_1 t^{A_2} \tag{5.12}$$

Where $\Delta_p(t)$ is the total time-dependant deflection, Δ_o is the initial deflection, A_1 and A_2 are creep parameters, and t is the time in hours.

As a first step, the application of a power model is suggested to predict the primary and secondary relative creep behaviour of SIP panels. The power model is simple in form and number of parameters. The obvious limitations of this model are that it is applicable only to constant load histories; therefore, cyclic, step and ramp loads can not be modeled. Also, it does not account for the effects of temperature and relative humidity. For this reason, phenomenological models are being developed such as those reported by Fridley et al. (1992) to model mechanosorptive effects under stress histories for hygrothermal materials. Although the power model has been the most used to describe creep behaviour of wood (Nielsen, 1972) and is widely used in the study of other materials (Morlier, 1994), mechanical models of various forms are more powerful and also widely used.

Linear mechanical models, as shown in Fig. 2.17, are made up of combinations of linear springs and linear dashpots. This two-element model is comprised of a spring in a series with a Kelvin body (parallel spring and dashpot). This model is presented in Equation 5.13 as

$$\Delta_2(t) = \Delta_o + A_1(1 - \exp(-\frac{t}{A_2})) \tag{5.13}$$

Where $\Delta_2(t)$ is the total time-dependant deflection, Δ_o is the initial deflection, and A_1 and A_2 are creep parameters (related to Kelvin body spring constant and Kelvin body viscous constant, respectively).

This two-element model (called Kelvin model herein) has been successfully used to model short-term creep experiments since the model fits in the form of primary creep well. That is, the exponential function decays relatively quickly and the deflection approaches a horizontal asymptote. Models of this form are limiting, in that they usually predict lower trends than measured for the creep behaviour beyond the experimental data.

The three-element model (called also Burger model) for time-dependant deflection is presented in the form given in Equation 5.14 as

$$\Delta_3(t) = \Delta_o + A_1(1 - \exp(-A_2 t)) + A_3 t \quad (5.14)$$

Where $\Delta_3(t)$ is the total time-dependant deflection, Δ_o is the initial deflection, and A_1, A_2 and A_3 are creep parameters (related to Burger body spring constants and Burger body viscous constants, shown in Fig. 2.17).

This Burger model is more adaptive to longer-term creep experimentation exhibiting secondary creep behaviour, since the exponential function decays into a sloped asymptote defined by the viscous term $A_3 t$. The most outstanding limitation of the three-element model is that it over-predicts the creep behaviour beyond the experimental data for some materials.

Given the limits of the two- and three-element models to predict creep behaviour beyond the time period of the experimental data, DinWoodie et al. (1984) have recommended a four-element model (called Fridley model herein after some modifications) that essentially redefines the viscous dashpot of the three-element model from linear to nonlinear. Equation 5.15 presents the mathematical form of this model as

$$\Delta_4(t) = \Delta_o + A_1(1 - \exp(-A_2 t)) + A_3 t^{A_4} \quad (5.15)$$

Where; Δ_4 (t) = total time dependent deflection; Δ_o = initial deflection; A_i = creep parameters.

5.2.4 Logarithmic Expression of Creep Model

The U.S. Bureau of Reclamation developed a mathematical model in the form of a parabolic curve for flexural creep prediction as per Equation 5.16 (Neville, 1970), where k is a creep constant.

$$C_{sp} = \Delta_o + (K)\, ln(t + 1) \quad (5.16)$$

Where Csp is the fraction increase in deflection due to creep, t is the time since loading, and K is a creep parameter obtained based on experimental data, and Δ_o = initial deflection.

5.2.5 Interpretation of results from creep models

To investigate the applicability of the creep models to SIPs based on the short-term experimental data and over number of years, the initial deflection, Δ_o, was simply considered as the measured experimental deflection immediately after loading the panels. A nonlinear least-square regression procedure (using Microsoft Excel) was used to determine the creep parameters in Equations 5.12 through 5.15 for each panel group. The resulting creep parameters and the corresponding summation of square of the errors obtained from the regression analyses are listed in Table 5.1. The individual experimental deflection versus time data for each tested panel group along with the deflection-time history obtained using creep models is depicted in Fig. 5.1 for panel group I and Fig. 5.2 for panel group II. In addition, Tables 5.2 and 5.3 present the deflection values obtained experimentally and using the creep models within the test period of about 8 months (5780 hours). Also, Tables 5.2 and 5.3 showed the predicted deflection of the tested panels, using the creep models, after 1, 5, 10, 50 and 75 years of service.

By inspection of the data listed in Tables 5.2 and 5.3, it can be observed that the power model agrees very well in the short term during the 8-month period of the flexural creep tests. For example after sustaining the triangular loading over the panels for 3 months (2160 hrs), the power model predicted the measured deflection of 10.85 mm as 10.05 mm for panel group I, an underestimation of 7.3%. Also, after 8 months of loading the power model underestimates the

experimental creep deflection by 0.23%. In case, of group II, the power model underestimates the experimental deflection by 0.92% after 3 month of loading and overestimate this value by 5.6% after 8 months of sustained loading. As such, the power model is adequately predicted the creep deflection within the 8-month period of the creep experiments.

A comparison of the total deflection of panel groups I and II listed in Tables 5.2 and 5.3 shows good correlation between the two-element (Kelvin) model prediction and the experimental data within the 8-month test period. For example after sustaining the triangular loading over the panels for 3 months (2160 hours), the two-element model predicted the measured deflection of 10.85 mm as 10.27 mm for panel group I, an underestimation of 5.3%. Also, after 8 months of loading the power model underestimates the experimental creep deflection by 2.6%. In case, of group II, the two-element model underestimates the experimental deflection by 0.25% after 3 month of loading and overestimate this value by 3.7% after 8 months of sustained loading. As such, the two-element model is adequately predicted the creep deflection within the 8-month period of the creep experiments.

Similarly, from inspection of Tables 5.2 and 5.3, the three-element (Burger) creep model appears to underestimate the experimental data at low times and over estimate it near the end of the 8-month period of the sustained loading. For example in case of group II, the three-element model underestimates the experimental deflection by 0.76% after 3 month of loading and overestimate this value by 5.4% after 8 months of sustained loading.

Tables 5.2 and 5.3 also present the predicted creep deflection of the tested panels using the four-element (Fridley) model. It can be observed that the predicted total deflection agrees very well the experimental data. For example after sustaining the triangular loading over the panels for 3 months, Fridley creep model predicted the measured deflection of 10.85 mm as 10.27 mm for panel group I, an underestimation of 5.4%. Also, after 8 months of loading the power model underestimates the experimental creep deflection by 2.53%. In case, of group II, the power model overestimates the experimental deflection by 3.83% after 3 month of loading and overestimate this value by 0.2% after 8 months of sustained loading.

In case of the prediction of creep deflection using the Logarithmic Expression model, results listed in Tables 5.2 and 5.3, the model appears to overestimate the experimental data at low times and underestimates the values at the end of the 8-month period of the sustained loading. However, the level of overestimation is acceptable. For example in case of group I, the Logarithmic Expression model overestimates the one-month experimental deflection by 2.9%, while it underestimates the value by 12.2% after 8 months of sustained loading.

5.2.6 Predication of creep deflection past the period of experimental creep tests

As a result of the success of the available creep models in predicting the experimental creep deflection of the tested panels, the extrapolation of such models past the modeled creep test time period was conducted. Tables 5.2 and 5.3 summarizes the predicted total deflection of the panel groups I and II, respectively, after 1, 5, 10, 50 and 75 years of service.

Results for the power model beyond the 8-month test period show significant increase in the total deflection that makes it realistically unacceptable form long-term creep deflection. For example, the power model increased the instantaneous deflection by about 2, 6 and 7 times after 10, 50 and 75 years of service, respectively. Also, for Group II, the increases in deflection due to creep after 10, 50 and 75 years are predicted as about 5, 7 and 24 times the instantaneous deflection, respectively.

As for the two-element (Kelvin) model, Tables 5.2 and 5.3 show and increase in fractional deflection by the extrapolation of the model pasted the experimentally modeled time scale up to about 5 years. No significant additional deflection past the 5 years is predicted using this model since the model is forced to a horizontal asymptote beyond the 5–year predication period.

As the case for the power model, the three-element (Bruger) model showed a significant increase in the total deflection that makes it realistically unacceptable form long-term creep deflection for times ranging from 5 to 75 years. For example, the model increased the instantaneous deflection by about 5, 25 and 38 times after 10, 50 and 75 years of service, respectively. Also, for Group II, the increases in deflection due to creep after 10, 50 and 75 years are predicted as about 6, 28 and 42 times the instantaneous deflection, respectively.

As the case for Kelvin model, Tables 5.2 and 5.3 show that the four-element (Fridley) model predicted an increase in fractional deflection by the extrapolation of the model pasted the experimentally modeled time scale up to about 5 years. No significant additional deflection past the 5 years is predicted using this model since the model is forced to a horizontal asymptote

beyond the 5–year predication period. For example, the predicted creep deflections of Group I are 0.44, 0.45, 0.45 and 0.45 times the instantaneous deflection after 1, 5, 10, 50 and 75 years of service, respectively.

In contrast to all the presented models above, Logarithmic Expression model predicts an increase in deflection due to creep at low time and long times past the experimental test time scale. For example, the predicted creep deflections of Group I are 0.29, 0.34, 0.36, 0.41 and 0.43 times the instantaneous deflection after 1, 5, 10, 50 and 75 years of service, respectively. Also, the predicted creep deflections of Group II are 0.26, 0.31, 0.33, 0.37 and 0.38 times the instantaneous deflection after 1, 5, 10, 50 and 75 years of service, respectively. Table 5.4 shows a summary of the relative creep constant after 75 years of service as predicted by Fridley's model and the Logarithmic Expression model. Also, Fig. 5.3 depicts the predicted relative creep constant with time as obtained from Fridley model and the Logarithmic Expression model. From the above mentioned discussions, one may suggest that the most realistic predicted relative creep deflection constant after 75 years of service are constants are 0.70, 0.45 and 0.43 from Kelvin, Fridley and Logarithmic Expression models, respectively. To cover the SIP configurations of the two tested groups I and II, a conservative relative creep deflection constant of 0.7 is proposed in this study.

5.3 EFFECT OF TEMPERATURE AND HUMIDITY ON CREEP DELFECTION

5.3.1 Humidex

Wood is hygroscopic organic material that adsorbs and losses moisture from surrounding air to be in equilibrium with surrounding different environmental conditions that could be dry,

wet, hot, corrosive vapor, or combination of some of them. Its service condition is considered to be dry condition when the average equilibrium moisture content (EMC) is 15% or less than 19%. The *Humidex* is a Canadian index to describe the weather feeling to the average person, where it is a combination of temperature and relative humidity in percentage as in Equation 5.17 (Masterton and Richardson, 1979).

Humidex = Air Temperature in Celsius + Relative Humidity in % (5.17)

Figures 5.4 and 5.5 depict the effect of the *Humidex* on the creep deflection for tested panel group I and II, respectively. It can be observed that the creep rate increases with the increase of the temperature and humidity (i.e. with increase in *Humidex*), as expected. During the creep tests, it was observed that the room temperature ranged between 22^{o}C and 25^{o}C, while the relative humidity ranged between 20 to 70%. The humidex varies between 22+20 = 42 up to 25+70 = 92.

5.3.2 Proposed Viscoelastic Creep Model

The phenomenological creep-strain response for wood-based structure is viscoelastic, with elastic spring and viscous dashpot (Findley, 1976). The common rheological models can be illustrated as of Kelvin-Voigt (solid) and Maxwell (fluid) as linear mode and of Burger model which is nonlinear (Hunt, 1998). Burger model consisted of elastic, viscoelastic, and viscoplastic deformations. Fridley developed Burger's model (Fridley 1992; Burger 1935) by multiplying the last term of the Equation 5.14 with time. The proposed model in this study is a modification to Fridley's model by replacing the fixed sustained stress (i.e. constants A_2, A_3 and A_4) with cyclic stress. This is achieved by adding the *Humidex* effect in the form of change in ambient temperature and relative humidity, and converting them into stress equivalency. This stress

equivalency is presented in Equation 5.18 in such a way that both temperature and relative humidity are variables.

$$\sigma_e = a \,.\, \sigma^m + b \,.\, T + c \,.\, \theta \tag{5.18}$$

Where σ_e is the stress equivalency; σ is the sustained stress (i.e. the soil pressure of 4.7 kPa per meter depth of the wall in this study), T is the temperature, θ is the relative humidity, and a, b, c and m are the stress equivalency coefficients.

Using experimental data for tested Groups I and II in this study, stress equivalency coefficients, a, b and c, were calculated using Levenberg-Marquart (LM) algorithm, namely: Nonlinear Least Squares Minimization (Betten, 2008, Bewick, 2003). The values of these constants are listed in Table 5.5.a for tested panel groups I and II, respectively.

Fridley (1992) presented the following creep model (Wu 2009; Pierce 1977) as the original form of the four-element model presented in Equation 5.15 before simplifying it by Taylor (1996) in the form of creep constants A_1, A_2, A_3 and A_4.

$$\varepsilon_{Creep}\,(t) = \varepsilon_e + \varepsilon_K + \varepsilon_V = \frac{\sigma_e}{K_e} + \frac{\sigma_e}{K_k}\,\{\,1 - \exp\,[\,-\frac{K_k}{\eta_k}\,t]\} + \frac{\sigma_e}{\eta_v}t^n \tag{5.19}$$

Where $\varepsilon_{Creep}(t)$ is the creep strain; t is the time, σ_e is the stress equivalency, K_e is the elastic spring constant, K_k and $\boldsymbol{\eta}_k$ are the spring constant and viscosity for the viscoelastic deformation, respectively, and $\boldsymbol{\eta}_v$ is the viscosity of dashpot for the viscoplastic deformation, n is power constant. It should be noted the instantaneous deflection, $\Delta_o = \frac{\sigma_e}{K_e}$.

Using statistical package for curve fit of the experimental data, the constants in Equation 5.19 were calculated and presented in Table 5.5.b. Figures 5.6.a and 5.7a show the plotted

average experimental data for groups I and II, respectively, versus the smooth Fridley curve per equation 5.14 that does not include the effects of the change in temperature and the relative humidity. The predicted deflection from the proposed creep model in equation 5.19 is also plotted against the average experimental data in the same Figure. It can be observed that the proposed creep model gives close results to the experimental data, given the change in the recorded daily temperature and relative humidity during the length of the creep tests. Figures 5.6.b and 5.7.b depict the change in the deflection recorded from each LVDT for each panel in groups I and II, respectively. Good correlation was observed. Results show that the rate of increase of creep deflection increases with increase of ambient temperature and/or the relative humidity.

To have a sense of the proposed mode in Equation 5.19, the total deflection is calculated as the short-term deflection plus the long-term deflection within the time of the creep test experiments as well as 5 year of service. It should be noted that the drawback of this equation is that it cannot accurately predict the short-term deflection at t = 0, however, it provides realistic values starting at t = 24 hrs. In case of panel group I, Fig. 5.8.a depicts the total deflection of the panel up to 8 months of sustained loading at 23° ambient temperature and different relative humidity of 25, 50 and 65%. It can be observed that the change of the relative humidity from 25 to 65% increased the total deflection after 8 months from 11.25 to 12.38 mm (an increase of 10.04 %).

Figure 5.8.b depicts similar trend but with constant relative humidity of 25% and different ambient temperature of 23, 30 and 35°. It can be observed that the total deflection after 8 months changed from 11.13 mm to 12.235 mm when the temperature changes from 23 to 35° (an

increase of 9.928 %). Similar observation is depicted from Figs. 5.8.c and 5.8.d for panel group II. Table 5.6 shows similar trend when applying equation 5.19 over 5 years of sustained loading. One may observe that the proposed creep model of Equation 5.19 predicts well the total deflection of the panel within the experimental test period of 8 month, given the fact that the total experimental deflections were 11.67 and 11.35 mm for panel groups I and II. However, the predicted deflection after 5 years for each model is very close to those predicted by the power model by comparing results of Table 5.6 with those in Tables 5.2 and 5.3 for groups I and II, respectively. It should be noted that the total deflections calculated in Fig. 5.8 and Table 5.6 assumed constant ambient temperature and relative humidity at all times of the sustained loading, which contradicts with the actual conditions recorded experimentally.

5.6 DESIGN TABLES FOR SIPS AS PERMANENT WOOD FOUNDATION

5.6.1 Strength Interaction Equation

The Canadian Standard CSA-O86.01 specifies that for preserved wood foundation, the strength interaction equation 5.20 of shall be applied to examine the combined effect of factored gravity load the factored soil pressure on the strength capacity of the wall.

$$\frac{M_f + P_f \Delta}{M_r} + \left[\frac{P_f}{P_r}\right]^2 \leq 1.0 \qquad (5.20)$$

Where M_f = maximum applied factored moment due to soil pressure, P_f = factored applied axial load on the wall, Δ = deflection due to lateral load at point where M_f is calculated, M_r = factored bending moment resistance of the wall, and P_r = factored compressive resistance of the wall. It should be noted that a load duration factor, K_D, of 0.65 is specified to the calculated resisting moment by code equations. However, in case of experimental data, this factor is applied to the

experimental resisting moment to be consistent with code requirements for the application of permanent loads such as soil pressure.

Since the resisting compressive loading of the tested SIP wall, P_r, was determined experimentally by applying the gravity wall load at an eccentricity of t/6, an additional applied factored moment of P_f.t/6 acts opposite to the applied factored moment due to soil pressure, M_f, and it should be considered in design as shown in the modified interaction equation 5.21.

$$\frac{M_f + P_f\Delta - P_f\frac{t}{6}}{K_D\, M_r} + \left[\frac{P_f}{P_r}\right]^2 \leq 1.0 \qquad (5.21)$$

5.6.2 Determination of Applied Factored Forces and Moments

Also, in this equation, the secondary moment $P_f.\Delta$ represent the added moment to the applied factored moment as a result of flexural deformation of the wall under soil pressure. Since this lateral deflection is calculated based on the soil pressure this is permanent as long as the structure exists, long-term effects should be considered. Based on inspection of results in reported in Tables 5.2 and 5.3 for the long-term creep results, it can be observed that Kelvin model for panel group II provides conservative, yet realistic values, for total deflection due to creep effects for both panel groups I and II. Given that the initial deflection is 8.03 mm and Kelvin predicted final deflection after 75 years is 13.69 mm, the predicted fractional creep deflection would be (13.69-8.03)/8.03 = 0.70. Since the experimental short-term deflection for both panel groups is 8.03 mm under sustained soil pressure, the factored short-term deflection due to factored soil pressure is 1.5 x 8.03 mm = 12.045 mm. By applying a creep constant of

1.70, the predicted total deflection due to creep effects after 75 years would be 1.7 x 12.045 = 20.48 mm.

The factored applied moment, M_f, is calculated based on the soil pressure distribution shown in Fig. 5.9 for slab-floor system. The intensity of the applied factored soil pressure, w_f, is taken as 1.5 times the specified soil pressure of 4.7 kN/m^2 per meter depth of the wall. It should be noted that the ground level is assumed 300 mm lower that the floor level for the calculation of the depth of the soil pressure.

$$M_f = \frac{w_f H^2}{6L}\left[L - H + \frac{2}{3}\sqrt{\frac{H^3}{3L}}\right] \tag{5.22}$$

5.6.3 Determination of Characteristic Values from Small Number of Samples

The structural design is based on random variables which are represented by their characteristic values. Thus, for further structural analyses, random variable is replaced by the characteristic value which is assumed to be deterministic. However, when only relatively small sample is available, the characteristic value is only estimated from the sample and in not random. The estimate is based on the assumption that the distribution of the variable is known and that its parameters can be approximated from a sample (Zupan et al., 2007). In engineering design based on available data, different distributions are usually prescribed for the determination of the resistance of different materials and for the determination of the resistance of the structures (among them: normal, log-normal, Gumbel and Weibull distributions). For most cases, formulae for the 75% confidence intervals for the estimates of 5% characteristic values based on normal or log-normal distribution are prescribed. In case of normal distribution, analytical formula for the characteristic value estimate within any

confidence internal based only upon the mean and the variance of the sample can be obtained. Analytical approach can easily be extended for log-normal distribution, as it is related to normal through the exponential map.

In this research, the log-normal distribution, as shown in Fig. 5.10, is used to determine the characteristic values for M_r and P_r since it is recommended by CSA.O86-01 for reliability analyses to determine the characteristic strength values of timber structures based on experimental data. The European Standard EN 14358 (EN 14358, 2006) specifies a procedure for the determination of the characteristics 5-percentile values from test results for wood structures. In this procedure, the characteristic value of a material parameter or a resistance shall be determined at a confidence level of 75%, where the confidence level is defined as the probability of which the characteristic value is greater than the estimator on the characteristic value. The characteristic value of m_k for a material strength parameter or a resistance m modeled as a stochastic variable is defined as the p -percentile in the distribution function for m, corresponding to an assumed infinitely large test series. In this case p = 5 % shall be assumed. It is assumed that n test values are available and that these may be assumed to originate from a homogeneous population. The test values, which are assumed to be logarithmically normally distributed and independent, are denoted m_1, m_2,…. m_n. The mean value ỹ and the standard deviation s_y for the stochastic variable $y = \ln m$ shall be determined as

$$\tilde{y} = \frac{1}{n}\sum_{i=1}^{n} \ln m_i \tag{5.23}$$

$$s_y = \sqrt{\frac{1}{n-1}\sum_{i=1}^{n}(\ln m_i - \tilde{y})^2} \tag{5.24}$$

The characteristic value shall be determined as

$$m_k = \exp(\tilde{y} - k_s s_y) \quad (5.25)$$

Where k_s is given in Table 5.7 and use s_y = 0.05 in Equation 5.25 in the case where the coefficient of variation is less than 0.05.

Based on the above-mentioned equations, the characteristic values for resisting compressive forces, P_r, of SIP panel groups I and II are calculated as 223.8 and 84.88 kN, respectively.

Also, the characteristic values for the resisting applied flexural loads for SIP panel groups I and II are calculated as 40.22 and 43.364 kN, respectively. In case of the resisting factored applied moment, M_r, the experimental data was obtained for panels subjected to two point loads at the quarter points simulating the uniformly distributed loading condition. However, the soil pressure is distributed linearly over the depth of the wall. To obtain the corresponding M_r, it was observed that the failure mode of the tested panels in flexure was due to shear at the interface between the top plywood facing and the foam core between the support and the quarter point location. As such, the ultimate shear force at this region is simply half the ultimate load carried by the panels experimentally. Equating this ultimate shear force at the mid-length between the support and the quarter point with the corresponding value in case of triangular load distribution, the equivalent intensity of the ultimate triangular load is then obtained. Using Equation 5.22 above, the corresponding factored resisting moment for a triangular soil pressure is them obtained as M_r in Equation 5.21 for each panel.

Other method to determine the characteristic strength values is based on an approximation of the design values based upon tested data as specified in ICC-ES AC04 (2004) for US market. The Acceptance criteria for SIPs set forth in AC04 includes testing three identical panels from each panel size. The average ultimate load carrying capacity of this

panel size will be basically the average of those for the three panels. However, AC04 specifies that when the results of each tested panel vary more than 15% from the average of the three panels, either the lowest test value is used or the average result based on a minimum of five tests may be used regardless of the variations. Since three identical panels were tested for each group and that some panels had strength values more that 15% from the average of the three panels, it was decided to consider the lowest strength value for both flexural and compressive loading. As such, the design compressive forces, P_r, for groups I and II, are taken as 285.47 and 173.69 kN, respectively, to apply equation 5.21. Also, in case of factored resisting bending moment from soil pressure, the factored jacking loads for flexural panels are taken as 56.20 and 49.77 kN, respectively. These values were considered in calculating the corresponding factored resisting moment due to soil pressure.

The characteristic values for compressive and flexural strength of the tested panel groups I and II based on the above-mentioned approaches are listed in Table 5.8. To develop design Tables for the served span length between the SIP basement wall and the nearest parallel basement wall of supporting element, Equation 5.21 was applied with different values of specified snow load of 1, 1.5, 2, 2.5 and 3 kPa. The following two loading cases were considered to determine the maximum gravity load that can be carried by the wall to satisfy the strength interaction equation 5.21.

Load Case 1 $\alpha_i S_i = \alpha_D D + \alpha_L L = 1.25 \text{ x } D + 1.5 \text{ x } L + 0.5\text{x}S$ (5.26)

Load Case 2 $\alpha_i S_i = \alpha_D D + \alpha_S S \text{ Is} = 1.25\text{x } D + 0.5\text{x } L + 1.5 \text{ x } S$ (5.27)

Three different house configurations were considered, namely: (i) house with roof and floor; (ii) house with roof and two floors; and (iii) house with roof and three floors. To conduct the

analyses, floor live load was assumed to be 1.9 kPa, roof dead load was assumed 0.5 kPa, floor dead load and partitions were assumed 0.47 kPa and exterior wall with brick veneer was assumed 1.9 kPa. Tables 5.9 and 5.10 present the results for the supported joist length in meters for panel groups I and II, respectively, based on the ICC-ES AC04 and the 5-percentile characteristic value per BS-EN 14358 approaches. It can be observed that the latter approach provides more critical served joist length than the AC04 approach.

CHAPTER VI

CONCLUSIONS

6.1 GENERAL

This study presents both experimental and theoretical investigation on the structural performance of SIPs as permanent wood foundation as an energy efficient alternative to the conventional concrete basement wall in houses and low-rise buildings. The objective of this research work is to contribute to the efficient design of structural insulated sandwich timber panels as permanent wood foundation by developing experimentally calibrated models capable of predicting their structural response when subjected to sustained flexural loading. Also, experimental testing to-collapse of selected SIP configurations was conducted to investigate their ultimate load carrying capacities in both flexural and shear that would lead to design tables for SIP use as permanent wood foundation. The following sections summarize the conclusions resulting from this research work as well as recommendations for future research.

6.2 CONCLUSIONS

Based on the experimental and theoretical findings, the following conclusions can be drawn:

1- During creep tests, the recorded ambient temperature was between 22ºC and 25 ºC, while the relative humidity ranged between 20 to 70%. It can be observed that the experimental long-term creep deflection did not increase smoothly with time due to the cyclic change in temperature and relative humidity over time.

2- After 8 months of sustained soil pressure, the panel experimental deflection increased by about 38 and 35% for groups I and II, respectively.

3- The tested SIP configurations are adequate for short-term serviceability limit state design of permanent wood foundation per CAN/CSA-O86.01.

4- Correlation between the experimental instantaneous deflection and that obtained by Canadian Standard CAN/CSA-O86.01 for stress-skinned panels and Diab's equation for SIPs with foam-spline connections revealed that the presence of lumber stud at the spline connection prevented the shear deformation of the core foam area. As such, instantaneous deflection of SIPs with lumber stud connection is basically the panel flexural deflection and the shear deflection of the lumber stud based on CSA-O86.01 for stress-skinned panel, ignoring the foam core area in shear deformation.

5- All creep models presented in this study agree very well with the experimental data in the short-term during the 8-month period of the flexural creep tests. In case of the prediction of creep deflection using the Logarithmic Expression model, the model appears to overestimate the experimental data at low times and underestimates the values at the end of the 8-month period of the sustained loading. However, the level of overestimation is acceptable.

6- Results for the power model beyond the 8-month test period show significant increase in the total deflection that makes it realistically unacceptable for long-term creep deflection.

7- The two-element (Kelvin) model and the four-element (Fridley) model predicted an increase in fractional deflection by the extrapolation of the model pasted the experimentally modeled time scale up to about 5 years. No significant additional deflection past the 5 years is predicted using this model since the model is forced to a horizontal asymptote beyond the 5–year predication period.

8- Both the power model and the three-element (Bruger) model showed a significant increase in the total deflection that makes it realistically unacceptable form long-term creep deflection for times ranging from 5 to 75 years.

9- In contrast to all the presented models above, Logarithmic Expression model predicted an increase in deflection due to creep at low time and long times past the experimental test time scale. For example, the predicted creep deflections of Group I were 0.29, 0.34, 0.36, 0.41 and 0.43 times the instantaneous deflection after 1, 5, 10, 50 and 75 years of service, respectively.

10- Based on the results from all creep models, it is suggested that the most realistic predicted fractional creep deflection constant after 75 years of service are constants are 0.70, 0.45 and 0.43 from Kelvin, Fridley and Logarithmic Expression models, respectively. To cover the SIP configurations of the two tested groups I and II, a conservative relative creep deflection constant of 1.7 is proposed in this study (i.e. fractional creep deflection of 0.70).

11- The proposed creep model in this study is a modification to Fridley's model by replacing the fixed sustained stress constants with cyclic stress which is a function of the ambient temperature and the relative humidity. Good correlation between the proposed mode and the experimental data was observed. Results show that the rate of increase of creep deflection increases with increase of ambient temperature and/or the relative humidity. It should be noted that the drawback of this equation is that it cannot accurately predict the short-term deflection at $t = 0$, however, it provides realistic values starting at $t = 24$ hrs. Also, the equation predicts large values of the total deflection over years which are not realistic for constant ambient temperature and relative humidity.

12- In case of compressive load tests of SIPs, No general failure trend is observed given the fact that the failure mode is somewhat different from one panel to the other. Failure of tested panels under eccentric compressive loadings occurred due to one of combinations of (i) crushing of OSB face near the top of the panels, (ii) delamination of the OSB-foam interface at that location, (iii) fracture of the lumber-spline as well as the OSB facing near the mid-height of the panel due to global flexural deformation of the panel, (iv) delamination at the OSB-foam interface between the panel footer and mid-height of the panel, and (v) complete separation of plywood face and foam from the OSB facing and the bottom plate footer. Given the general linear shape of such relationship between the applied load and corresponding axial shortening of the wall, it can be concluded that the failure was sudden, as observed during testing.

13- In case of flexural loading, it was observed that the failure mode of the panel was due to shear failure at the interface between the top plywood face and foam core. Delamination (debonding) between the top foam-Plywood interface and the foam core at the support location going towards the quarter point of the panel suddenly occurred at failure. Noise was heard when approaching failure load and shear failure was abrupt causing a sudden drop in the applied jacking load as depicted in the flexural load-deflection.

14- The CAN/CSA-O86.01 was used to develop design tables for the supported joist length of the SIP basement wall for single, double and triple-storey residential building. The characteristic 5-percentile value per BS-EN 14358: 2006 gives more conservative value than the basic average provided by ICC AC-04. As such, design tables based on the former is recommended for use in practise. However, it is safe to recommend a maximum

served joist span of 7.75 m for the SIP foundation wall for a low-rise residential building up to three stories.

6.3 RECOMMENDATIONS FOR FUTURE RESEARCH

1. Study the influence of the elastic properties of PWF and the stresses of mechanical connections.
2. Study the effect of climatic changes on modulus of elasticity, crack, and stability of the PWF structural elements.
3. Study the racking behaviour of the wall under seismic loading.
4. Establish design procedure and guidelines for SIPs as roof, floor and walls in low-rise residential construction.

REFERENCES

Allen, H. 1969. Analysis and Design of Structural Sandwich Panels. Pergamon Press, Oxford, UK.

ANSI / AF&PA PWF. 2007. Permanent Wood Foundation Design Specification with Commentary. American Forest & Paper Association. (www.awc.org).

APA. 1990. Supplement 4: Design and Fabrication of Plywood Sandwich Panels. APA – The Engineering Wood Association, Tacoma, WA, USA. (www.apawood.org).

ASTM. 2002. Standard Test Methods of Conducting Strength Tests of Panels for Building Construction, ASTM E72-02. American Society for Testing Materials, Philadelphia, PA, USA.

ASTM. 1988. Standard Test Methods of for Flexural Creep of Sandwich Construction, ASTM C 480-62. American Society for Testing Materials, Philadelphia, PA, USA.

ASTM. 2009. Standard Specifications for Structural Insulated Panel (SIP) Adhesives for Laminating Oriented Strand Board (OSB) to Rigid Cellular Polystyrene Thermal Insulation Core Materials, ASTM D7446 - 09. American Society for Testing Materials, Philadelphia, PA, USA.

ASTM. 2006 Standard Test Methods for Determining Structural Capacities of Insulated Panels, ASTM E1803 – 06. American Society for Testing Materials, Philadelphia, PA, USA. (http://www.astm.org/Standards/E1803.htm).

Aviles, F. and Carlsson, L.A. 2007. Post-buckling and debond propagation in sandwich panels subject to in-plane compression. Engineering Fracture Mechanics, Vol. 74, No. 5, pp. 794-806.

Betten, J. 2008. Creep Mechanics. Springer.

Bewick, V., Cheek, L., Ball, J. 2003. Statistical Review 7: Correlation and regression. Crit Care. Vol 7, No. 6, pp. 451-459.

BS-EN 14358. 2006. Timber structures – Calculation of characteristic 5-percentile values and acceptance criteria for a sample. British Standards.

Burgers, J.M. 1935. Mechanical considerations model systems-phenomenological theories of relaxation and of viscosity. In: J.M. Burgers, Editor, First Report on Viscosity and Plasticity, Nordemann Publishing Company, New York.

Butt, A.S. 2008. Experimental Study on the flexural behavior of structural insulated sandwich timber panels. M.Sc. Thesis, Ryerson University.

Canadian Standard Association. 1992 Construction of Preserved Wood Foundation, CAN/CSA-S406-92. Etobicoke, Ontario, Canada.

Canadian Standard Association. 2001 Engineering Design of Wood, CAN/CSA-O86.01. Toronto, Ontario, Canada.

Canadian Standard Association. 2005. National Building Code of Canada. Etobicoke, Ontario, Canada.

Canadian Wood Council. 2001. Wood Design Manual. CWC, Ottawa, Ontario, Canada.

Cheung, Y. K. 1968a. The finite strip method in the analysis of elastic plates with two opposite simply supported ends, Proc. Inst. Civ. Eng., Vol. 40, pp. 1–7.

Cheung, Y. K. 1968b. Finite strip method analysis of elastic slabs, J. Eng. Mech. Div., Proc. ASCE, Vol. 94 (EM6), pp.1365–1378.

Chong, K. P. 1986. Sandwich panels with cold-formed thin facings, Keynote paper, Proc. IABSE International Colloquium on Thin-Walled Metal Structuresin Buildings, Stockholm, Sweden, Vol. 49, pp. 339–348.

Chong, K.P., Hartsock, J.A. 1972. Flexural wrinkling mode of elastic buckling in sandwich panels. Proc. ASCE Specialty Conf. on Composite Materials Pittsburgh.

Chong, K.P., Hartsock, J.A. 1974. Flexural wrinkling of foam-filled sandwich panels. J. Eng. Mech. Div., Proc. ASCE.

Chong, K.P. and Hartsock, J. A. 1993. Structural Analysis and Design of Sandwich Panels with Cold-Formed Steel Facings. Journal of Thin-Walled Structures, Vol. 16, pp. 199-218.

Cox, H.L. and Riddell, J.R. 1949. Buckling of a longitudinal Stiffened Panel. Aeronautical Quarterly, Vol. 1, pp. 225-244.

Cox, H. L. and Riddell, J. R.. 1945. Sandwich Construction and Core Materials III: Instability of Sandwich Struts and Beams. ARC Technical Report ARC/R&M-2125, UK. (http://aerade.cranfield.ac.uk)

Davies, J.M. 1986. The Analysis of Sandwich Panels with Profiled Faces. Eighth Int. Specialty conf. on Cold-Formed Steel Structures, St. Louis, Missourri, U.S.A., November 11-12.

Davies, J.M. 1987. Design Criteria for Structural Sandwich Panels, Journal of Structural Engineering, ASCE, Vol. 65A, No.12, pp. 435-441.

Davies, J.M. & Hakmi, M.R. 1990. Local Buckling of Profiled Sandwich Plates. Proc. IABSE Symposium, Mixed Structures including New Materials, Brussels, Sep, pp. 533-538.

Davies, J.M. & Hakmi, M.R. 1992. Postbuckling Behaviour of Foam-Filled Thin-Walled Steel Beams. Journal of Construction Steel Research, Vol. 20, pp. 75-83.

Davies, J.M. 1993. Sandwich Panels. Journal of Thin-Walled Structures, Vol. 16, pp. 179-198.

Davies, J.M. 2001. Light Weight Sandwich Construction. Blackwell Science.

DIAB AB. 2003. DIAB Sandwich handbook, Sandwich Concept. 09.03. DIAB AB, Sweden.

Dinwoodie, J.M. 2000. Timber, Its Nature and Behaviour. Taylor & Francis. 2nd Edition.

Dinwoodie, J. M.; Pierce, C. B.; Paxton, B. H. 1984. Creep in chipboard. Part 4: The influence of temperature and moisture content on the creep behaviour of a range of boards at a single stress level. Wood Sci. Technol. Vol. 18, pp. 205-224.

Eringen, A.C. 1951. Buckling of a Sandwich Cylinder Under Uniform Axial Compression Load. Jour. Appl. Mech., Vol. 18, No. 2, 1951, pp. 195- 202.

Findley, W., J. Lai and K. Onaran. 1976. Creep and Relaxation of Nonlinear Viscoelastic Materials,North-Holland, New York.

Fridley, K.J., R.C. Tang, and L.A. Soltis. 1992 Creep behavior model for structural lumber. J. of Structural Engineering, Vol. 118, No.8, pp. 2261-2277.

Gerhards, C. C. 1985. Time-Dependent Bending Deflections of Douglas-Fir 2 by 4s. Forest Products Journal, Vol. 35, No. 4, pp.18-26.

Gibson, L. J. & Ashby, M. F. 1988. Cellular solids: Structure and properties. Oxford: Pergamon Press.

Goodier, J.N. 1946. Cylindrical buckling of sandwich plates. Trans. ASME J. Appl. Mech. Vol. 13, No. 4, pp. A253–A260.

Goodier, J.N., and Neou, I.M., 1951. The evaluation of theoretical critical compression in sandwich plates. J. Aero. Sci. Vol. 18, pp. 649-657.

Gough, G.S., Elam, C.F., De Bruyne, N.D., 1940. The stabilization of a thin sheet by a continuous supporting medium. J. Roy Aero. Soc. Vol. 44, pp. 12-43.

Gupta, N. and Woldesenbet, E . 2005. Characterization of Flexural Properties of Syntactic Foam Core Sandwich Composites and Effect of Density Variation. Journal of Composite Materials, Vol. 39, No. 24, pp. 2197-2212.

Gupta, N., Woldesenbet, E. and Kishore, 2002. Compressive fracture features of syntactic foams-microscopic examination. Journal of Materials Science, Vol. 37, No. 15, pp. 3199-3209.

Hassan, T.K. Reis, E.M. 2003. Innovative 3-d FRP sandwich panels for bridge decks. NC State University.

Heath, W.G. 1960. Sandwich construction, Part 2: The optimum design of flat sandwich panels. Aircraft Eng. Vol. 32, pp. 230–235.

Hemp, W.S. 1948. On a Theory of Sandwich Construction, Report, No. 15. College of Aeronautics, Cranfield, England. March, 10 pp., AMR1 (1614).

Hoff, N.J. and Mautner, S.E., 1945. The buckling of sandwich-type panels, J. Aero. Sci. Vol. 12, pp. 285–297.

Hossain, K. M., and Wright, H. D. 2004a. Experimental and theoretical behaviour of composite walling under in-plane shear. Journal of Constructional Steel Research, Vol. 60, No. 1, pp. 59-83.

Hossain, K. M. A., and Wright, H. D. 2004b. Performance of double skin-profiled composite shear walls - Experiments and design equations. Canadian Journal of Civil Engineering, Vol. 31, No. 2, pp. 204-217.

Hoyle, R.J., Griffith, M.C., and Itani, R.Y., 1985. Primary Creep in Douglas-fir Beams of Commercial Size and Quality. Wood and Fiber Science, Vol. 17, No. 3, pp. 300-314.

Hunt, D.G. 1998. A Unified approach to creep of wood. The Royal Society, UK.

Huang, J.S. and Gibson, L.J. 1990. Creep of Sandwich Beams with Polymer Foam Cores. Journal of Materials in Civil Engineering, Vol. 2, pp. 171-182.

Huang, J.S. and Gibson, L.J. 1991. Creep of Polymer Foams. Journal of Materials Science, Vol. 26, pp. 637-647.

Hunt, D.G. 1999. A Unified Approach to Creep of Wood. Proceedings: Mathermatical, Physical and Engineering Sciences. The Royal Society, pp 4077-4095.

ICC AC04. 2004. Acceptance Criteria for Sandwich Panels. ICC Evaluation Service Inc., USA.

Institute for Research in Construction. 2005. National Building Code of Canada, NBCC-2005. National Research Council, Ottawa, Ontario, Canada.

Jungbluth, O., Berner, K. 1986. Verbund- Und Sandwichtragwerke: Tragverhalten, Feuerwiderstand, Bauphysik. Springer-Verlag.

Kuhhorn, A., 1993. Nichtlineare Theorie und finites Element fur Sandwichtragwerke zur Beschreibung des globalen und lokalen (Knittern) Versagens. ZAMM Z. Angew. Math. Mech. 73 (4–5), T438–T443.

Kuhhorn, A., 1991. Geometrisch Nichtlineare Theorie Für Sandwichschalen Unter Einbeziehung des Knitterphanomens. VDI-Verlag, Reihe Vol. 18, No. 100.

Kuhhorn, A. and Schoop, H. 1992. A Nonlinear Theory for Sandwich Shells Including the Wrinkling Phenomena. Archive Applied Mechanics, Vol. 62, pp. 413–427.

Liu, Q., and Zhao, Y. 2007. Effect of Soft honeycomb Core on Flexural Vibration of Sandwich Panel using Low Order and High Order Shear Deformation Models. Journal of Sandwich Structures and Materials, Vol. 9, pp 95.

Mahendran, M. and Jeevaharan, M. 1999. Local Buckling Behaviour of Steel Plate Elements Supported by a Plastic Foam Material. Structural Engineering and Mechanics, Vol.7 No. 5, pp. 433-445.

Masterton, J.M., Richardson, F.A 1979. A method of quantifying human discomfort due to excessive heat and humidity. Downsview, Ontario, Canada: AES, Environment Canada, CL11-79, 1979.

Meyer-Piening. H. –R. 2006. Sandwich Plates: Stresses, Deflection, Buckling and Wrinkling Loads – A Case Study. Journal of Sandwich Structures and Materials, Vol. 8, No. 381.

Mindlin, R., 1951. Influence of rotatory inertia and shear on flexural vibrations of isotropic, elastic plates. J. Appl. Mech. Vol. 18, pp. 31–38.

Mohamed, M. 2009. Experimental study on the structural behavior of insulated sandwich foam-timber panels under combined axial compression and bending. M.Sc. Thesis, Ryerson University.

Morlier, P., Palka, L.C. 1994. Basic Knowledge, In Creep in Timber Structures. (ed. P. Morlier), RILEM Report 8. E and FN Spon, London, pp. 9-42.

National Forest Products Association (NFPA). 1991. National Design Specification for Wood Construction. Washington, DC.

Neville, A.M. 1970. Creep of concrete: plain, reinforced and prestressed. North-Holland Publishing Company, Amsterdam.

Nielsen, A. 1972. Rheology of building materials. National Swedish Building Research, Stockholm, Sweden.

Novak, C.A. 2009. Intrinsic Materials: Modernism, Sustainability and Fiber Cement Panels. (http://continuingeducation.construction.com/article.php?L=176&C=592&P=5). Accessed 2010.

NRC Canadian Construction Materials Centre. 2006. Evaluation report CCMC; 13016-R, 10741-R. (http://www.nrc-cnrc.gc.ca/ccmc/registry/eval/eval13000_e.shtml). Accessed 2010.

NTA. 2009. Engineered design of SIP panels using NTA listing report data. Report NTA IM 14 TIP 01.

Oehlers, D.J. 1993. Composite profiled beams. Journal of Structural Engineering, ASCE, Vol. 119, No. 4, pp. 1085-1100.

Olsson, R. 2002. Engineering Method for Prediction of Impact Response and Damage in Sandwich Panels, J. Sandwich Structures and Materials, Vol. 4, pp. 3–29.

PCI Sandwich Wall Panel Committee. 1997. PCI Report – Precast Sandwich Wall Panels. PCI Journal, Chicago, IL. (May-June).

Pflug, J., Vangrimde, B., Verpoest, I. Material efficiency and cost effectiveness of sandwich materials. Katholieke Universiteit Leuven, Belgium. (www.mtm.kuleuven.be/Research/C2/poly/phds/jp/jp_sampe_us_2.pdf). Accessed 2010.

Pierce, C.B., and Dinwoodie, J. M. 1977. Creep in chipboard, Part 1: Fitting 3- and 4-element response curves to creep data. Journal of Materials Science, Vol. 12, pp. 1955-1960.

Plantema, F.J. 1966. Sandwich Construction, John Wiley & Sons, Inc., New York .

Raville, M.E. 1955a. Supplement of analysis of long cylinders of sandwich construction under uniform external lateral pressure, facings of moderate and unequal thickness, Report no. 1844-A. U.S. Department of Agriculture, Forest Products Lab.

Raville, M.E. 1955b. Buckling of sandwich cylinders of finite length under uniform external lateral pressure, Report no. 1844-B. U.S. Department of Agriculture, Forest Products Lab.

Reddy, J.N. 2004. Mechanics of laminated composite plates and shells: theory and analysis. CRC Press.

Reissner, E., 1945. The effect of transverse shear deformation on the bending of plates. J. Appl. Mech. Vol. 12, pp. 69–77.

Reissner, E. 1950. On a variational theorem in elasticity, Journal of Mathematics and Physics, Vol. 29, pp. 90-95.

RSMeans. 2007. RSMeans SIPs Cost Study, Report Jan. Reed Construction Data/RSMeans. (http://www.sips.org/wp-content/uploads/2011/06/

RSMeansSIPSCostStudyReportJan2007.pdf). Accessed Sep, 2011.

Said, M.N.A. 2006. Task 2: Literature Review: Building Envelope, Heating, and Ventilating Practices and Technologies for Extreme Climates, B-1239.2. National Research Canada. (http://www.nrc-cnrc.gc.ca/obj/irc/doc/pubs/b-1239.2/b1239.2.pdf). Accessed 2011.

Sennah, K, Zarghooni, M. H., Butt, A. 2009. Long-term Flexural Creep Behavior of Structural Insulated Sandwich Foam-Timber Panels for Residential Construction. Technical Report Submitted to Thermapan Structural Insulated Panels Inc., Fort Erie, Ontario, Canada, 69 pages.

Sennah, K , Zarghooni, M. 2010. Development of Creep Model for Structural Insulated Timber-Foam Panels for Roof Construction under Sustained Loading. Proceedings of the 2nd International Structures Specialty Conference, Canadian Society for Civil Engineering, Winnipeg, Manitoba, pp. 1-10.

Schwarz, H.R. 1984. Methode der Finiten Elemente. BG Teubner, Stuttgart.

Shaw, T. Side-by-Side Study Proves SIP Advantage. Brock University, Canada. (http://www.grandcountysips.com/Comparison.pdf). Accessed Sep, 2011.

Stamm, K., Witte, H., 1974. Sandwichkonstruktionen. Springer-Verlag, (in German).

Straalen, I.J. 1998. Comprehensive Overview of Theories for Sandwich panels. (www.dogma.org.uk/vtt/modelling/workshop/straalen2.pdf). Accessed 2010.

Structural Board Association (SBA). 2004. OSB Design Manual Construction Sheathing and Design Rated Oriented Strand Board.

Swinton, M.C. 2005. Performance Guidelines for Basement Envelope Systems and Materials. Report B1018.1. National Research Council Canada. (http://www.nrc-cnrc.gc.ca/obj/irc/doc/rr199.pdf). Accessed 2011.

Taylor, S. B. 1996. Experimental Measurement of The Flexural Creep Behavior of Structural Insulated Panel (SIP) Sandwich Beams. The Pennsylvania State University, USA.

Tham, L. G., Chong, K. P., and Cheung, Y. K. 1982. Flexural bending and axial compression of architectural sandwich panels by finite-prism-strip methods, J. Reinf. Plast. Compos. Mater., Vol. 1, pp. 16–28.

Thermapan. 2007. Thermapan PWF Foundation SIP Installation Manual. Thermapan Inc.

Thomsen, O.T. 1995. Localised Loads, Chapter 12 of the book of D. Zenkert, An Introduction to Sandwich Construction. EMAS Publishing.

Thomson, W. 1865. On the elasticity and viscosity of metals. Proc. Roy. Soc. London, Vol. 14, pp. 289–297. [Introduces what is often referred to as the Kelvin-Voigt model for viscoelastic solids. Thomson is better known as Lord Kelvin.]

Triantafillou, T.C. and Gibson, L.J. 1987. Minimum weight design of foam core sandwich panels for a given strength. Materials Sci. and Engineering, Vol. 95, pp. 55-62.

Voigt, W. 1892. Ieber innere Reibung fester korper, insbesondere der Metalle. Annalon der Physik, Vol. 283, pp. 671–693.

Wiedemann, J. 1996. Leichtbau 1: Elemente. Springer Berlin, Heidelberg.

Williams D., Legget D.M.A. and Hopkins H.G. 1941. Flat Sandwich Panels under Compressive End Loads. Royal Aircraft Establishment Report No. A.D. 3174, June.

Wineman, A.S., Rajagopal, K.R. 2001. Mechanical Response of Polymers, An Introduction. Cambridge University Press, Cambridge.

WOlfel, E., Nachgiebiger V. 1978. Eine Naherungslösung und deren AnwendungsmOglichkeiten. (Elastic bond: an approximate solution and its applications). Stahlbau, Vol. 6, pp. 173-80 (in German).

Wong, B., Helling, D. E. and Clark, R. W. 1988. A creep rupture model for two-phase eutectic solders. IEEE Transactions on Components, Hybrids and Manufacturing Technology, Vol. II, No. 3, Sept., pp. 284-290.

Wu, Q., Lee, J.N., Cai, Z., Zhou, D. 2009. Creep behavior of borate-treated strandboard: effect of zinc borate retention, wood species, and load level. Maderas. Ciencia y tecnología. Vol. 11, No. 1, pp. 19-32.

Yoon, K.J., Kim, C.K. and Park, H.C. 2002. Nonlinear Flexural Deflection of Thermoplastic Foam Core Sandwich Beam, Journal of Composite Materials, Vol. 36, pp. 1529–1540.

Yoshii, A. 1992. Optimum design of advanced sandwich composite using foam core. Advances in Composite Materials, Vol. 2, pp. 289–305.

Zarghooni, M.H. 2009. Flexural creep behavior of structural insulated timber panels. M.Sc. Thesis, Ryerson University.

Zenkert, D. 1997. The Handbook of Sandwich Construction. EMAS Publishing Co. Ltd. UK.

Zenkert D, Hallstrom S, Shipsha A. 2002. Design Aspects of Marine Sandwich Structures, Composites for Marine Structures, 6–8, University of Maryland. pp. 28–32.

Zupan, D., Srpcic, J., Turk, G. 2007. Characteristic value determination from small samples. Structural Safety, Vol. 29, pp. 268-278.

APPENDIX

Table 2.1. Viscoelastic models (Taylor, 1996)

Model		Equation
Power	Power	$\Delta_p(t) = \Delta_o + A_1 t^{A_2}$
2 element	Kelvin	$\Delta_2(t) = \Delta_o + A_1(1 - \exp(-\frac{t}{A_2}))$
3 element	Burger	$\Delta_3(t) = \Delta_o + A_1(1 - \exp(-A_2 t)) + A_3 t$
4 element	Fridley	$\Delta_4(t) = \Delta_o + A_1(1 - \exp(-A_2 t)) + A_3 t^{A_4}$

Where; Δ (t) = total time dependent deflection; Δ_o = initial deflection; A_i = creep parameters associated with creep deflection equations.

Table 2.2. K_{cr} Based on load type[1] (ASCE7, 2010)

Load Type[2]	EPS/XPS Core	Urethane Core
D, F, H, T	4.0	7.0
L	3.0	5.0
E, W, S, R, Lr, Fa	1.0	1.0

[1] Table values are for OSB facings used dry service conditions.

[2] Load type are as defined in ASCE 7-10. Where Dead load is D, Live Load is L, Snow load is S, Rain and Ice is R, Earthquake is E, Roof Live Load is Lr, Wind load is W, Flood Load is Fa, lateral earth pressure is H, and self-straining load is T.

Table 3.1 Description of the tested panels

Groups	Test No	Test Type	Panel Size (WxLxT), mm	OSB Thickness	Plywood Thickness	Connection Type	Specimen Name
I	1	Long-term creep	1220x3048x260.3 (4'x10'x10.25")	11 mm (7/16")	15.5 mm (5/8")	Lumber	BW1
	2	Long-term creep	1220x3048x260.35 (4'x10'x10.25")	11 mm (7/16")	15.5 mm (5/8")	Lumber	BW2
	3	Long-term creep	1220x3048x260.35 (4'x10'x10.25")	11 mm (7/16")	15.5 mm (5/8")	Lumber	BW3
II	4	Long-term creep	1220x2743.2x209.55 (4'x9'x8.25")	11 mm (7/16")	15.5 mm (5/8")	Lumber	BW4
	5	Long-term creep	1220x2743.2x209.55 (4'x9'x8.25")	11 mm (7/16")	15.5 mm (5/8")	Lumber	BW5
	6	Long-term creep	1220x2743.2x209.55 (4'x9'x8.25")	11 mm (7/16")	15.5 mm (5/8")	Lumber	BW6
III	7	Eccentric axial load test (t/6 eccentricity)	1220x3048x260.35 (4'x10'x10.25")	11 mm (7/16")	15.5 mm (5/8")	Lumber	BW1
	8		1220x3048x260.35 (4'x10'x10.25")	11 mm (7/16")	15.5 mm (5/8")	Lumber	BW2
	9		1220x3048x260.35 (4'x10'x10.25")	11 mm (7/16")	15.5 mm (5/8")	Lumber	BW3
IV	10	Eccentric axial load test (t/6 eccentricity)	1220x2743.2x209.55 (4'x9'x8.25")	11 mm (7/16")	15.5 mm (5/8")	Lumber	BW4
	11		1220x2743.2x209.55 (4'x9'x8.25")	11 mm (7/16")	15.5 mm (5/8")	Lumber	BW5
	12		1220x2743.2x209.55 (4'x9'x8.25")	11 mm (7/16")	15.5 mm (5/8")	Lumber	BW6
V	13	Flexural test (4 Point Loading)	1220x3048x260.35 (4'x10'x10.25")	11 mm (7/16")	15.5 mm (5/8")	Lumber	BW1
	14		1220x3048x260.35 (4'x10'x10.25")	11 mm (7/16")	15.5 mm (5/8")	Lumber	BW2
	15		1220x3048x260.35 (4'x10'x10.25")	11 mm (7/16")	15.5 mm (5/8")	Lumber	BW3

Table 4.1. Load combination for ultimate limit states (NBCC, 2005)

Case	Load Combination	
	Principal Loads	Companion Loads
1	1.4D	
2	1.25D +1.5L	0.5S
3	1.25D +1.5S	0.5L

Note: D is dead load due to the weight of the building components, L is live load due to intended use and occupancy and S is the snow load.

Table 4.2. Instantaneous deflection of tested specimens at the start of flexural creep testing

Specimen No.	Experimental deflection, mm	Experimental deflection-to-span ratio	Average ratio	Deflection limit
BW1	7.690	1/396	1/379	1/300
BW2	8.023	1/380		
BW3	8.390	1/363		
BW4	8.140	1/337	1/341	1/300
BW5	7.240	1/378		
BW6	8.715	1/314		

Table 4.3. Recorded creep deflection and creep recovery of the tested specimens

Species	Location	Creep		Relative Creep %	Recovery	
		ID (mm)	MD (mm)		IRD (mm)	PD (mm)
BW1	0.45L	7.690	10.995	43	7.4225	2.7275
BW2		8.023	11.2767	41	6.5133	4.450
BW3		8.390	11.08	32	7.8600	2.615
Average		8.0343	11.12	38.6		
BW4	0.45L	8.140	11.35	39	7.7100	3.310
BW5		7.240	10.02	38	7.0100	2.340
BW6		8.715	11.115	28	8.3125	2.135
Average		8.03167	10.8283	35		

Where: ID = Instantaneous deflection, MD = Maximum deflection, IRD = Instantaneous recovery deflection, PD = Permanent deflection.

Table 4.4. Compression test failure modes

Name	Failure Type
BW1	Overall deflection, with failure of the OSB face with yielding / fracture at about 200 mm from the top of the wall, per Figures 4.5 to 4.8.
BW2	Overall deflection for the panels towards the OSB face, leads to delamination (debonding) of the interface between the core (lumber and EPS) and the OSB face. flexure failure of the core lumber, and separation of the bottom lumber footer, per Figures 4.9 to 4.13.
BW3	Overall deflection, with failure of the face with yielding / fracture at about 200 mm from the top of the wall, per Figures 4.14 to 4.16 .
BW4	Global flexural deformation as well as delamination of OSB side form the core foam. This is in addition to OSB crushing at about 100 mm from the top of the panel, per Figures 4.17 to 4.19.
BW5	Crushing in the OSB face within the first 50 mm from the top of the wall, per Figures 4.20 to 4.21.
BW6	Crushing Failure of the OSB at about 200 and 400 mm from the top of the panel, per Figures 4.22 to 4.24.

Table 4.5. Axial load test results per panel width

Panel	Panel Size, mm	Experimental Axial Load	Axial Displacement, mm			Lateral Displacement, mm		
		kN	POT-1	POT-2	Average	LVDT-3	LVDT-4	Average
BW1	1220x3048x26.35	291.46	22.07	23.24	22.655	4.39	4.94	4.665
BW2		341.83	25.01	44.69	34.85	5.66	3.39	4.525
BW3		285.47	23.18	23.33	23.255	8.43	9.83	9.13
Average		306.25						
BW4	1220x27432209.5	173.69	13.2	27.46	20.33	4.48	16.18	10.33
BW5		182.86	15.64	51.83	33.735	13.92	12.98	13.45
BW6		292.94	20.44	34.13	27.285	7.31	14.17	10.74
Average		216.5						

Note: Three tests of each type are required with none of the results varying more than 15 % percent from the average of the three, unless the lowest test value is used.

Table 4.6. Flexural load test results per panel width

Panel	Size	Experimental ultimate jacking load	Maximum deflection (mm)				
			LVDT-1	LVDT-2	LVDT-3	LVDT-4	Average
		kN	mm	mm	mm	mm	mm
BW1	1220x3048x260.35	64.87	28.5	27.54	26.83	25.82	27.1725
BW2		56.20	38.35	37.6	37.49	36.78	37.555
BW3		89.11	54.96	51.39	47.9	45.7	49.9875
Average		70.06	38.238				
BW4	1220x2743.2x209.5	51.54	23.93	27.88	27.09	25.98	26.22
BW5		49.77	33.7	41.16	40.24	43.3	39.6
BW6		50.99	20.8	28.44	30.33	32.83	28.1
Average		50.77	31.31				

Note: Three tests of each type are required with none of the results varying more than 15 % percent from the average of the three, unless the lowest test value is used.

Table 5.1. Creep parameters obtained for the creep models

Specimens	Model	A1 (K for Log. Exp)	A2	A3	A4	SSE
Group I	Power	0.0219327539845	0.589028101282			7.628
	Kelvin	3.61043265888	2237.21019600			5.015
	Burger	0.999735917564	0.0014875056222	.00046786900318		8.852
	Fridley *	**3.60944090980**	**0.0004419719749**	**0.0117031861254**	**2.0715620782E-08**	5.013
	Log. Exp	0.25515642375				54.02
Group II	Power	0.0032322780244208	0.8205188972397			14.22
	Kelvin	5.65848285006871	5337.9813778277			12.25
	Burger	0.999737178565103	0.0005084573927	0.0005156577294		13.68
	Fridley *	**3.60944090980833**	**0.0004419719749**	**0.0117031861254**	**2.0715620782E-08**	18.29
	Log. Exp	0.229702				85.16

(*) Constants used in Equation 5.16

N.B. Constants referred to equations in Table 2.1

Table 5.2. Prediction for creep-deflection for panels BW1, BW2 and BW3

Years	Hours	Experimental Results, mm	Power Model, mm	Kelvin Model, mm	Burger Model, mm	Fridley Model, mm	Log. Exp. Model, mm
	0	8.0343*	8.0343*	8.0343*	8.0343*	8.0343*	8.0343*
	24	8.71	8.176886	8.072824	8.08059	8.084087	8.855617
	720	9.44	9.091464	9.027812	9.028328	9.029782	9.713392
	1440	9.835	9.624521	9.747932	9.590379	9.745425	9.890076
	2160	10.85	10.0535	10.26989	10.00441	10.26601	9.993474
	5780	11.67	11.63987	11.37213	11.73813	11.37491	10.24455
1	8760		12.64046	11.57278	13.13257	11.58028	10.35063
5	43800		19.92074	11.64473	29.5267	11.65544	10.76126
10	87600		25.91428	11.64473	50.01936	11.65544	10.93812
50	438000		54.17455	11.64473	213.9607	11.65544	11.34878
75	657000		66.62149	11.64473	316.424	11.65544	11.45223

(*) Instantaneous deflection

Table 5.3. Prediction for creep-deflection for panels BW3, BW4 and BW5

Years	Hours	Experimental Results, mm	Power Model, mm	Kelvin Model, mm	Burger Model, mm	Fridley Model, mm	Log. Exp. Model, mm
	0	8.03167*	8.03167*	8.03167*	8.03167*	8.03167*	8.03167*
	24	8.42	8.078153	8.057054	8.056171	8.081457	8.771053
	720	8.42	8.748803	8.745665	8.709422	9.027152	9.543257
	1440	8.755	9.296142	9.369567	9.29322	9.742795	9.702315
	2160	9.885	9.794212	9.914745	9.811867	10.26338	9.795398
	5780	11.35	11.98107	11.77394	11.959	11.37228	10.02143
1	8760		13.58577	12.59369	13.53694	11.57765	10.11692
5	43800		28.82772	13.68861	31.61722	11.65281	10.48659
10	87600		44.75633	13.69015	54.20302	11.65281	10.64581
50	438000		145.5793	13.69015	234.8895	11.65281	11.0155
75	657000		199.8707	13.69015	347.8185	11.65281	11.10863

(*) Instantaneous deflection

Table 5.4. Predicted relative creep after 75 Years based on Logarithmic Expression and Fridley's Model

		Creep Deflection		
Type	Model	ID, mm	MD, mm @75 years	Relative Creep, C_t
Group I	Fridley	8.0343	11.65544	0.4507
	Log Expression	8.0343	11.45223	0.4254
Group II	Fridley	8.03167	11.65281	0.4508
	Log Expression	8.03167	11.10863	0.3831

ID: instantaneous deflection
MD: Maximum deflection

Table 5.5.a. Stress equivalency constants for the proposed creep model in Equation 5.18

Panel No.	a	b	c	m
BW1, BW2 and BW3	0.001	0.007689	0.003223	0.001
BW4,BW5, and BW6	0.001	9.94E-5	0.000949	0.001

Table 5.5.b. Creep Coefficients obtained by Least-Squares for the proposed creep model in Equation 5.19

Panel No.	K_e	K_k	η_k	η_v	n	SSE*
BW1, BW2 and BW3	--	0.275646	160417	9.190288	0.542119	3.855977
BW4,5,6	--	0.345007	160417	8.377447	0.754815	3.929337

. (*) SSE: Summation of Square of Errors.

Table 5.6. Predicted total deflection using the proposed creep model with different temperatures and relative humidifies

a. Predicted total deflection for group I

Group I	Temperature in C			Relative Humidity in %			Proposed Creep Model
	23.5			40			
	Relative Humidity in %			Temperature in C			
	22	44	65	22.5	23.5	24.5	

Years	Hours	Stress Equivlancy			Stress Equivlancy			Parameters
		0.2526	0.32351	0.39119	0.30292	0.31061	0.3183	
	24	8.18827	8.2315	8.27275	8.21895	8.22364	8.22832	
	168	8.47663	8.60079	8.71931	8.56475	8.57822	8.59168	
	720	9.00844	9.28189	9.54291	9.20252	9.23217	9.26182	
1	8640	11.7903	12.8446	13.851	12.5386	12.6529	12.7673	
2	17280	13.5106	15.0478	16.5152	14.6016	14.7683	14.935	
3	25920	14.8634	16.7804	18.6102	16.224	16.4318	16.6397	
4	34560	16.0222	18.2644	20.4048	17.6136	17.8567	18.0999	
5	43800	17.1234	19.6747	22.1101	18.9342	19.2109	19.4875	
10	87600	21.3003	25.0242	28.5787	23.9433	24.3471	24.7509	
50	438000	39.9568	48.9176	57.4712	46.3167	47.2884	48.2601	
75	657000	47.8209	58.9892	69.6499	55.7475	56.9586	58.1697	

a	0.001
m	0.001
b	0.00769
c	0.00322
Kk	0.27565
nk	160417
nv	9.19029
n	0.54212
Stress	4.7
ID	8.0343

b. Predicted total deflection for group II

Group II	Temperature in C			Relative Humidity in %			Proposed Creep Model
	23.5			40			
	Relative Humidity in %			Temperature in C			
	22	44	65	22.5	23.5	24.5	

Years	Hours	Stress Equivlancy			Stress Equivlancy			Parameters
		0.02422	0.04509	0.065022	0.0412	0.0413	0.0414	
	24	8.0635	8.09094	8.117138	8.08582	8.08595	8.08608	
	168	8.16995	8.28917	8.402973	8.26693	8.26749	8.26806	
	720	8.44648	8.80412	9.14551	8.7374	8.7391	8.7408	
1	8640	10.7389	13.073	15.30107	12.6375	12.6487	12.6598	
2	17280	12.6003	16.5393	20.29919	15.8043	15.8231	15.8418	
3	25920	14.2364	19.586	24.69248	18.5879	18.6134	18.6389	
4	34560	15.7416	22.3888	28.73396	21.1486	21.1802	21.2119	
5	43800	17.2517	25.201	32.78897	23.7178	23.7557	23.7935	
10	87600	23.5911	37.0061	49.81128	34.5031	34.567	34.6309	
50	438000	60.4647	105.671	148.823	97.2367	97.4519	97.6671	
75	657000	79.2334	140.622	199.2199	129.168	129.46	129.753	

a	0.001
m	0.001
b	9.94E-05
c	0.00095
Kk	0.34501
nk	160417
nv	8.37745
n	0.75482
Stress	4.7
ID	8.03167

Table 5.7. Values of the factor Ks in Equation 5.22 (BS-EN-14358)

Number of test specimens n	Factor Ks
3	3.15
5	2.46
10	2.10
15	1.99
20	1.93
30	1.87
50	1.81
100	1.76
500	1.71
∞	1.65

Table 5.8 Characteristic Strength of tested panel groups per ICC AC-04 and BS-EN-14358

Specimens	Design compressive load		Design total applied flexural load	
	AC-04	BS-EN-14358	AC-04	BS-EN-14358
Group I	285.47	223.765	56.20	40.22354
Group II	173.69	84.878	49.77	43.364

Table 5.9. Design Tables for PWF made of SIPs of 3 m height

a. Using basic average per ICC AC-04

Group I	Supported joist Length [(1)], m Specified Snow Load, kPa					Load Case 1
	1	1.5	2	2.5	3	
Roof and Floor	116.7441	109.9568	103.9154	98.50322	93.62692	
Roof and 2 Floors	65.6673	63.39514	61.27496	59.292	57.43336	
Roof and 3 Floors	44.77236	43.66962	42.6199	41.61946	40.66491	
Group I	Supported joist Length [(1)], m Specified Snow Load, kPa					Load Case 2
	1	1.5	2	2.5	3	
Roof and Floor	135.414	111.4707	94.72228	82.34934	72.83534	
Roof and 2 Floors	94.27846	84.30662	74.3623	66.51641	60.16813	
Roof and 3 Floors	71.20523	67.7876	61.20636	55.78993	51.25421	

(1) Supported joist length means the distance between the PWF exterior wall and the nearest parallel wall. Maximum supported length of roof is based on 0.5 kPa dead load, 1.9 kPa live load for floors and a specified snow load as shown on flat roofs. Wall with brick veneer

b. Using 5-percentile characteristic value per BS-EN-14358

Group I	Supported joist Length [(1)], m Specified Snow Load, kPa					Load Case 1
	1	1.5	2	2.5	3	
Roof and Floor	87.98683	82.87144	78.31816	74.23917	70.56404	
Roof and 2 Floors	48.96959	47.27519	45.69412	44.21538	42.82936	
Roof and 3 Floors	33.00808	32.1951	31.4212	30.68363	29.9799	
Group I	Supported joist Length [(1)], m Specified Snow Load, kPa					Load Case 2
	1	1.5	2	2.5	3	
Roof and Floor	102.0578	84.0124	71.38958	62.06444	54.894	
Roof and 2 Floors	70.30558	63.53958	56.04482	50.13159	45.34707	
Roof and 3 Floors	52.49551	51.08965	46.12955	42.04734	38.62889	

Table 5.10. Design Tables for PWF made of SIPs of 2.74 m height

Using basic average per ICC AC-04

Group II	Supported joist Length [(1)], m Specified Snow Load, kPa					Load Case 1
	1	1.5	2	2.5	3	
Roof and Floor	63.69567	59.99252	56.6963	53.74343	51.08291	
Roof and 2 Floors	35.07703	33.86333	32.73081	31.67158	30.67877	
Roof and 3 Floors	23.36947	22.79389	22.24597	21.72378	21.22554	
Group II	Supported joist Length [(1)], m Specified Snow Load, kPa					Load Case 2
	1	1.5	2	2.5	3	
Roof and Floor	73.882	60.81849	51.68054	44.92986	39.73901	
Roof and 2 Floors	50.36005	45.99775	40.57212	36.2914	32.82777	
Roof and 3 Floors	37.16643	36.98496	33.39423	30.43903	27.96433	

(1) Supported joist length means the distance between the PWF exterior wall and the nearest parallel wall. Maximum supported length of roof is based on 0.5 kPa dead load, 1.9 kPa live load for floors and a specified snow load as shown on flat roofs. Wall with brick veneer

Using 5-percentile characteristic value per BS-EN-14358

Group II	Supported joist Length [(1)], m Specified Snow Load, kPa					Case 1
	1	1.5	2	2.5	3	
Roof and Floor	27.44125	25.84586	24.42579	23.15364	22.00744	
Roof and 2 Floors	14.02616	13.54084	13.08798	12.66443	12.26744	
Roof and 3 Floors	8.538201	8.327907	8.127722	7.936936	7.754901	
Group II	Supported joist Length [(1)], m Specified Snow Load, kPa					Case 2
	1	1.5	2	2.5	3	
Roof and Floor	31.8297	26.2017	22.26491	19.3566	17.12029	
Roof and 2 Floors	20.13734	19.81666	17.4792	15.63499	14.1428	
Roof and 3 Floors	13.57902	15.93379	14.38684	13.11368	12.04754	

Figure 1.1. Comparison of SIP with I-beam section

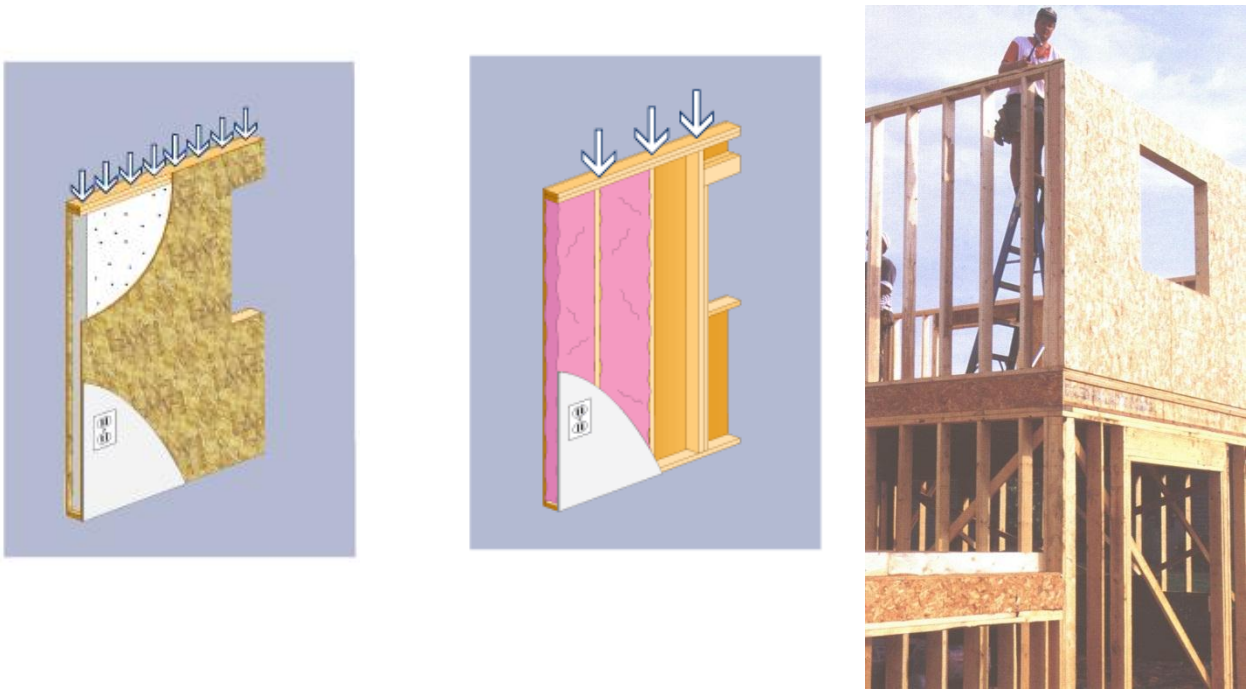

Figure 1.2. Comparison of SIP with stud wall system

(a) Industrial

(b) Commercial

(c) Residential

Figure 1.3. Use of SIPs in industrial, commercial and residential buildings (http://planetpanels.com/tag/structural-insulated-panels/)

Treated plywood exterior OSB interior face

Figure 1.4. View of the proposed SIP foundation wall

Figure 1.5. Views of the use of SIPs as preserved wood foundation in residential construction

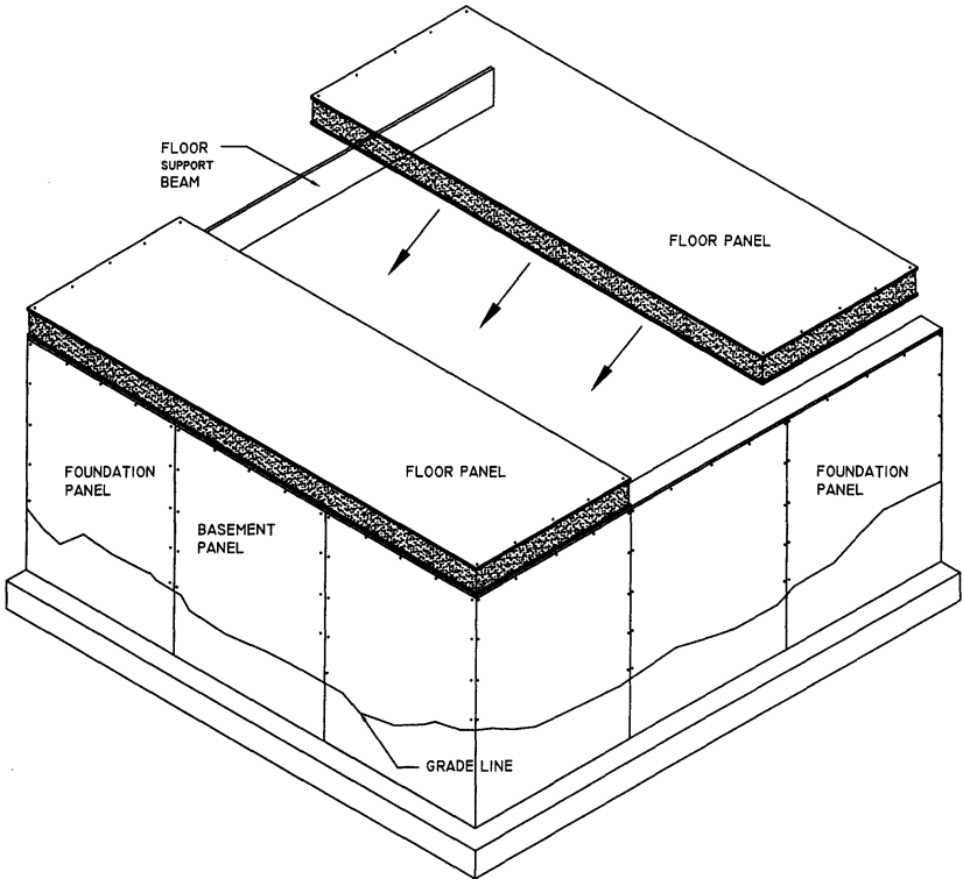

Figure 1.6. Typical floor and basement wall construction using SIPs

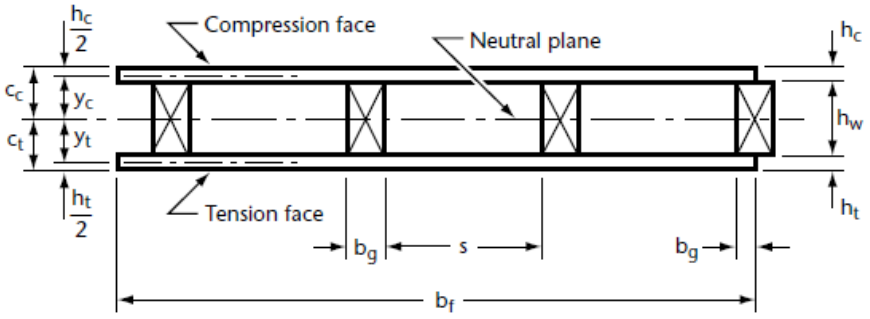

h_c = flange thickness under compression, mm
b_g = stud thickness, mm
c_t = distance from neutral axis to tension face, mm
c_c = distance from neutral axis to tension compression, mm
s = spacing between studs, mm
h_t = flange thickness under tension, mm
b_f = width of flange, mm
$y_t = c_t - h_t$, mm
$y_c = c_c - h_c$, mm

Figure 1.7. Schematic Diagram of Stressed-Skin Panel (CWC, 2005)

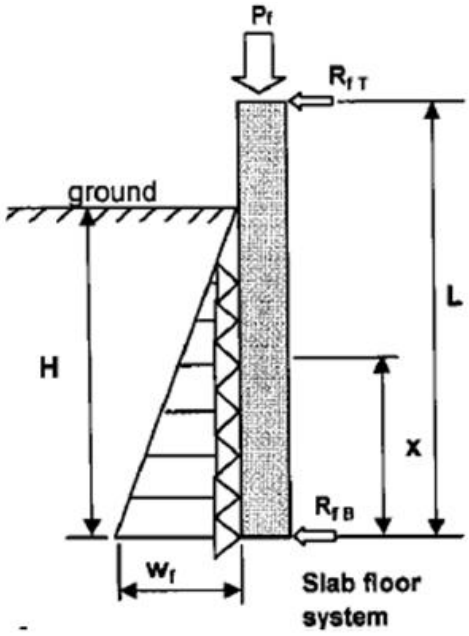

Legend

L = Panel height (mm)
X = Location of maximum bending moment (mm)
H = Height of backfill (mm)
P_f = Factored axial load, N
W_f = Maximum factored lateral load, N/mm
R_{fT} = Inward reaction at top of panel, N
R_{fb} = Inward reaction at bottom of panel, N

Figure 1.8. Loading of the permanent wood foundation (CWC, 2005)

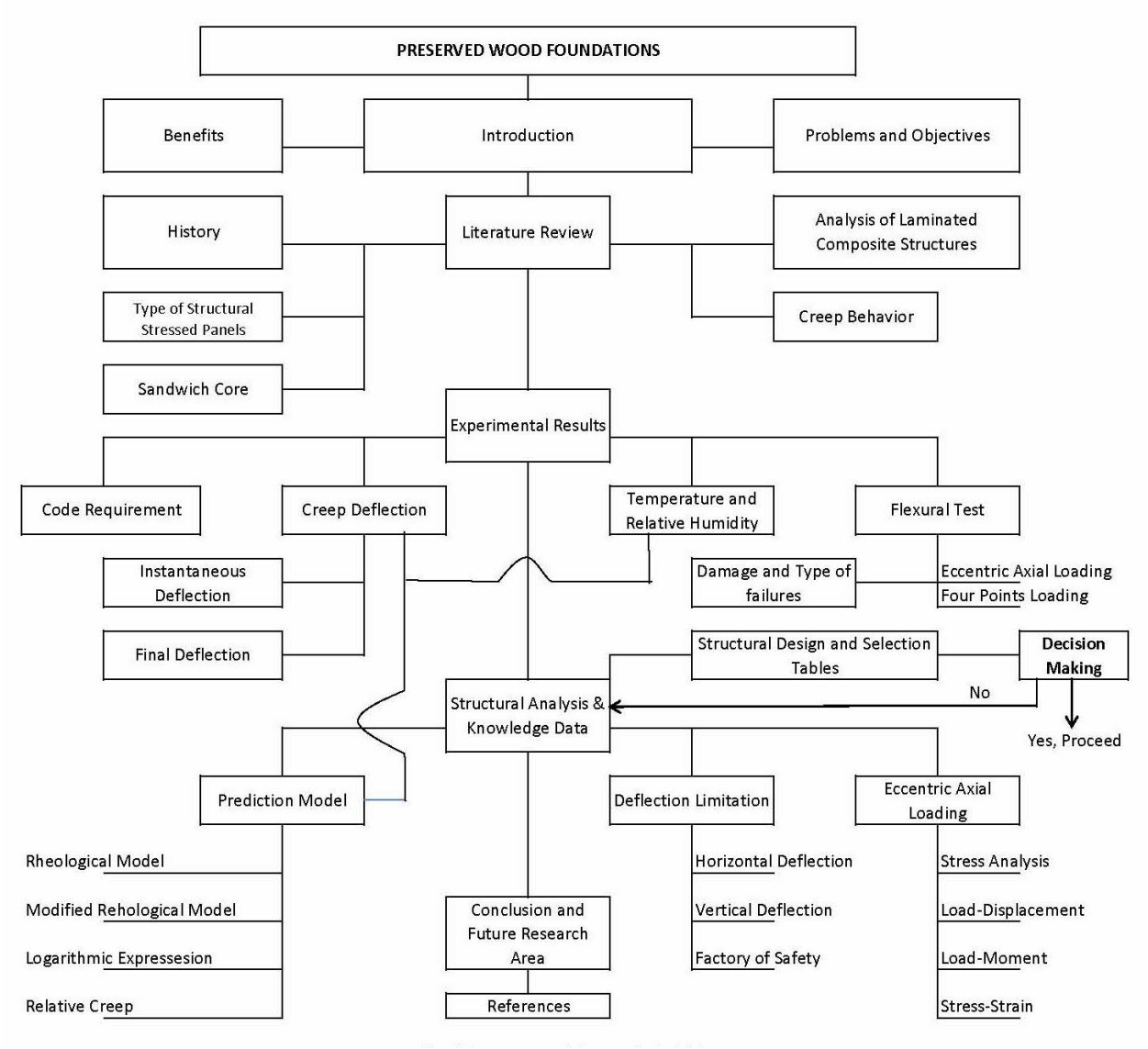

Figure 1.9. Flow Chart of Thesis structure and research activities

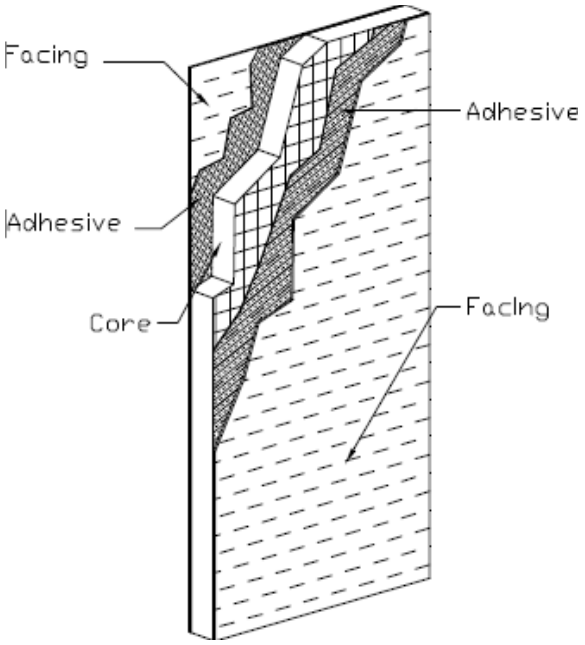

Figure 2.1. Cross Sectional View of SIP (http://www.sips.org/)

Figure 2.2. View of Lightweight Structural Cold-Formed Steel (CFS) (http://www.steelframing.org)

Figure 2.3. View of Steel SIP (www.steelsip.com)

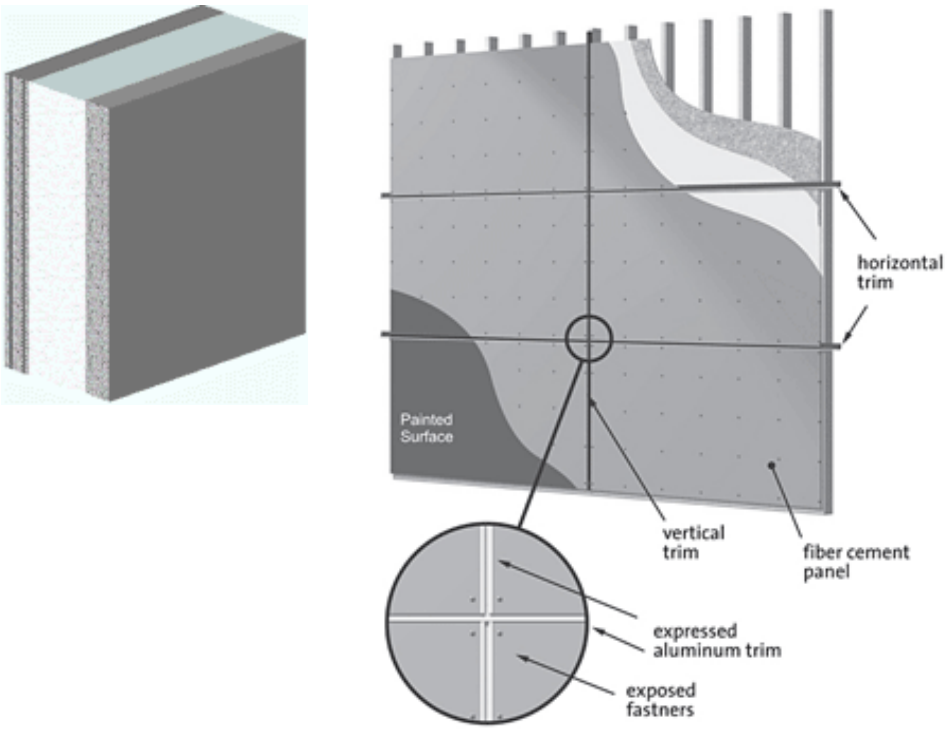

Figure 2.4. View of Structural Insulated Panel Made of Fiber Cement (Novak, 2009)

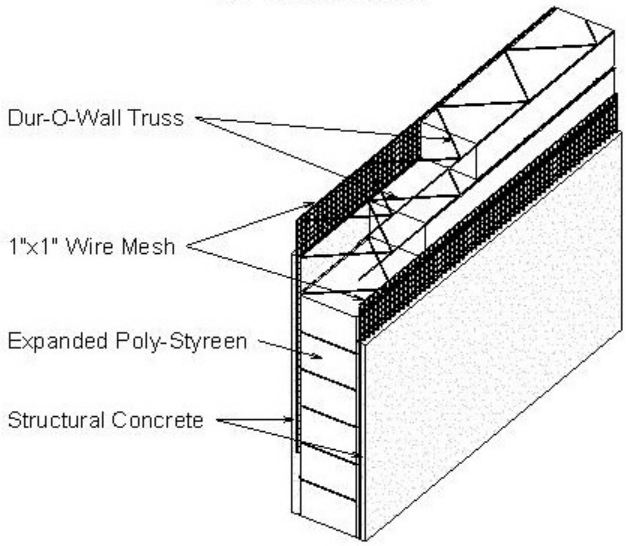

Figure 2.5.a. K-Panel Detail for Concrete Sandwich Panel
(http://www.cswall.com/CSW/Walls/index.cfm)

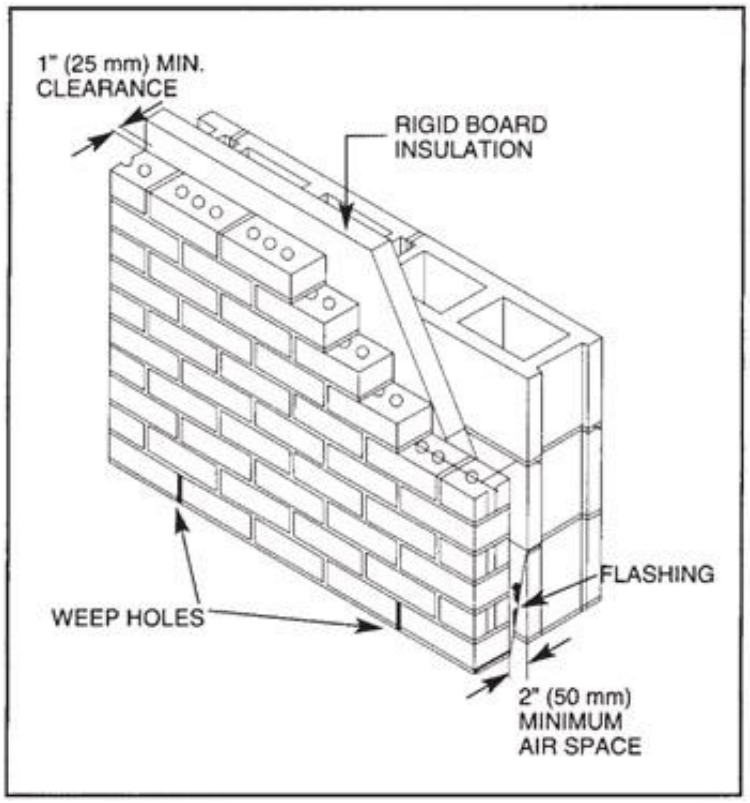

Figure 2.5.b.Brick clad masonry concrete panel (Brick Industry Association.)

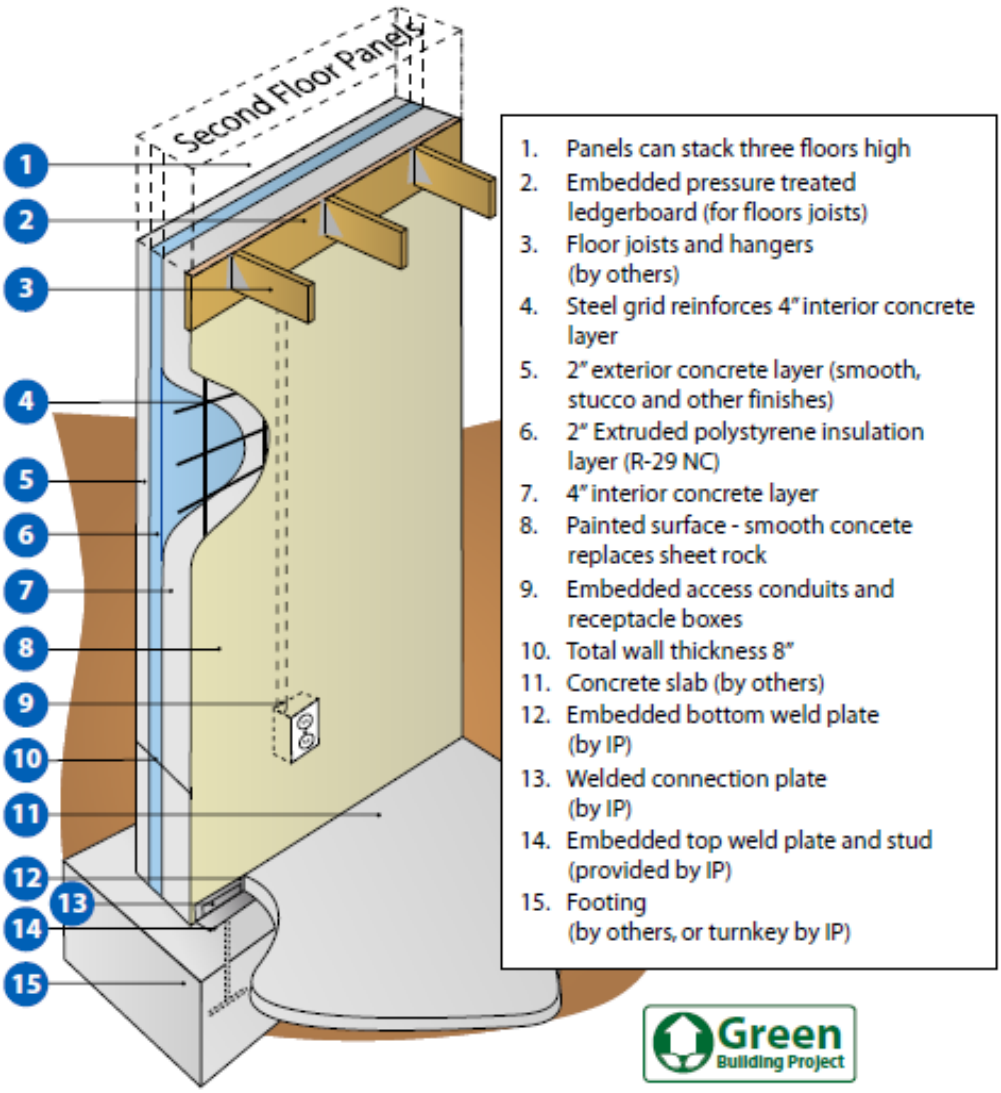

Figure 2.6. Insulated Precast Concrete (IPC) System
(http://www.international-precast.com/Residential-Wall-Panels.aspx)

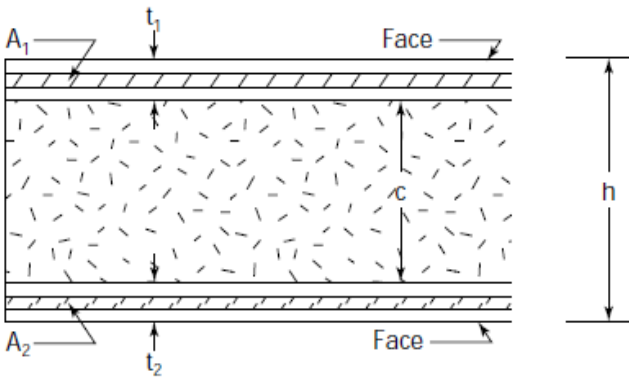

A_1= Cross-Sectional Area for top face t_1 = face thickness for top face
A_1= Cross-Sectional Area for top face t_1 = face thickness for bottom face
C = Core depth h = total panel thickness

Figure 2.7. Cross section for Plywood Sandwich Panel (APA, 1990)

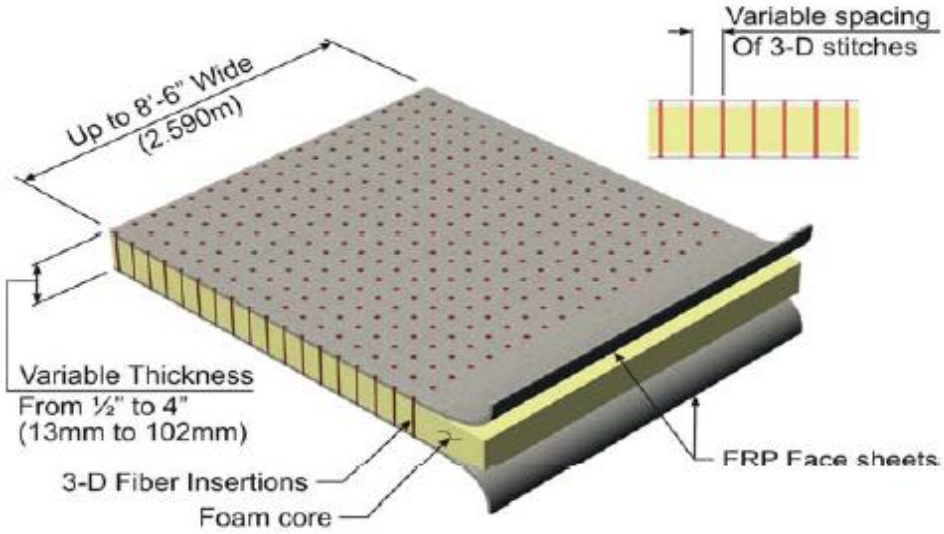

Figure 2.8. Schematic diagram of FRP Sandwich Panel (Hassan et al, 2003)

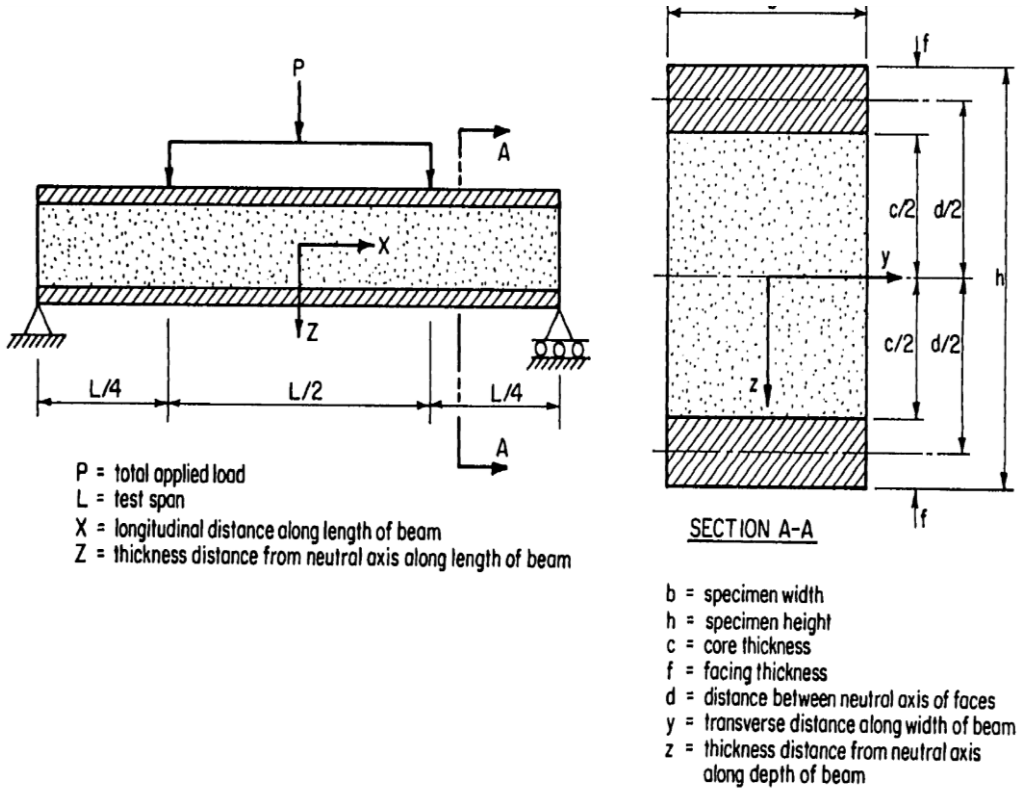

Figure 2.9. Dimensions of Sandwich Panel (Taylor, 1996)

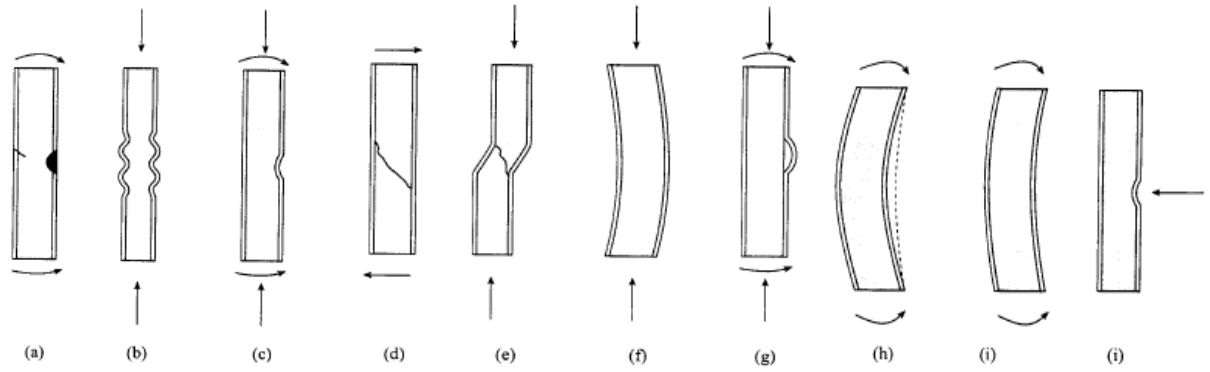

Figure 2.10. Failure Modes of walls
(a) failure of the face; yielding or fracture, (b) wrinkling of the face, (c) dimpling of the face, (d) shear failure of the core materials, (e) shear crimping of the core materials, (f) overall buckling, (g) delamination of the interface between the core and the face (h) long-term creep (i) overall deflection and (j) local deflection (Source; Straalen et al, 2010)

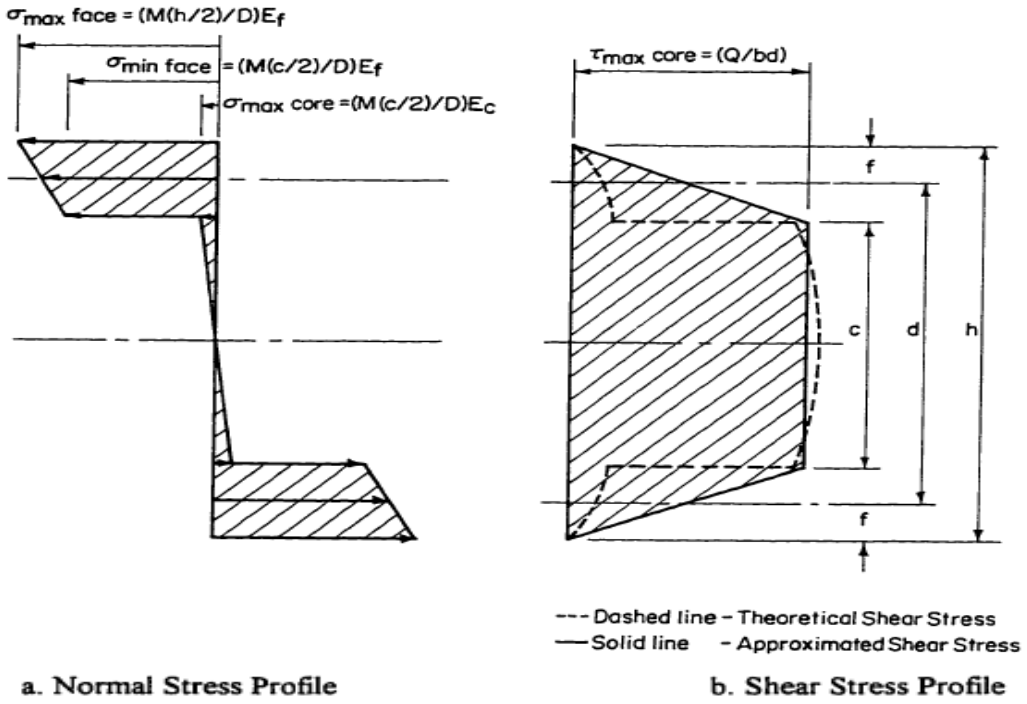

Figure 2.11. Flexural Stress and Shear Stress Distribution across the Depth of the Sandwich Panel (Taylor, 1996)

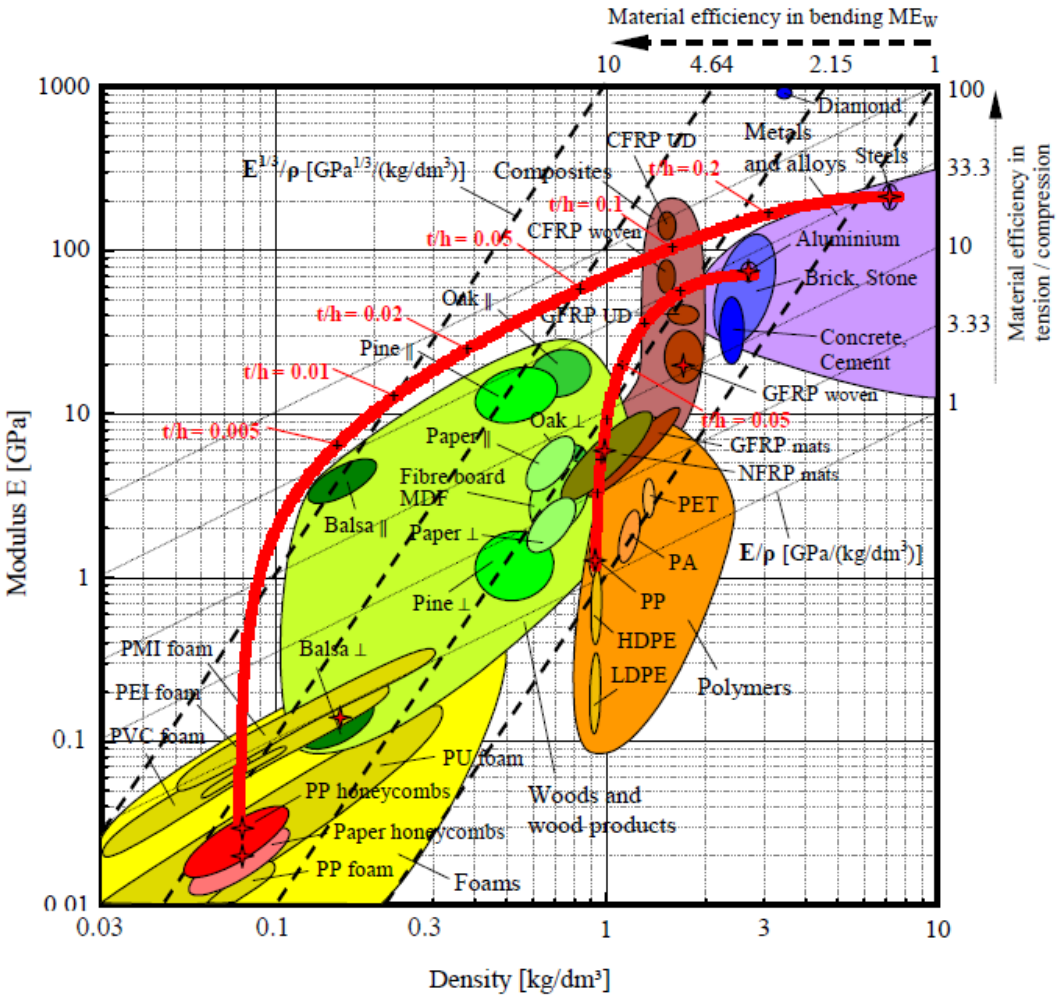

Figure 2.12. Sandwich Selection with chart for modulus versus density (Jochen Pflug et al., 2008)

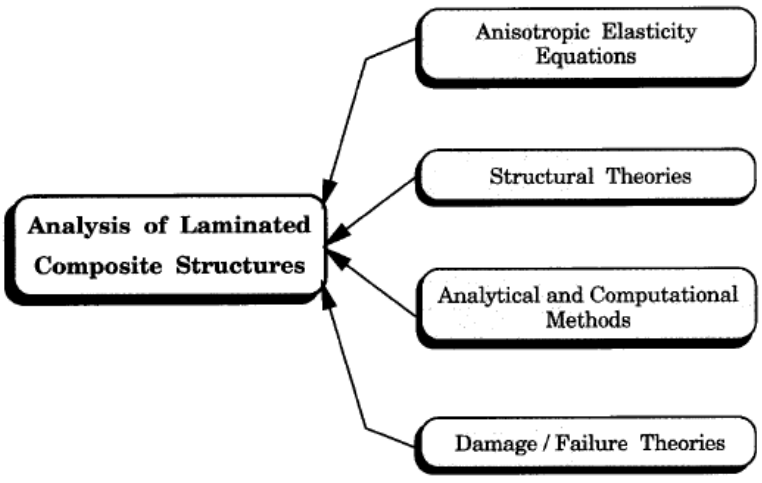

Figure 2.13. Basic blocks in analysis for composite materials (Reddy, 2004)

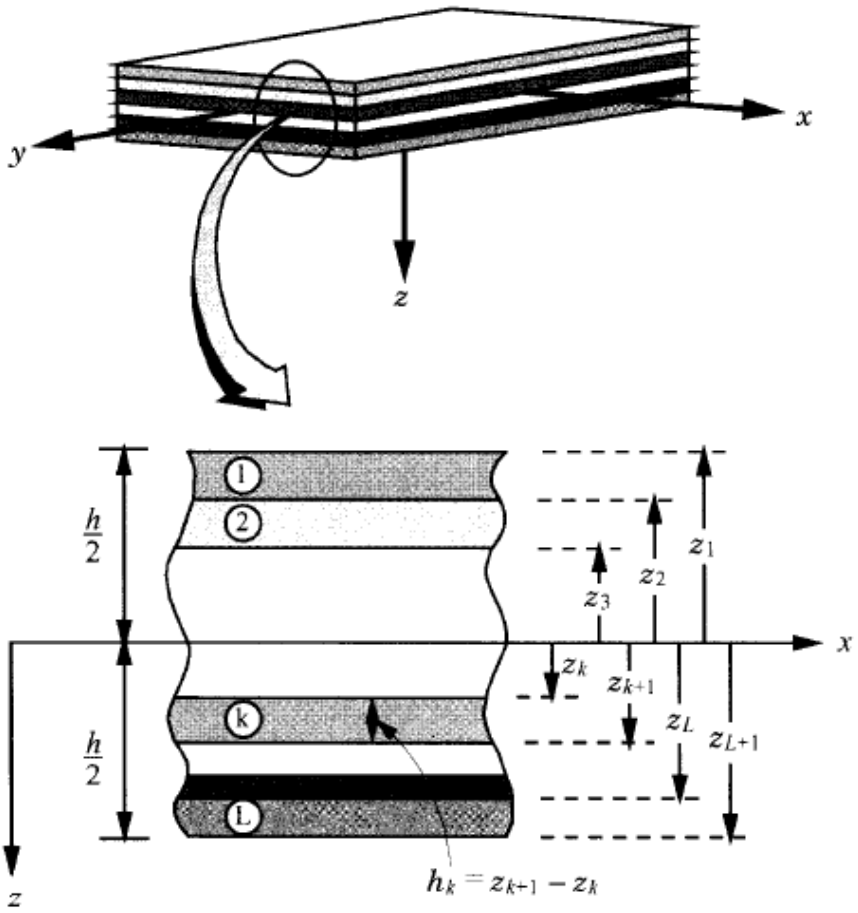

h = Total Thickness of the Laminated Plate

Z = is the z-axis

k^{th} is the location of the lamina layers

Figure 2.14. Coordinate system and layer numbering used for a laminated plate (Reddy, 2004)

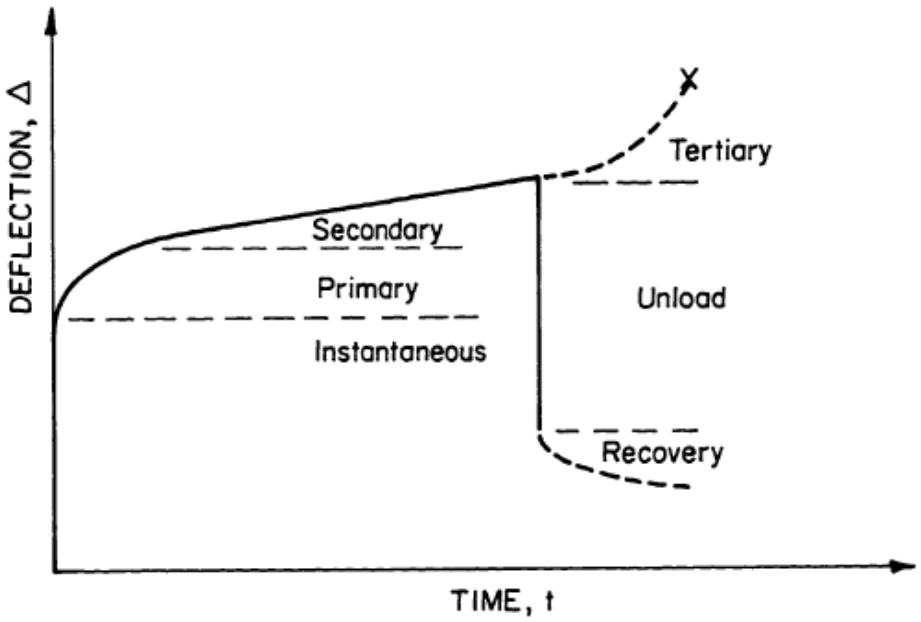

Figure 2.15. Schematic Diagram of Flexural Creep Behavior

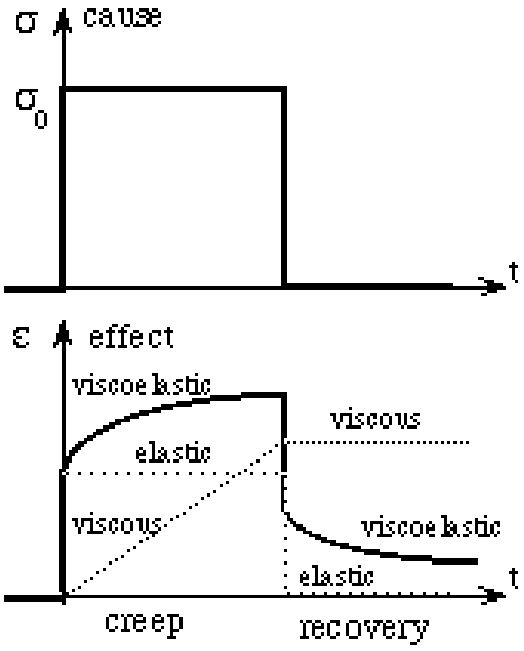

a. Creep and recovery: Stress, σ, and strain, ε, vs. time, t (http://silver.neep.wisc.edu/~lakes/VEnotes.html)

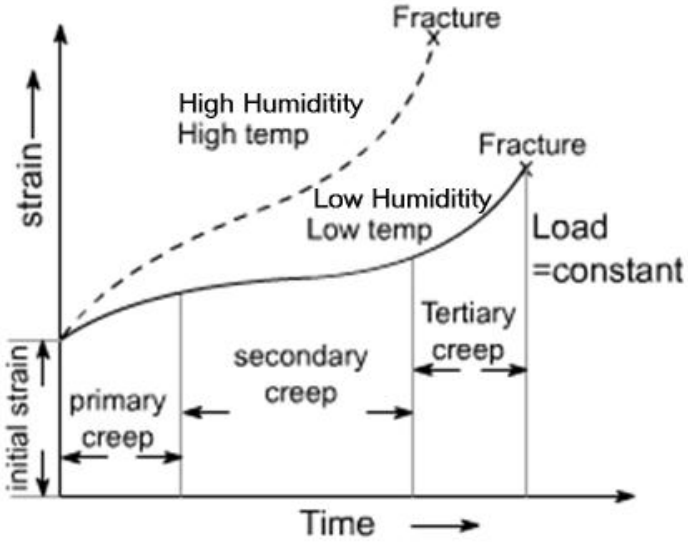

b. Regions of creep behaviour: Strain, ε, vs. time, t, for different humidity and temperature levels

Figure 2.16. Schematic Diagram of Viscoelasticity Demonstration on creep

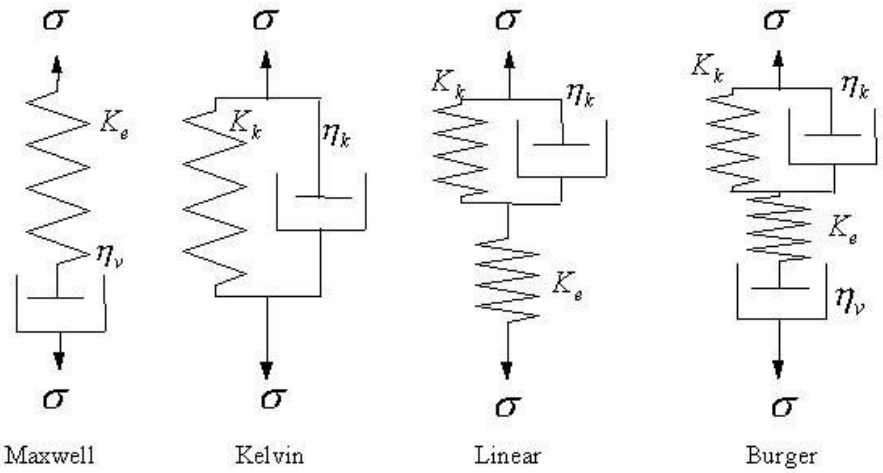

Where

σ = Stress

K_e, K_k = the elastic modulus (E) represented as spring

$\boldsymbol{\eta_v}$ = $\boldsymbol{\eta_k}$ = the viscosity represented as dashpot

Figure 2.17. Commonly used creep models for a viscoelastic material, (Wu. Q., 2009)

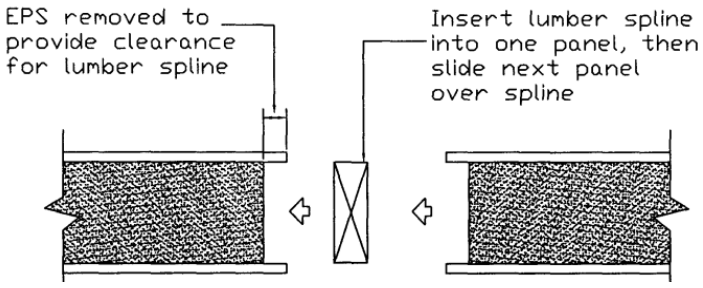

Figure 3.1. Typical section at panel lumber-spline connection before assembly

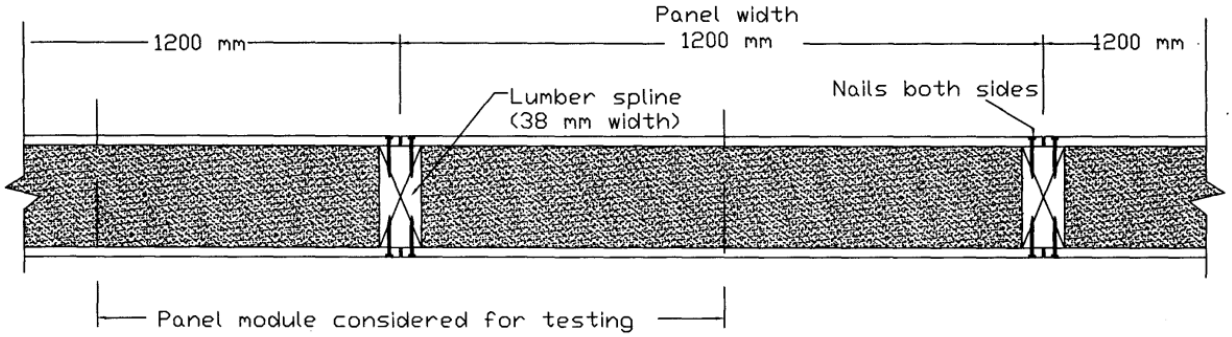

Figure 3.2. Typical section at panel lumber-spline connection before and after assembly

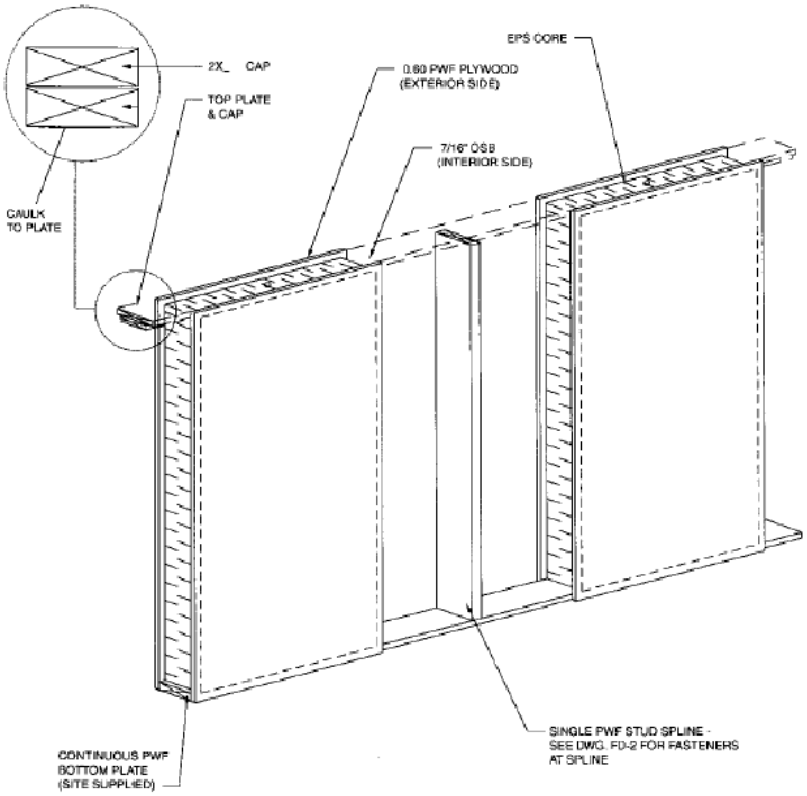

Figure 3.3. Schematic diagram of SIP Wall with Lumber-Spline Connection during assembly

Loading Area; 1200 mm X 2700 mm

Pile	Length mm	Layers Num	Quantity Per layer	Unit Wt N	Total Wt N	Total Bricks
1	200	7	12	28.8	2419.2	84
2	200	7	12	28.8	2419.2	84
3	200	6	12	28.8	2073.6	72
4	200	6	12	28.8	2073.6	72
5	200	5	12	28.8	1728	60
6	200	5	12	28.8	1728	60
7	200	5	12	28.8	1728	60
8	200	4	12	28.8	1382.4	48
9	200	4	12	28.8	1382.4	48
10	200	3	12	28.8	1036.8	36
11	200	3	12	28.8	1036.8	36
12	200	2	12	28.8	691.2	24
13	200	2	12	28.8	691.2	24
14	100	1	6	28.8	172.8	6
14	2,700.00	OK		OK	20,563.20	714.00
Pile	mm	Test Value			N	Num

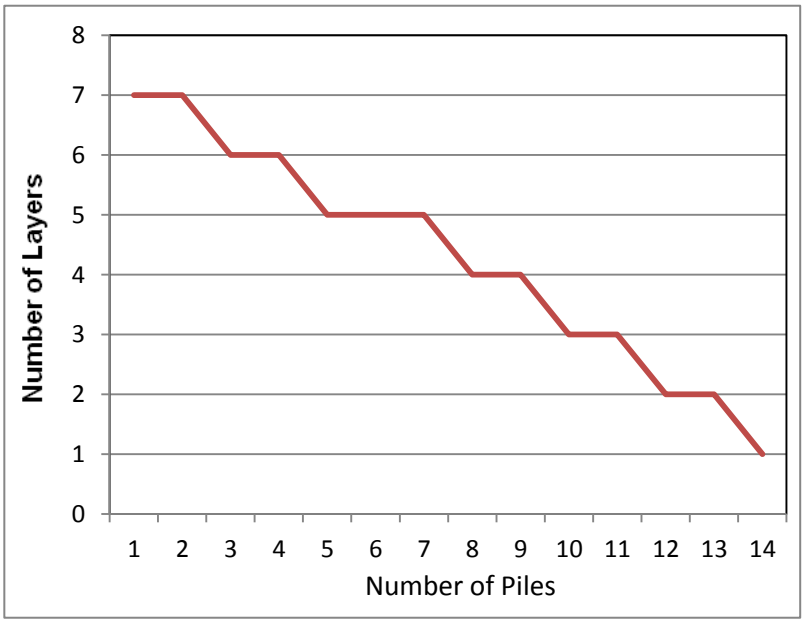

Figure 3.4. Simulated Triangular Load Arrangement for Specimens BW1, BW2 and BW3

Loading Area ; 1200 mm X 2400 mm

Pile	Length mm	layers Num	Quantity Per layer	Unit Wt N	Total Wt N	Total Bricks
1	200	6	12	28.8	2073.6	72
2	200	6	12	28.8	2073.6	72
3	200	6	12	28.8	2073.6	72
4	200	5	12	28.8	1728	60
5	200	5	12	28.8	1728	60
6	200	4	12	28.8	1382.4	48
7	200	4	12	28.8	1382.4	48
8	200	3	12	28.8	1036.8	36
9	200	3	12	28.8	1036.8	36
10	200	2	12	28.8	691.2	24
11	200	2	12	28.8	691.2	24
12	200	1	12	28.8	345.6	12

12	2,400.00	OK		OK	16,243.20	564.00
Pile	mm		Test Value		N	Num

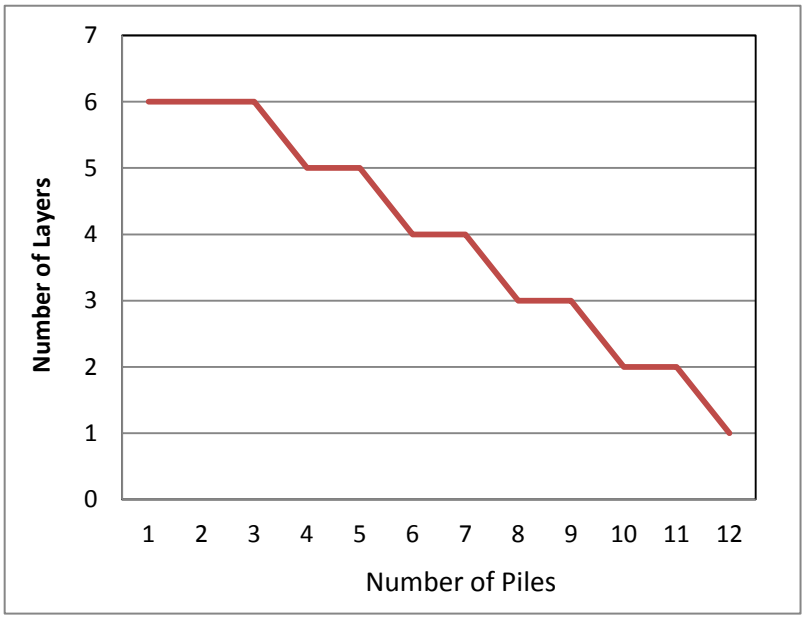

Figure 3.5. Simulated Triangular Load Arrangement for Specimens BW4, BW5 and BW6

Figure 3.6. View if the SIP panel before applying sustained loading

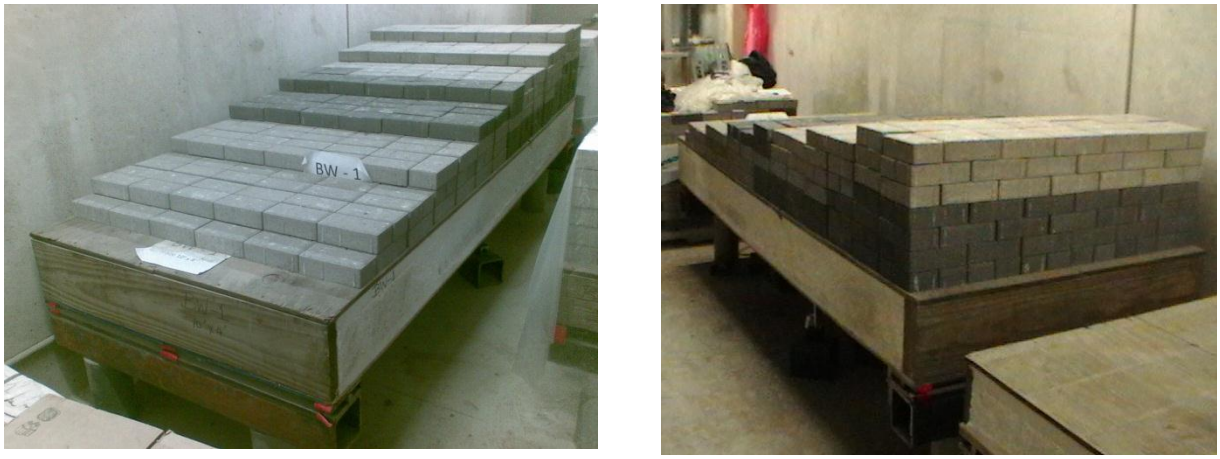

Figure 3.7. Views of specimen BW1 during creep testing

Figure 3.8. Views of specimen BW2 during creep testing

Figure 3.9. Views of specimens BW3 during creep testing

Figure 3.10. Views of specimen BW4 during creep testing

Figure 3.11 Views of specimen BW5 during creep testing

Figure 3.12. View of specimen BW6 during creep testing

Figure 3.13. View of the dial gauges under the specimen during creep testing

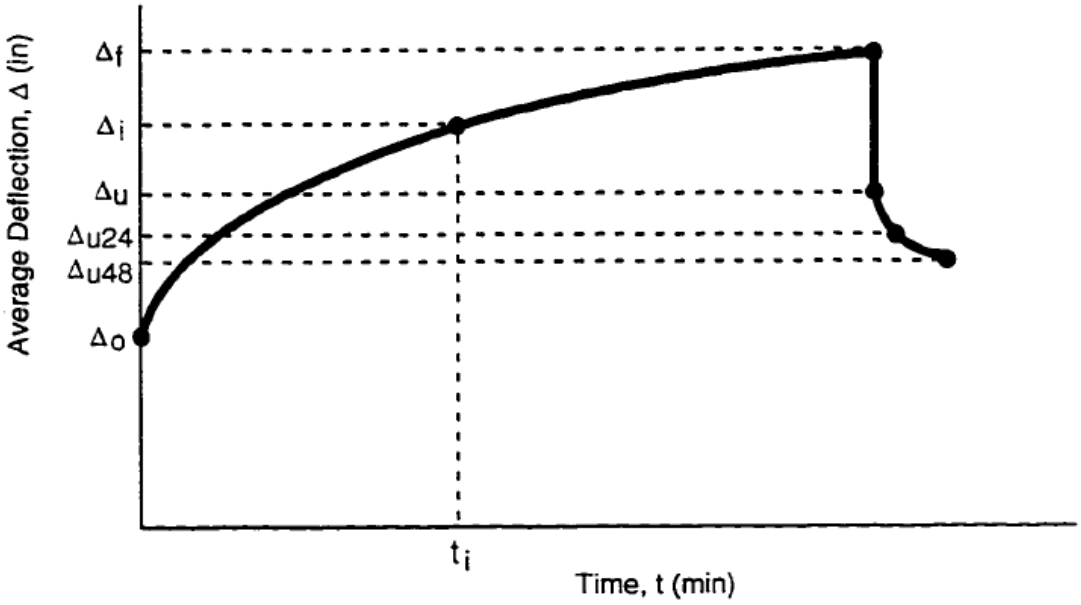

Figure 3.14. Typical flexural creep curve (Taylor, 1996)

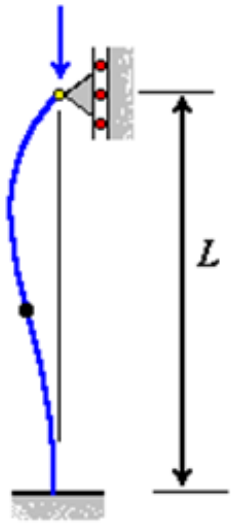

Figure 3.15. Fixed-pinned column assumption for wall testing

(http://physicsarchives.com/index.php/courses/899)

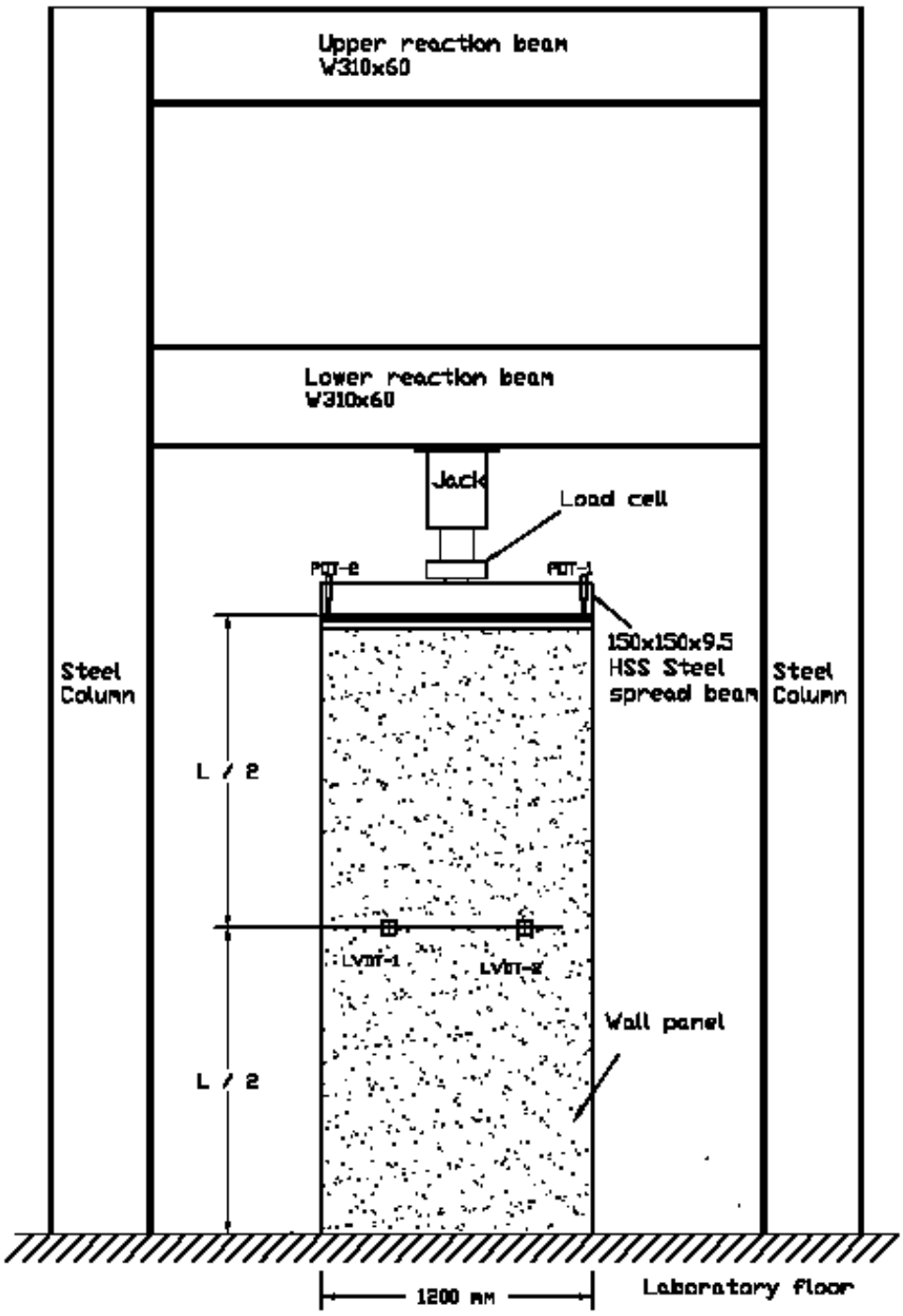

Figure 3.16. Schematic diagram of the elevation of the test setup for axial loading test

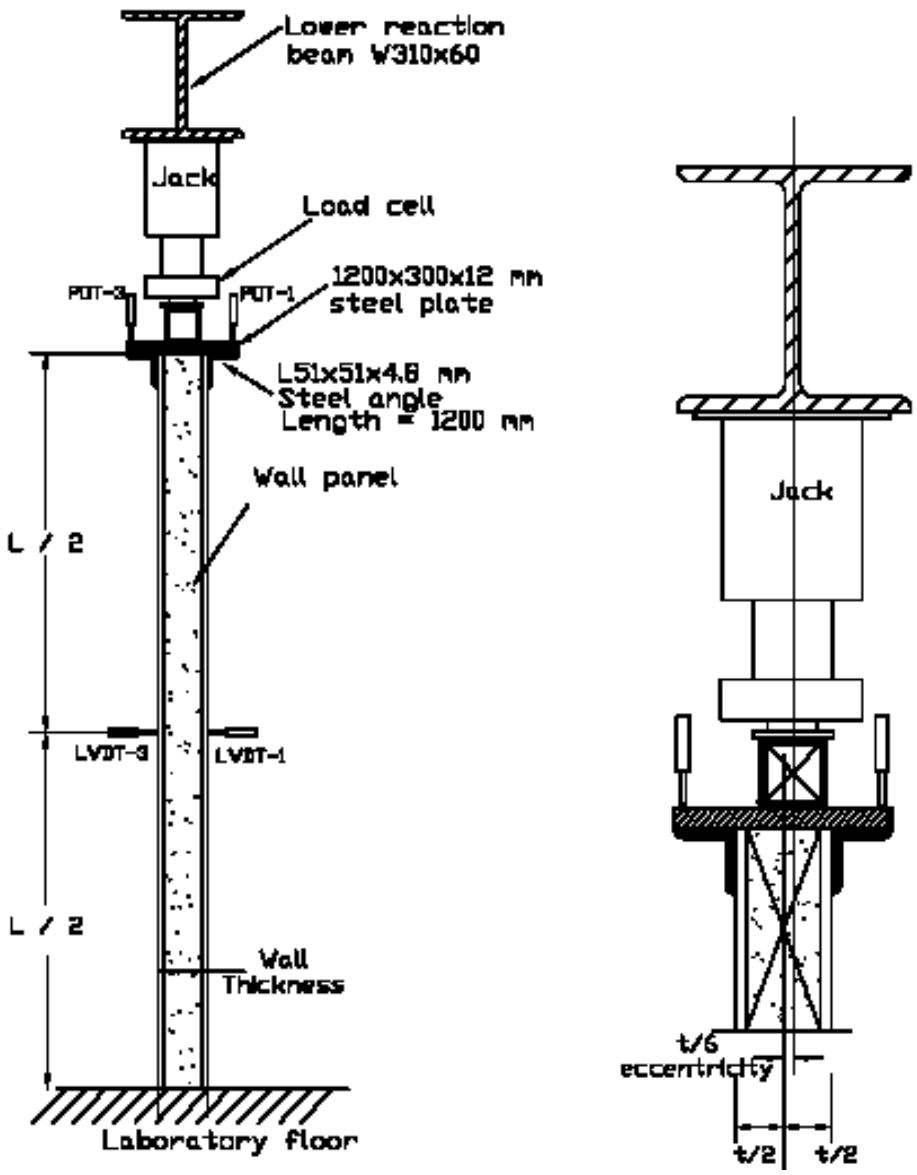

Figure 3.17. Schematic diagram of the side view of the test setup for axial loading test

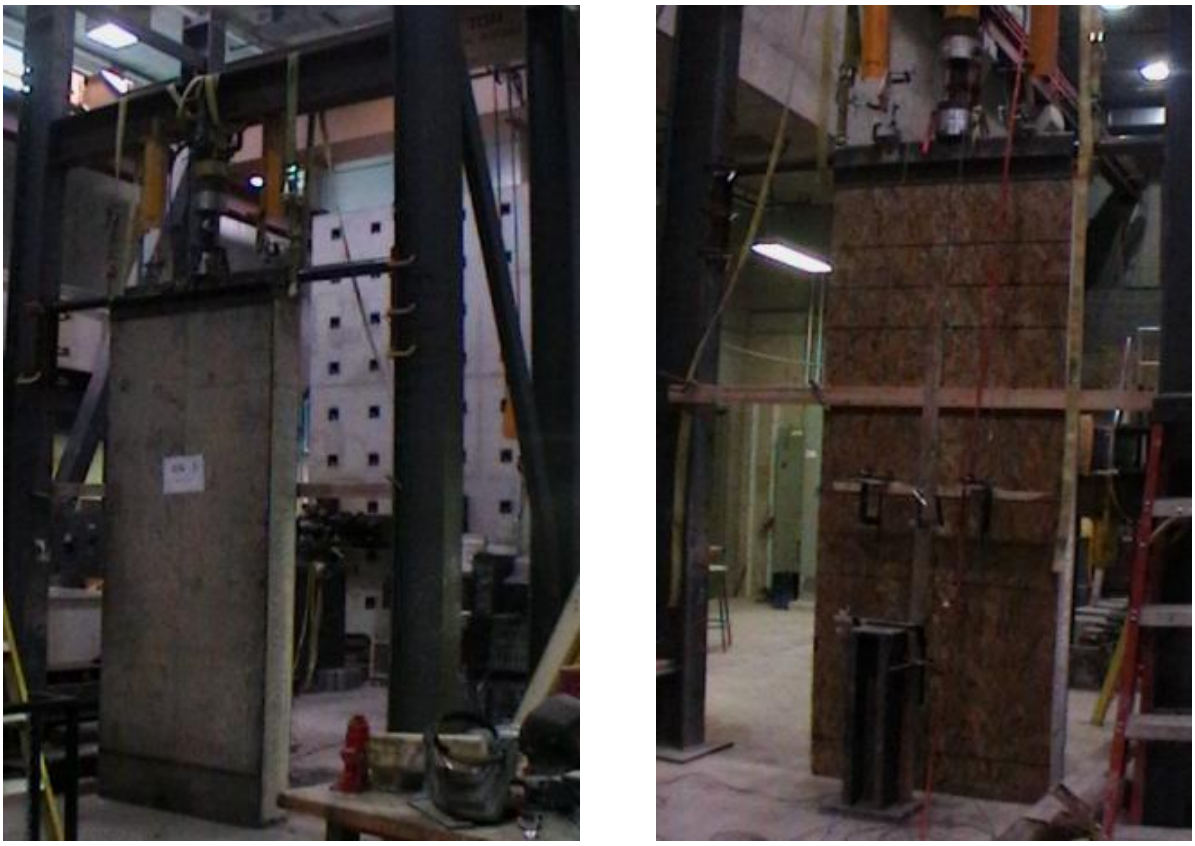

Figure 3.18. Views of the test setup for Axial load Testing

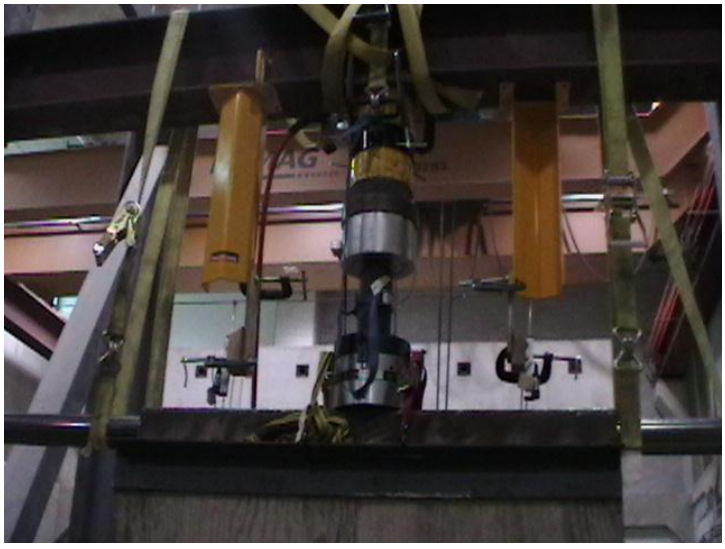

Figure 3.19. Close-up view of the test setup

Figure 3.20. View of the data acquisition system and the pump used in the tests

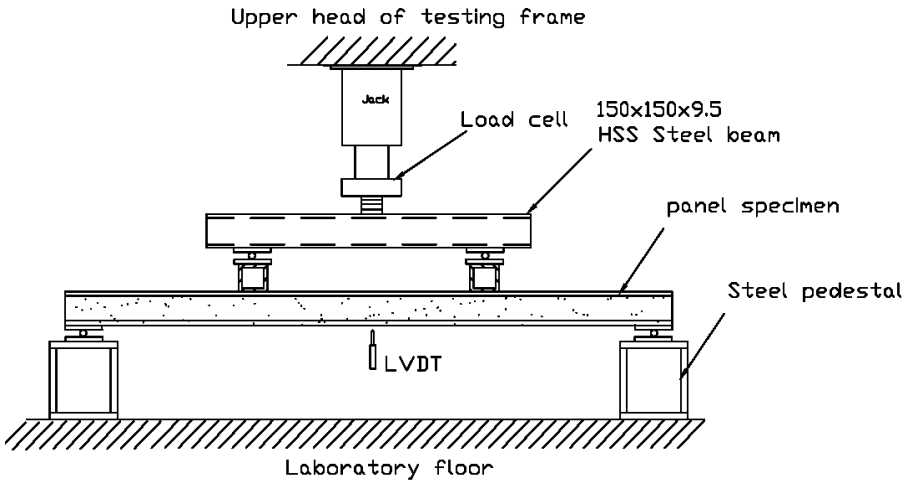

Figure 3.21. Schematic diagram of the elevation of the test setup for flexural loading test

Figure 3.22. View of Specimen BW4 before testing

Figure 3.23. Views of the bearing plate assembly used to transfer applied loading to the supports

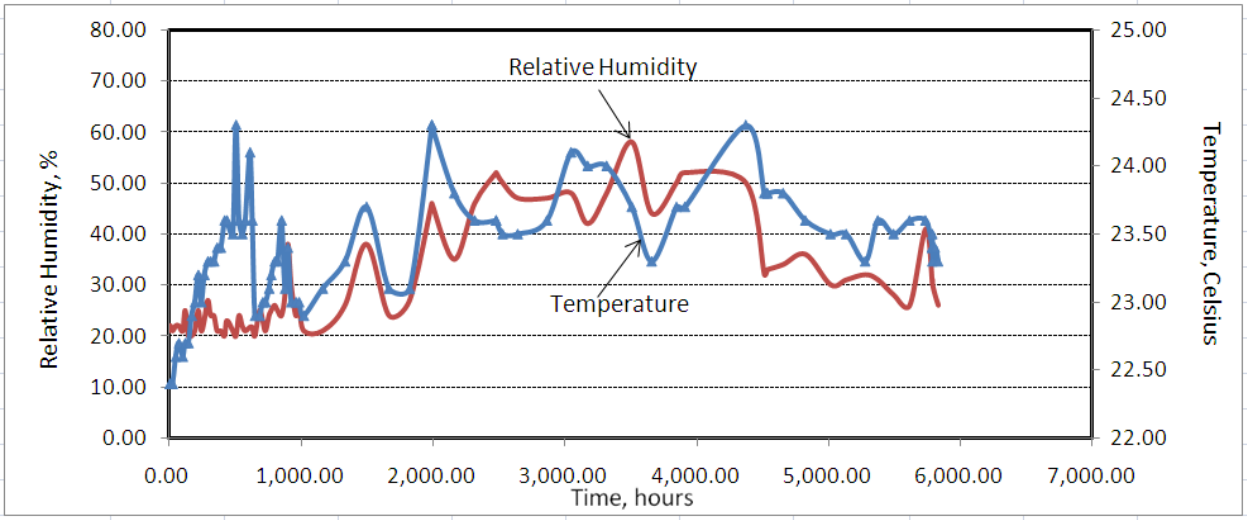

Figure 4.1. Recorded temperature and Relative Humidity with time during creep testing for specimens BW1, BW2, BW4 and BW5

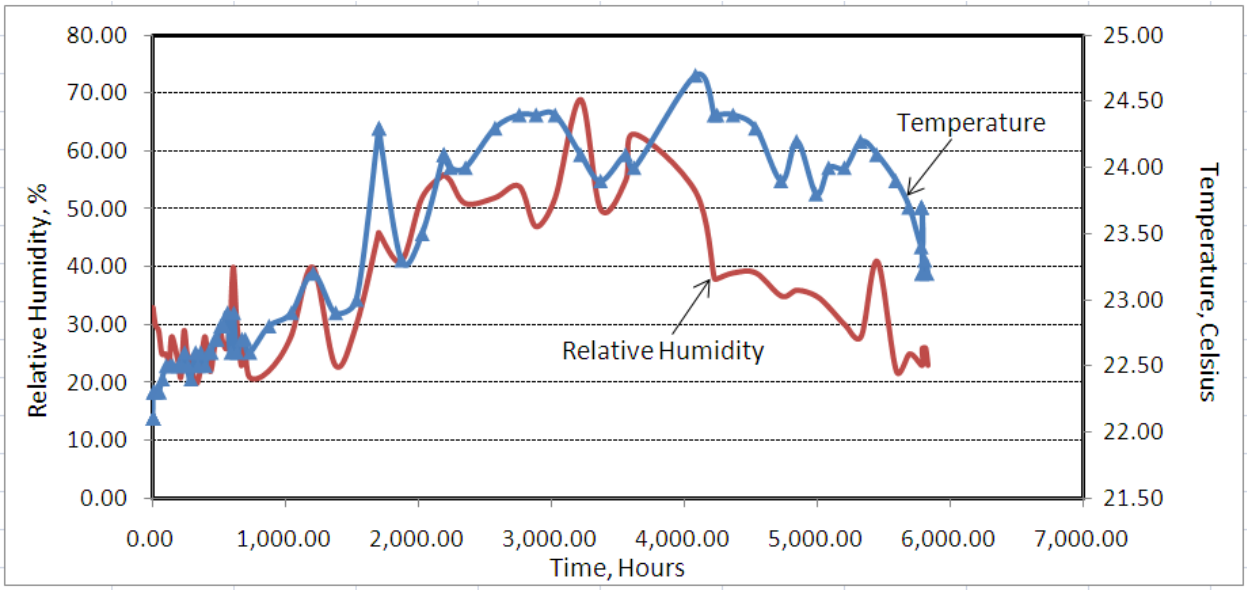

Figure 4.2. Recorded temperature and Relative Humidity with time during creep testing for specimens BW3 and BW6

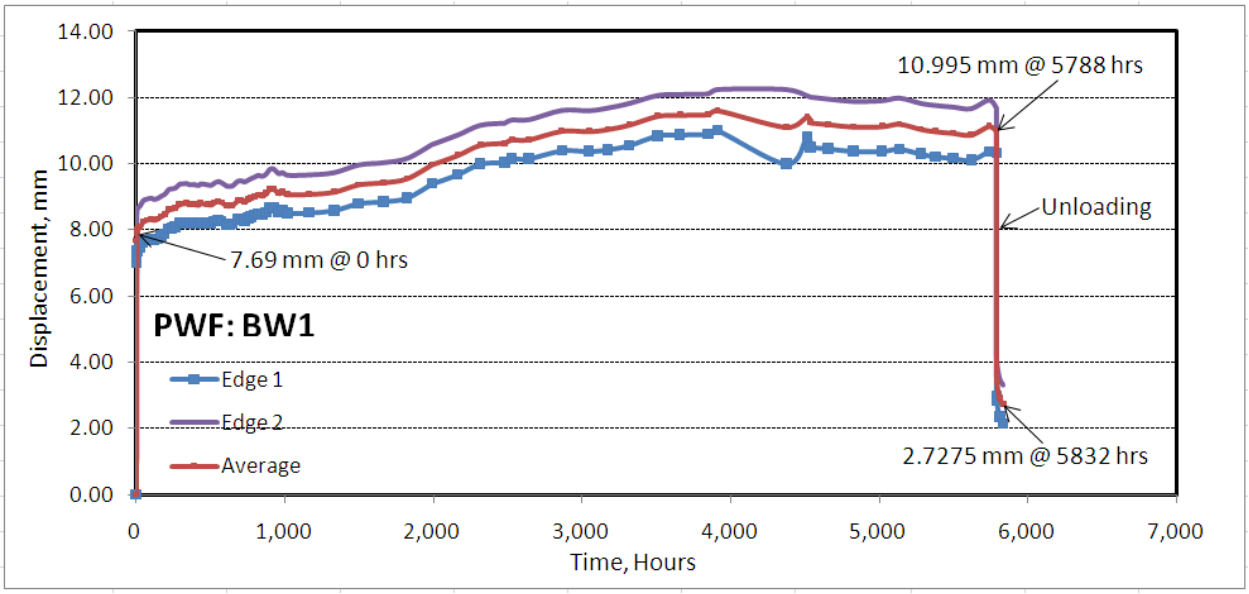

Figure 4.3.a Creep deflection-time relationship for specimen BW1

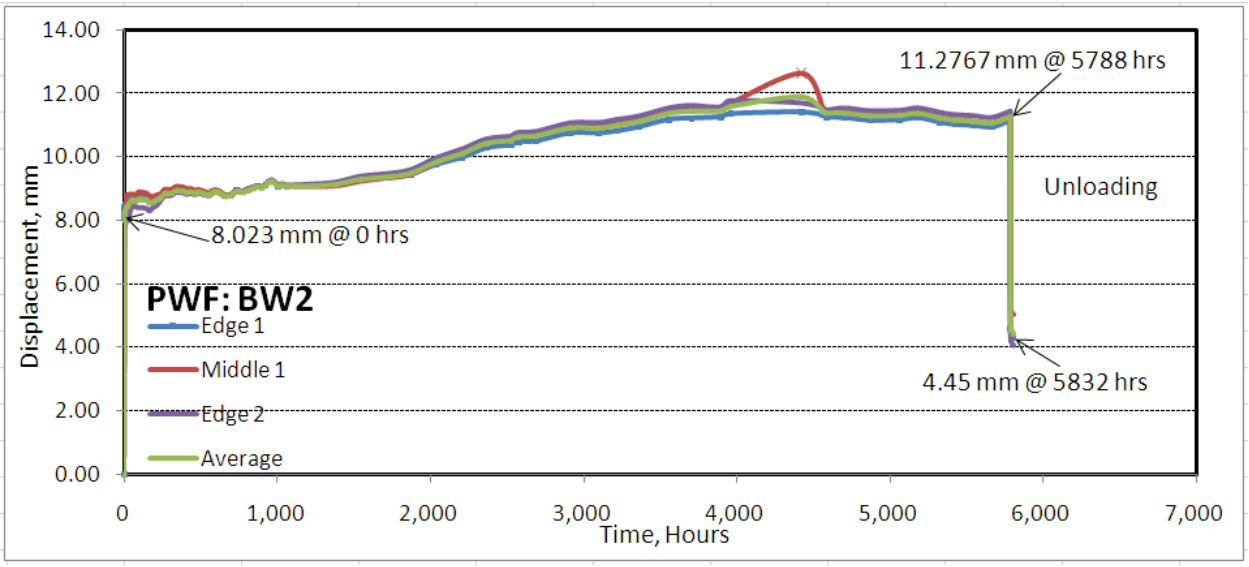

Figure 4.3.b Creep deflection-time relationship for specimen BW2

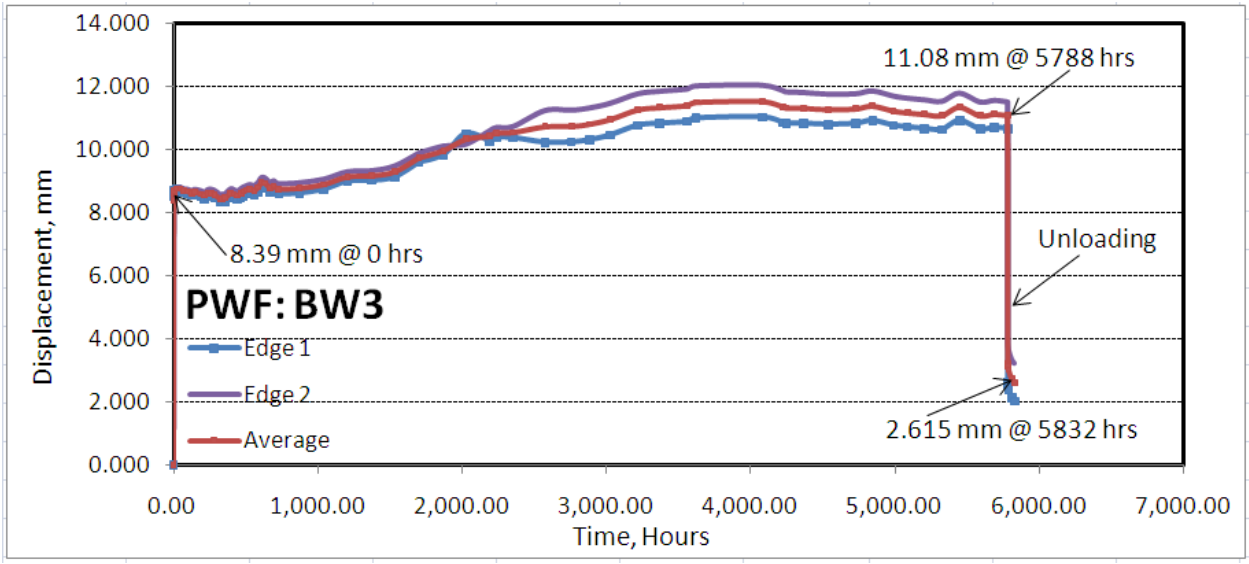

Figure 4.3.c Creep deflection-time relationship for specimen BW3

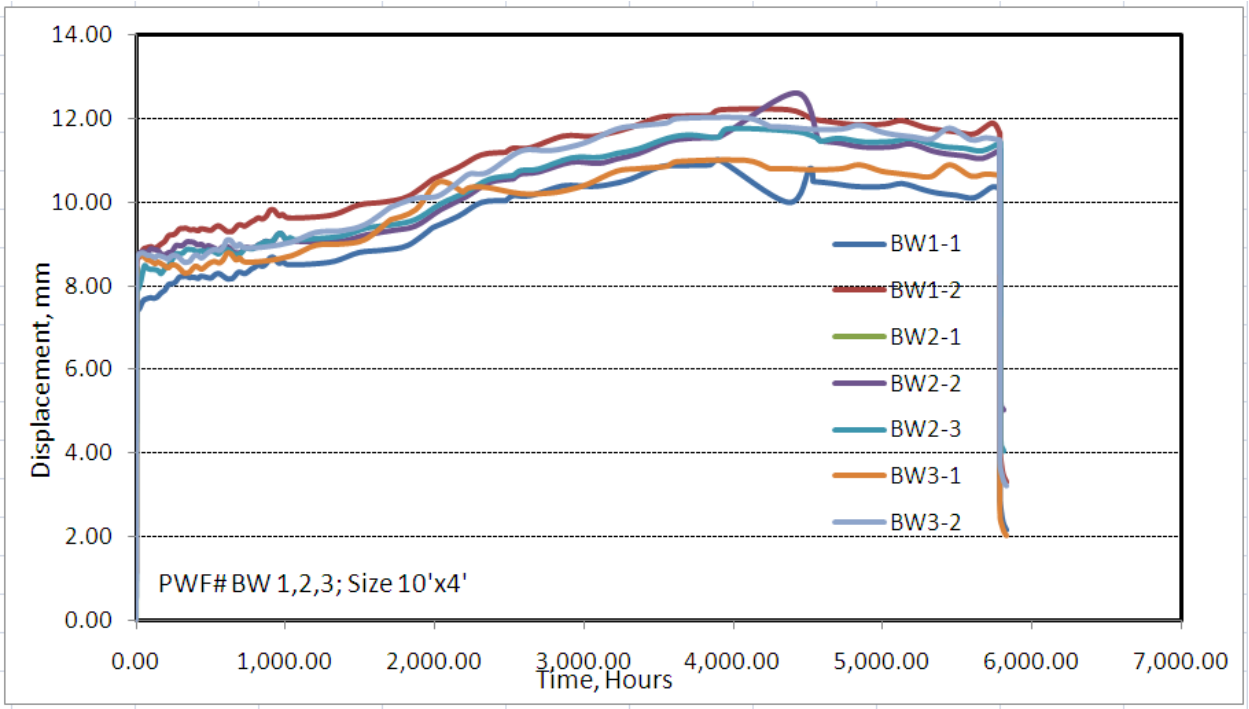

Figure 4.3.d Creep deflection-time relationship for PWF Group I

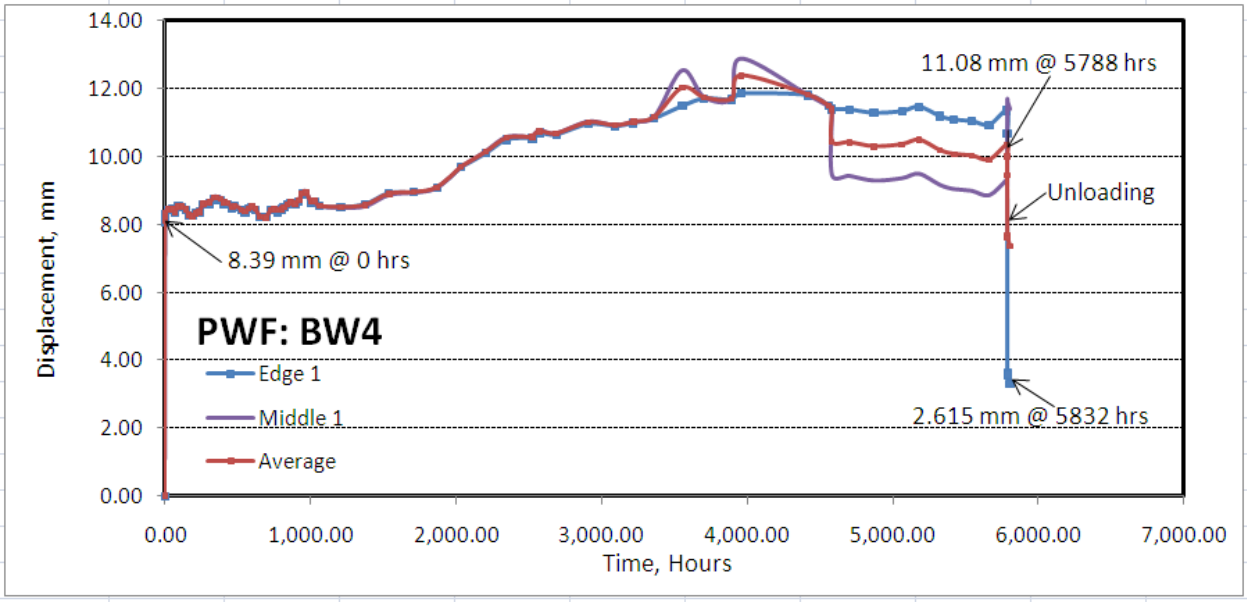

Figure 4.4.a Creep deflection-time relationship for specimen BW4

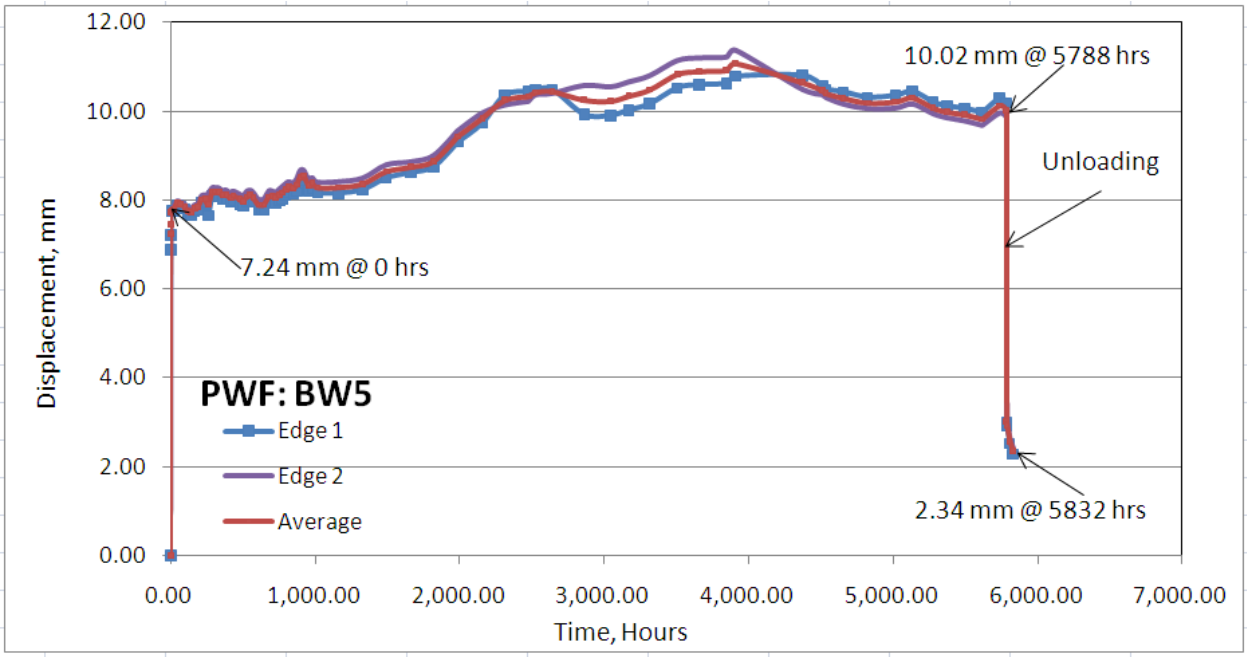

Figure 4.4.b Creep deflection-time relationship for specimen BW5

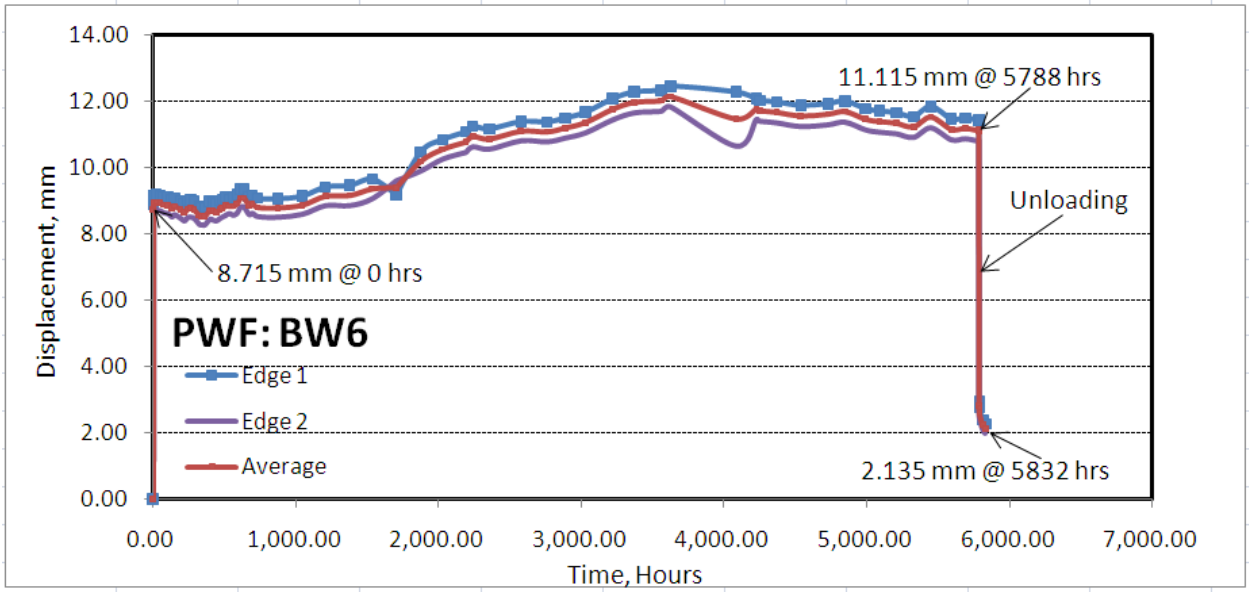

Figure 4.4.c Creep deflection-time relationship for specimen BW6

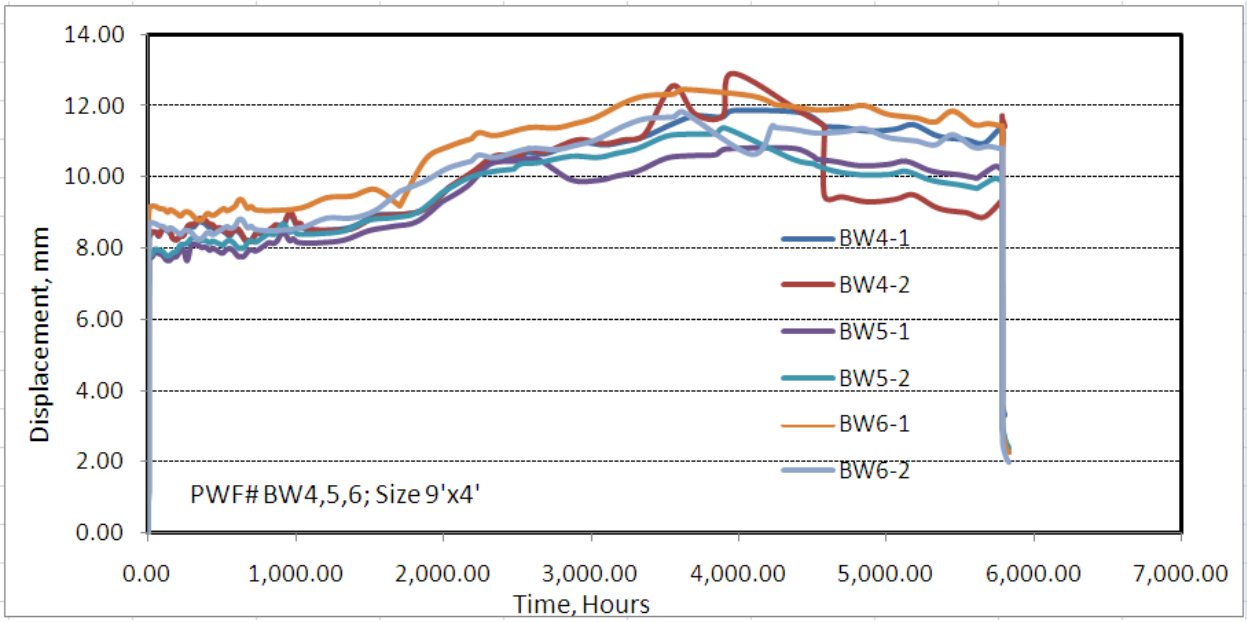

Figure 4.4.d Creep deflection-time relationship for PWF Group II

Figure 4.5. View of front and back faces of specimen BW1 before axial load testing

Figure 4.6. View of specimen BW1 after failure showing crashing of OSB face near the top of the wall

Figure 4.7. Close-up view of specimen BW1 after failure showing crashing of OSB face near the top of the wall

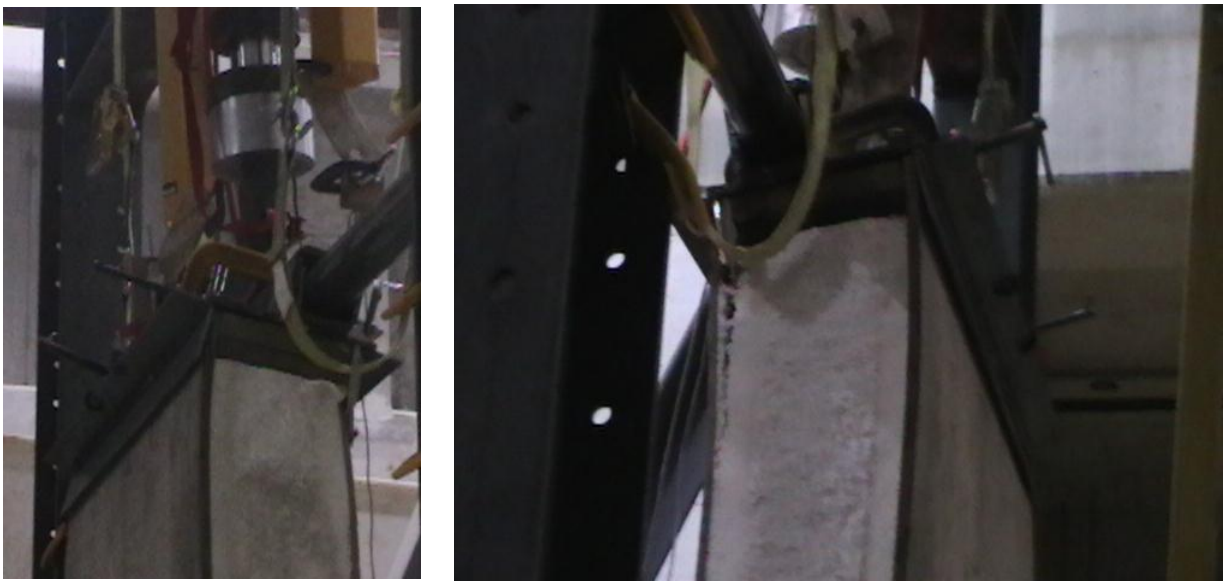

Figure 4.8. Views of top sides of specimen BW1 after failure showing delamination at the OBS-foam interface

Figure 4.9. Views of front and back faces of specimen BW2 before axial load testing

Figure 4.10. Views of crushing failure mode of the OSB face, delamination at OSB-foam interface and fracture of the lumber stud at the connection of specimen BW2 at the end of axial load testing

a)

b)

c)

d)

Figure 4.11. Views of delamination at OSB-foam interface of specimen BW2 at the end of axial load testing

Figure 4.12. Views of back face of of specimen BW2 at the end of axial load testing

Figure 4.13. Views of fracture of the lumber stud at the connection and diagonal crack of the foam after splitting from the OSB face of specimen BW2

Figure 4.14. View of specimen BW3 before axial load testing

Figure 4.15. View of specimen BW3 after failure due to crushing of OSB face at the top of the wall

Figure 4.16. Close-up views of specimen BW3 after failure showing crashing of OSB face near the top of the wall

Figure 4.17. View of specimen BW4 before axial load testing

Figure 4.18. View of specimen BW4 after failure showing crashing at the bottom of the OSB face and OSB-foam delamination along the length of the wall

Figure 4.19. a) Close-up view of OSB-foam delamination near the top of the wall, b) Close-up view of the OSB-foam delamination and OSB crushing at the bottom of specimen BW4

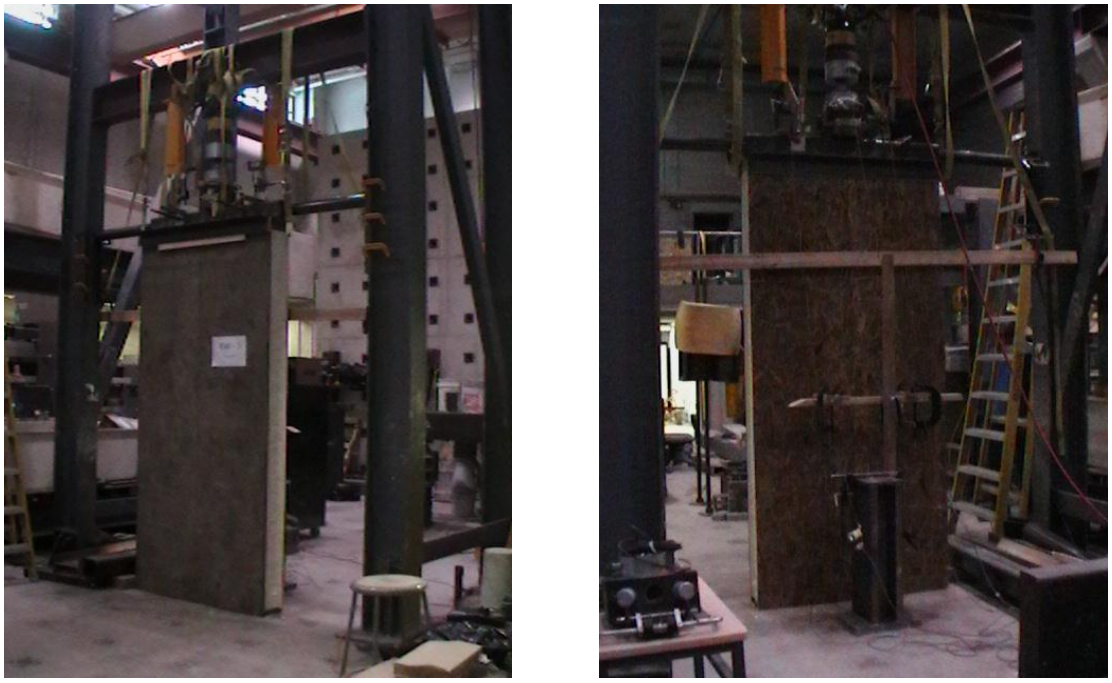

Figure 4.20. Views of the front and back faces of specimen BW5 before axial load testing

Figure 4.21. Close-up views of specimen BW5 after failure showing crashing of OSB face near the top of the wall

Figure 4.22. View of specimen BW6 before axial load testing

Figure 4.23. View of specimen BW6 after failure due to crushing of OSB face at the top of the wall

Figure 4.24. Close-up views of specimen BW3 after failure showing crashing of OSB face near the top of the wall

Figure 4.25. View of specimen BW1 before flexural load testing

Figure 4.26. View of deformed shape of specimen BW1 after flexural load testing

Figure 4.27. Views of shear failure at the interface between the top plywood face and foam core of specimen BW1 after flexural load testing

Figure 4.28. View of specimen BW2 before flexural load testing

Figure 4.29. View of deformed shape of specimen BW2 after flexural load testing

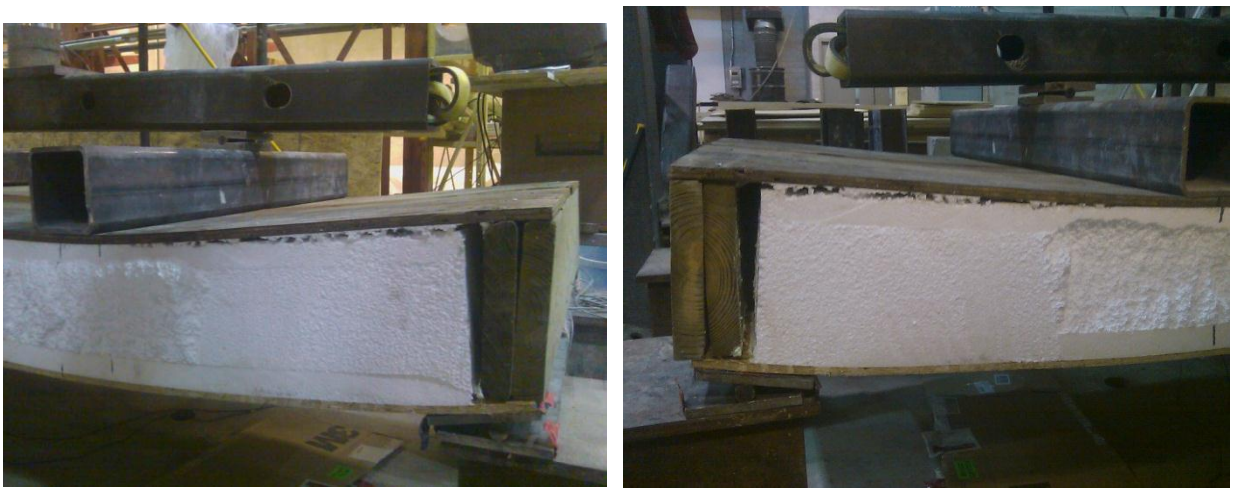

Figure 4.30. Views of shear failure at the interface between the top plywood face and foam core of specimen BW2 after flexural load testing

Figure 4.31. View nail tearing failure at the end of OSB face at the support location of specimen BW2 after flexural load testing

Figure 4.32. View of specimen BW3 before flexural load testing

Figure 4.33. View of deformed shape of specimen BW3 after flexural load testing

a) Before test b) After test

Figure 4.34. Views of west edge of end of the specimen BW3 before and after flexural test showing shear failure at the interface between the top plywood face and foam core

Figure 4.35. View of the east edge of the end of specimen BW3 showing shear failure at the interface between the top plywood face and foam core

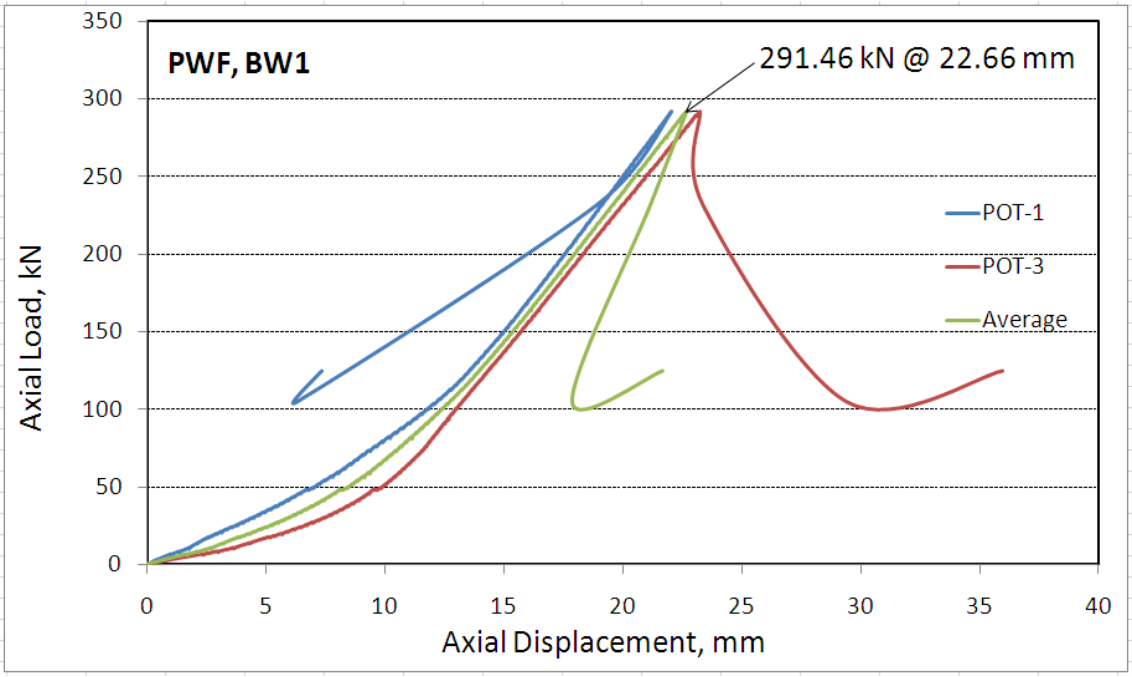

Figure 4.36. Axial load axial displacement curves for the 2 POTs for BW1, along with the average curve

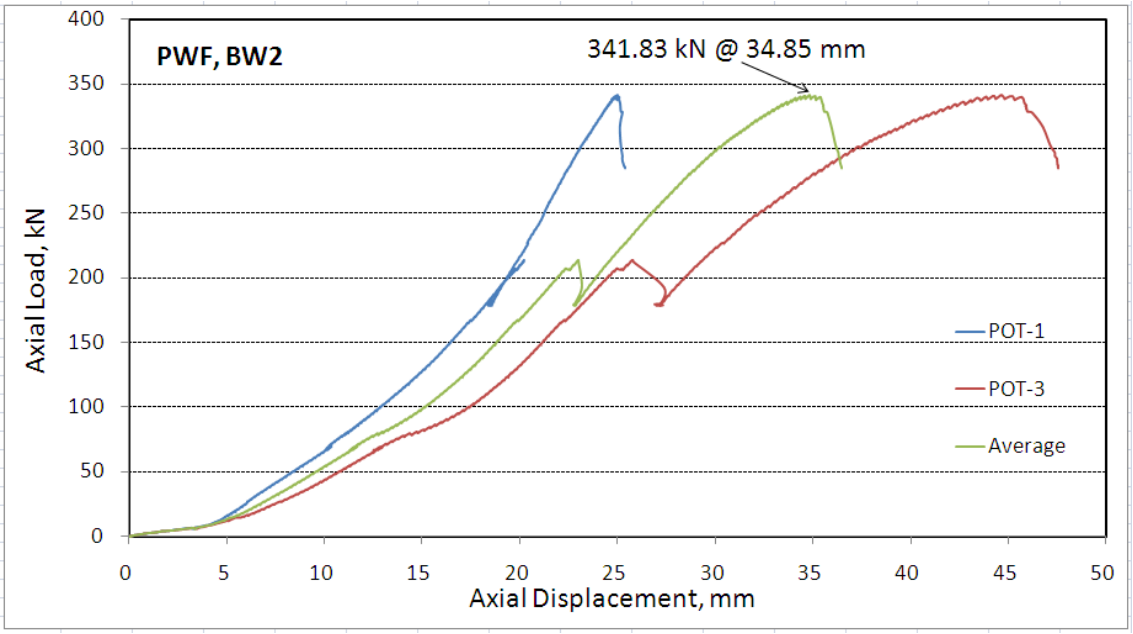

Figure 4.37. Axial load axial displacement curves for the 2 POTs for BW2, along with the average curve

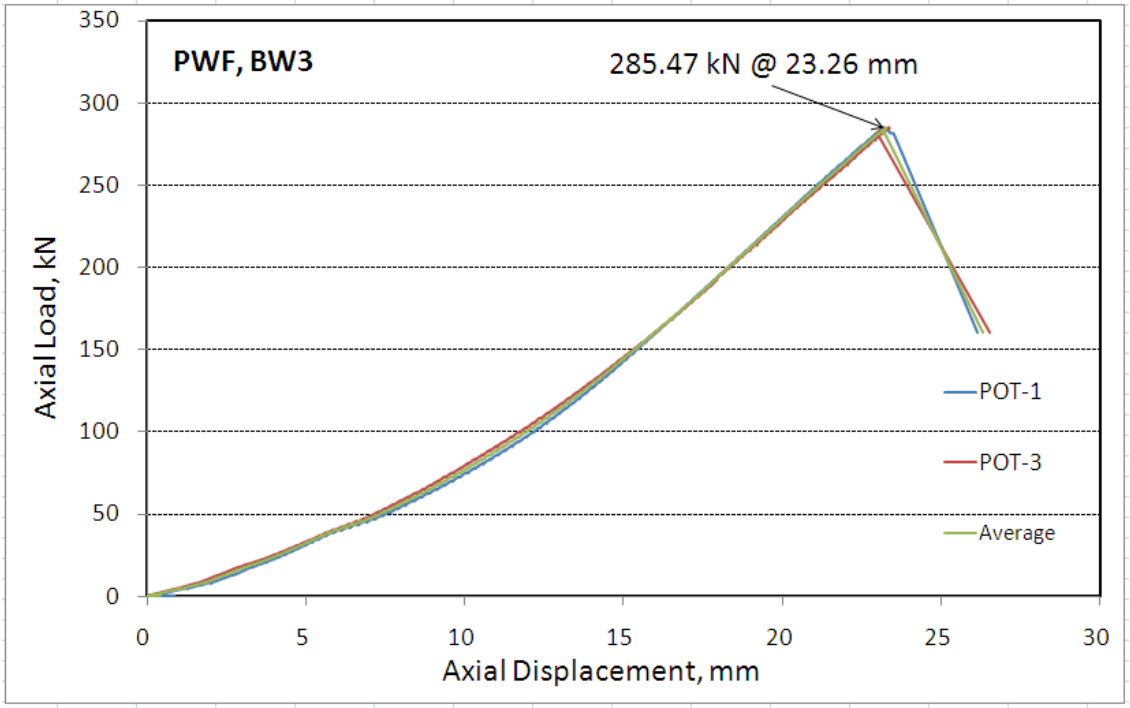

Figure 4.38. Axial load axial displacement on curves for the 2 POTs for BW3, along with the average curve

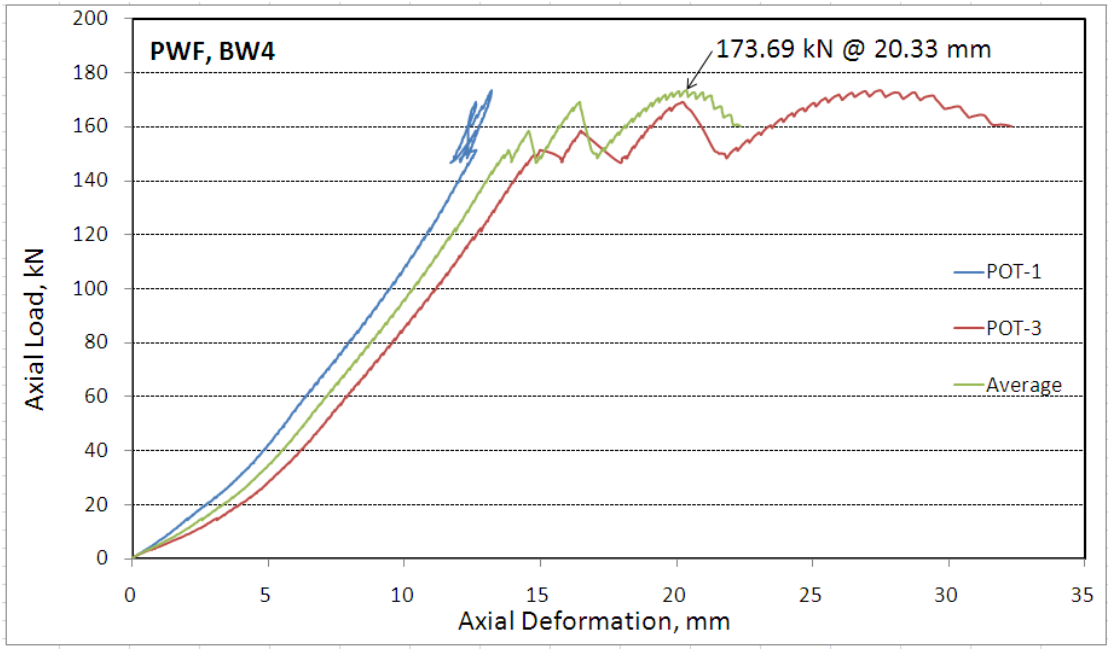

Figure 4.39. Axial load axial displacement curves for the 2 POTs for BW4, along with the average curve

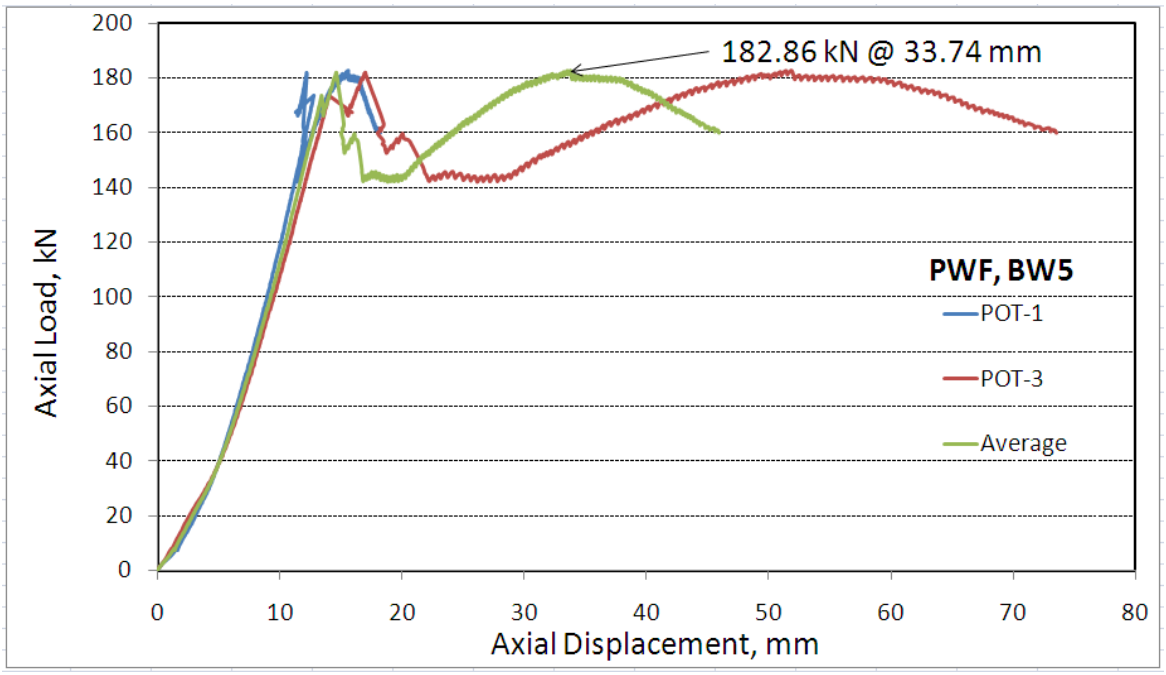

Figure 4.40. Axial load axial displacement curves for the 2 POTs for BW5, along with the average curve

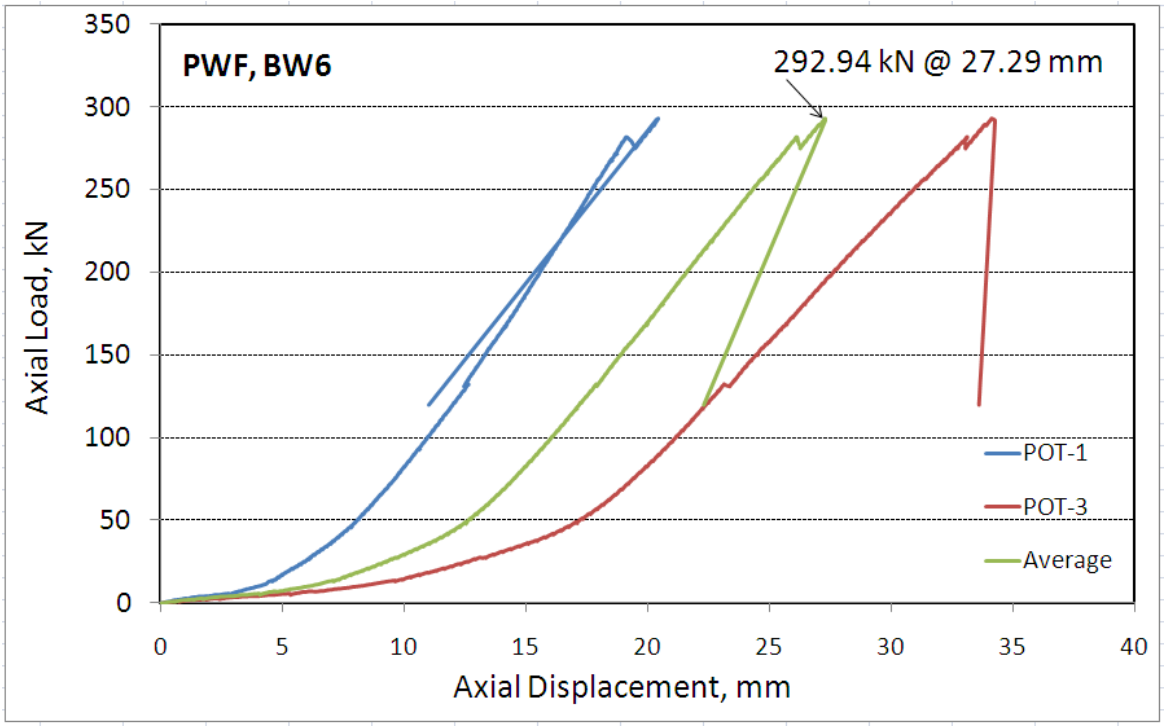

Figure 4.41. Axial load axial displacement curves for the 2 POTs for BW6, along with the average curve

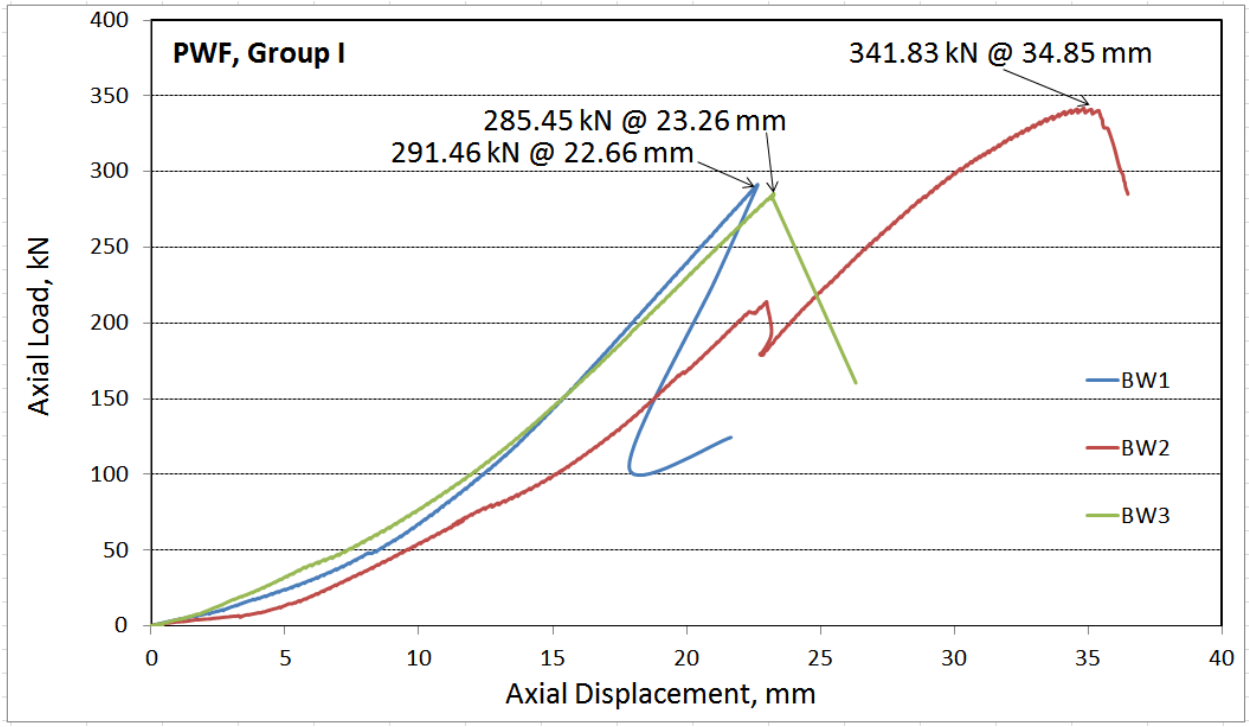

Figure 4.42. Former 4.36-4.38 for axial displacement, first group

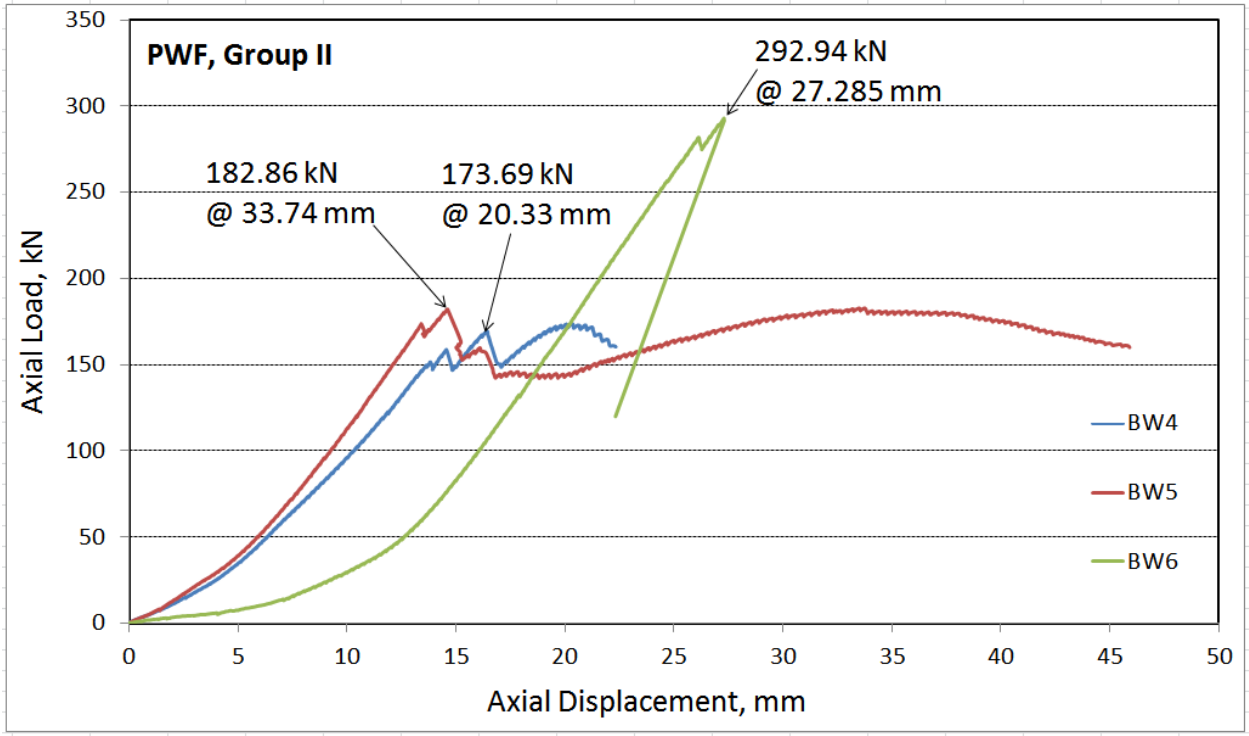

Figure 4.43. Former 4.39-4.41 for axial displacement, second group

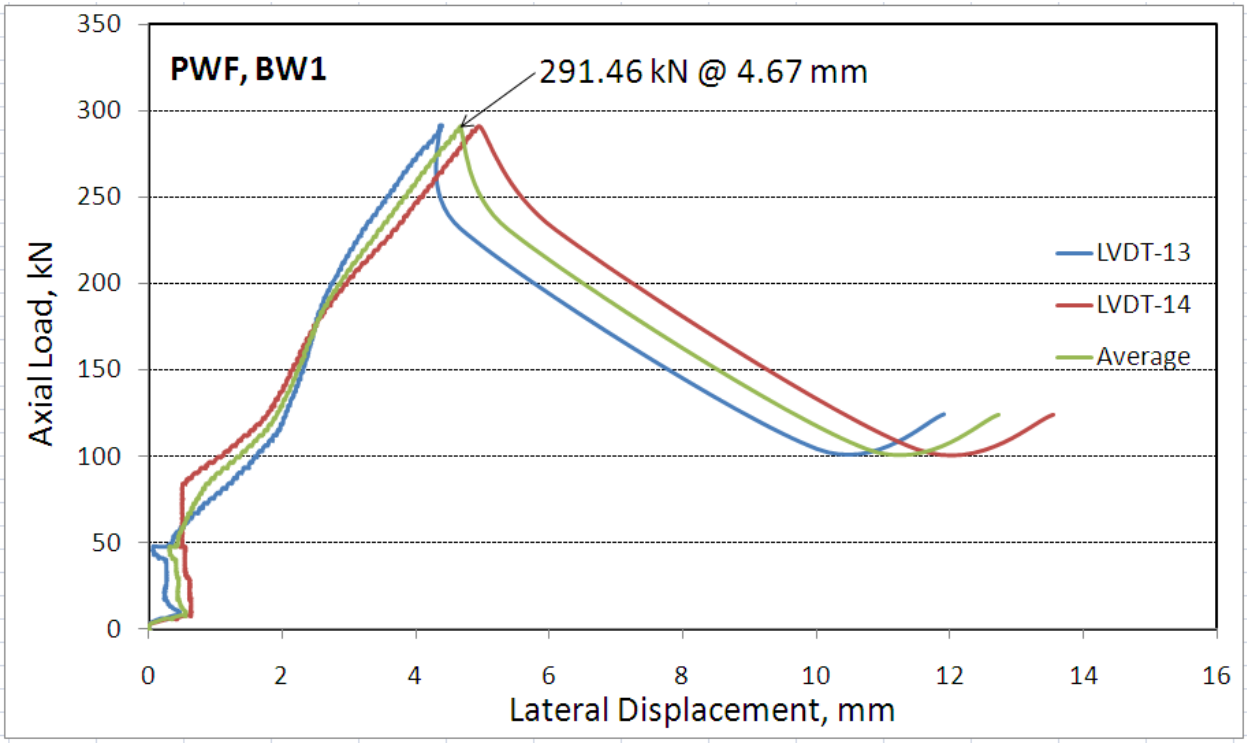

Figure 4.44. Axial load-lateral displacement for 2 LVDTs for BW1

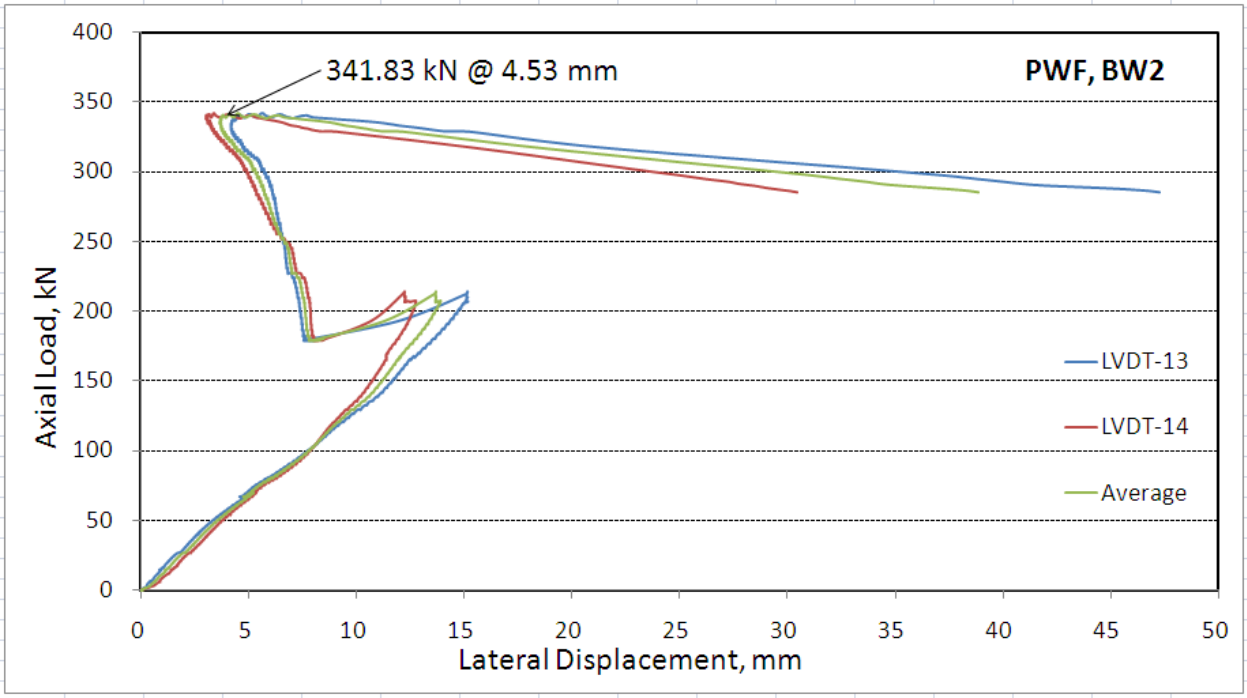

Figure 4.45. Axial load-lateral displacement for 2 LVDTs for BW2

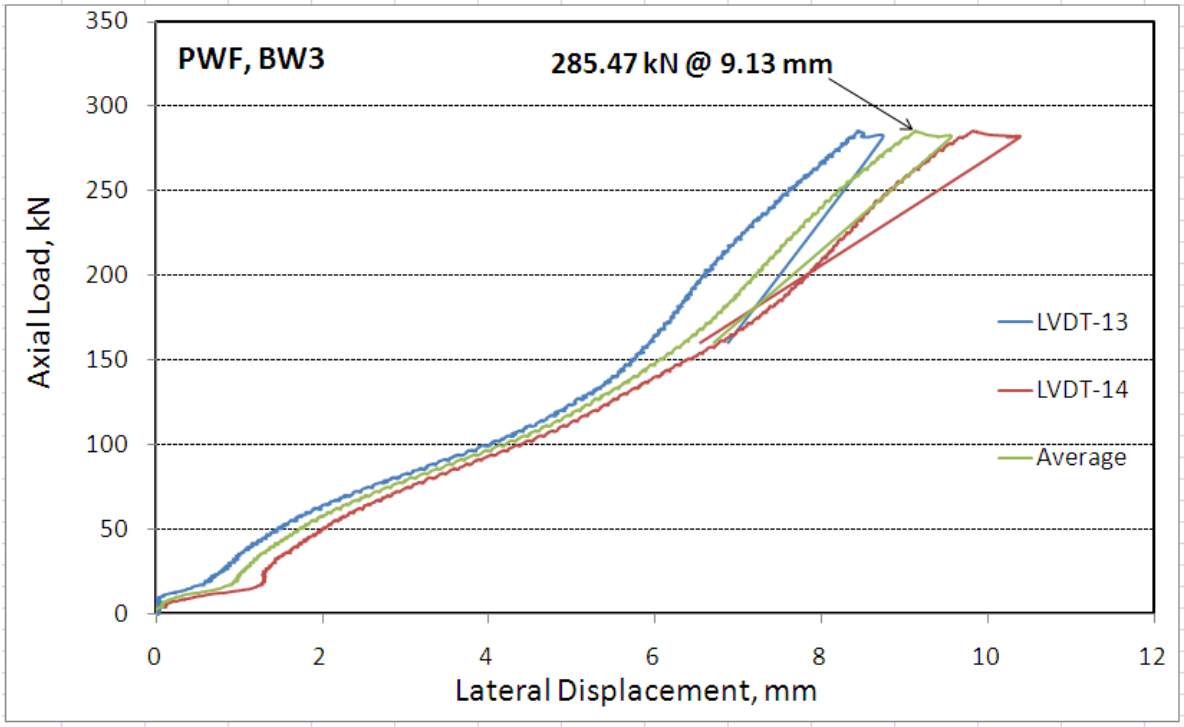

Figure 4.46. Axial load-lateral displacement for 2 LVDTs for BW3

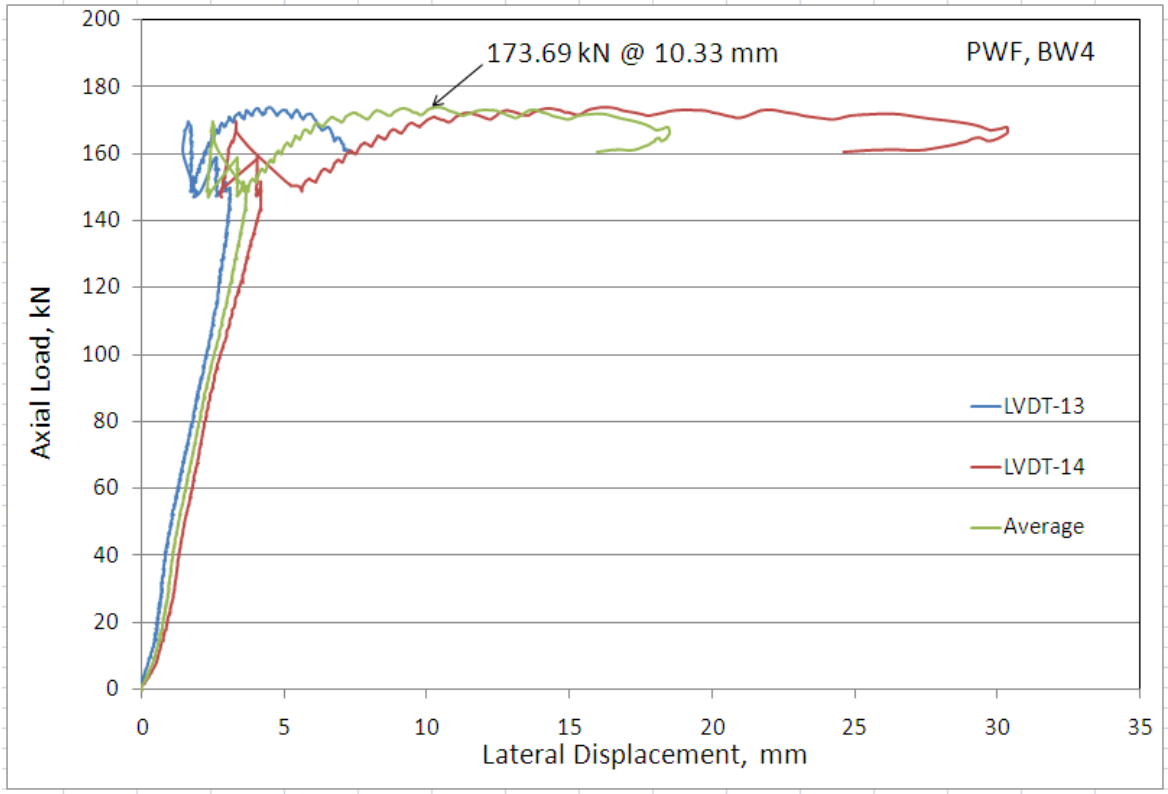

Figure 4.47. Axial load-lateral displacement for 2 LVDTs for BW4

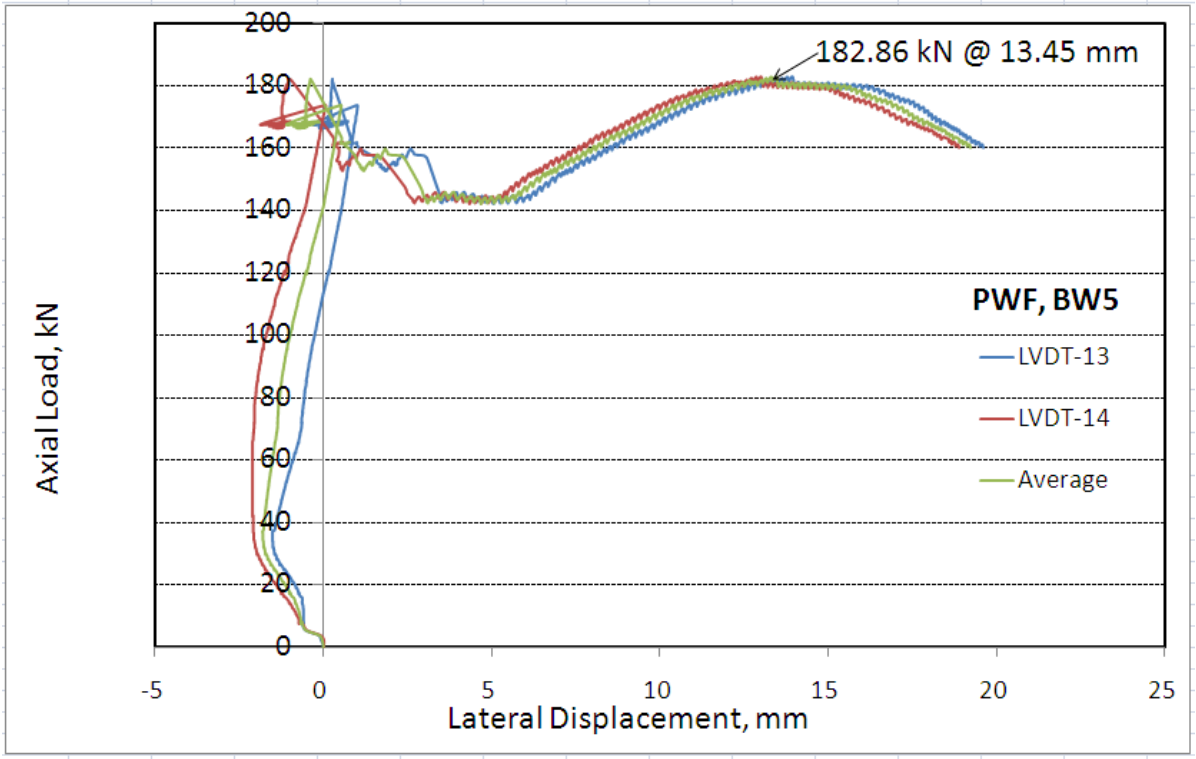

Figure 4.48. Axial load-lateral displacement for 2 LVDTs for BW5

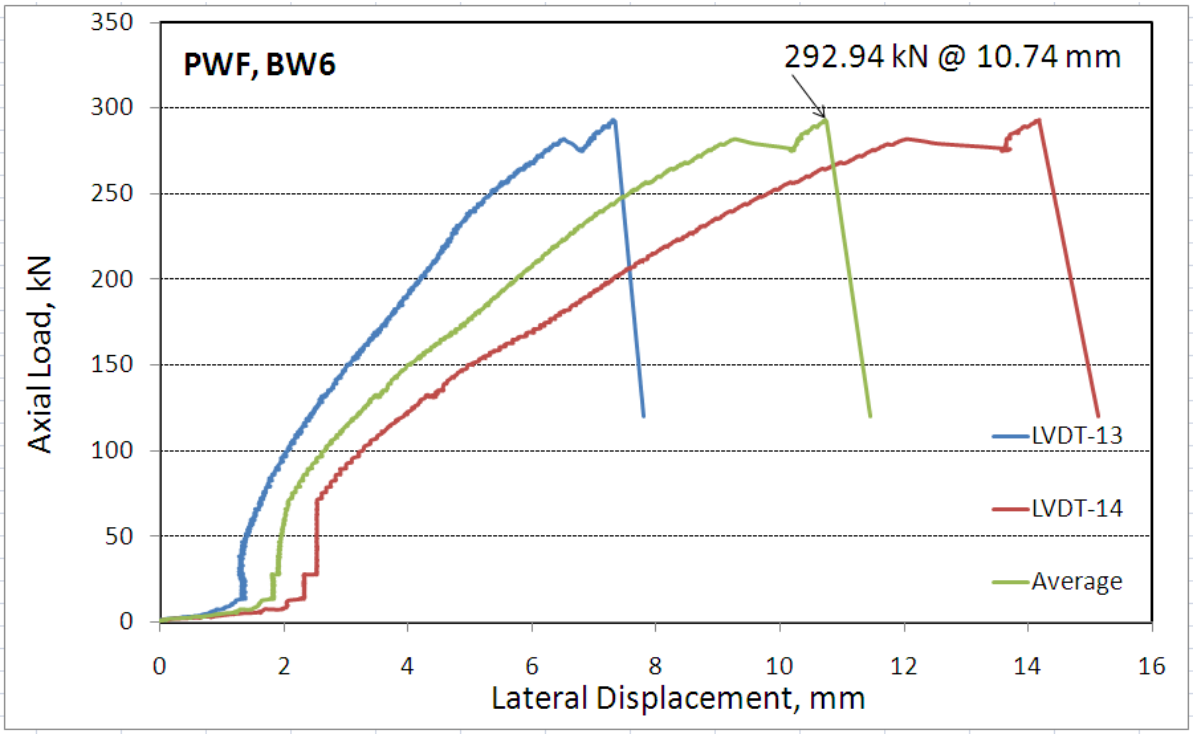

Figure 4.49. Axial load-lateral displacement for 2 LVDTs for BW6

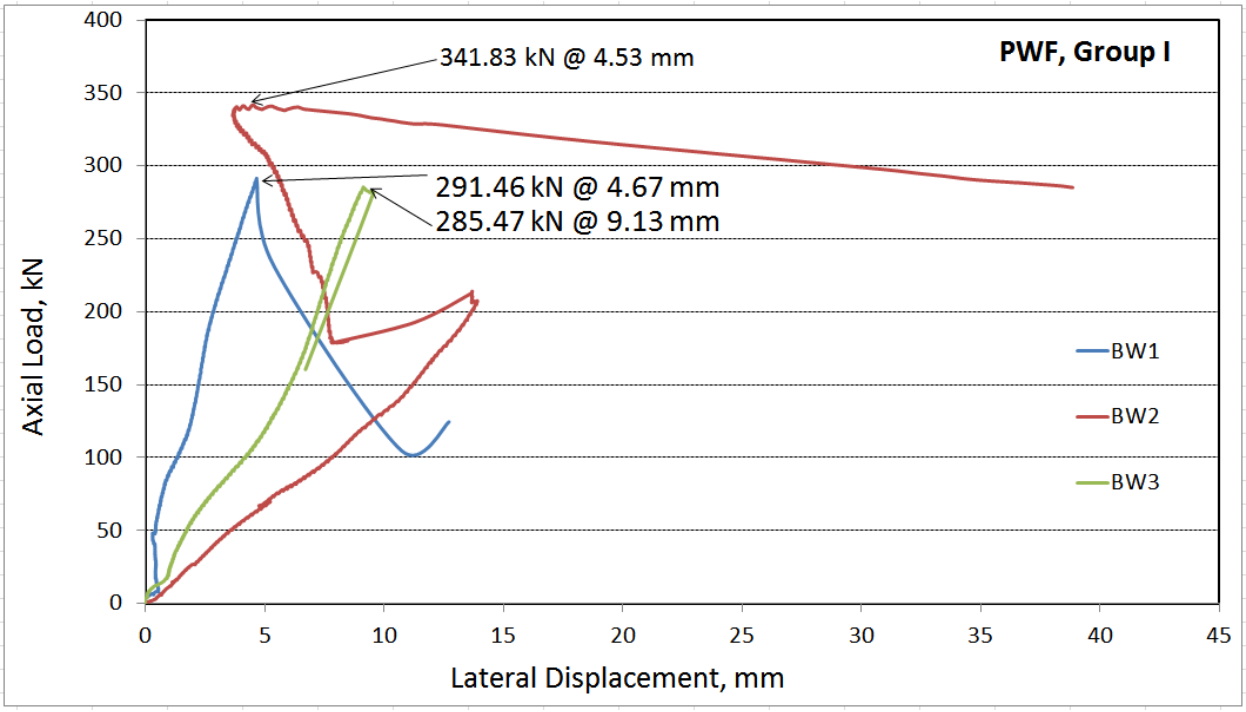

Figure 4.50. Former 4.44-4.46 for axial displacement, first group

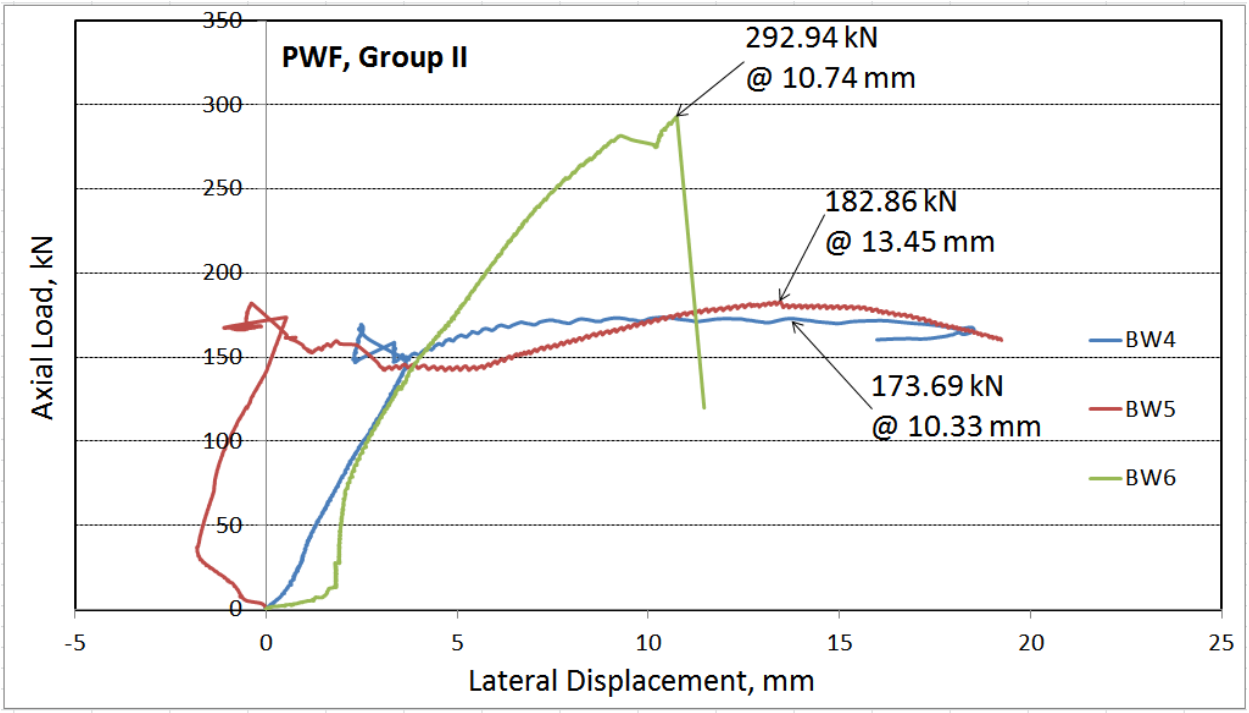

Figure 4.51. Former 4.47-4.49 for axial displacement, first group

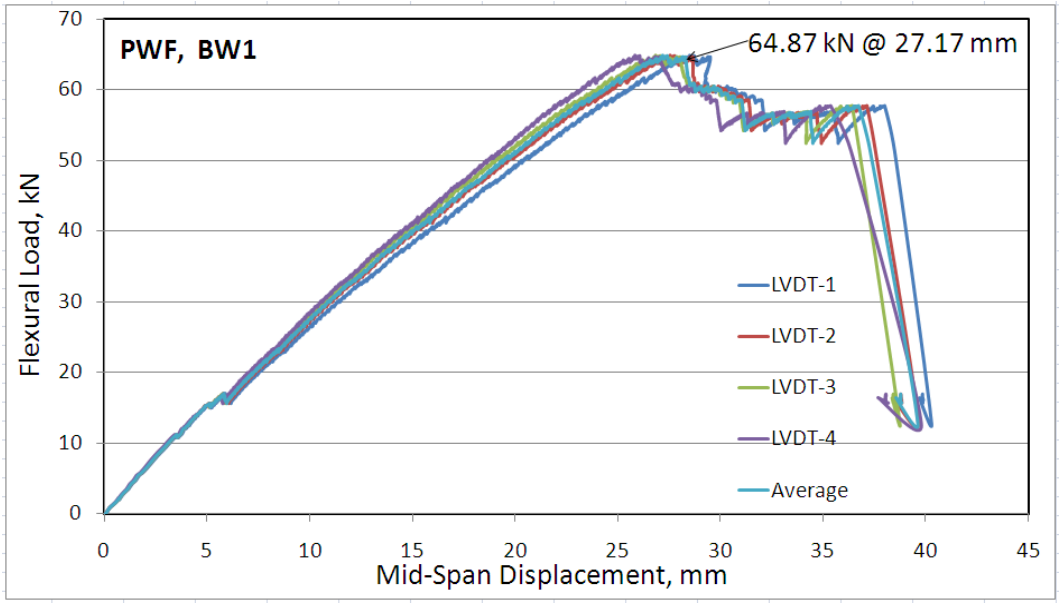

Figure 4.52. Flexural load-deflection curves for the 4 LVDTs for BW1, along with the average curve

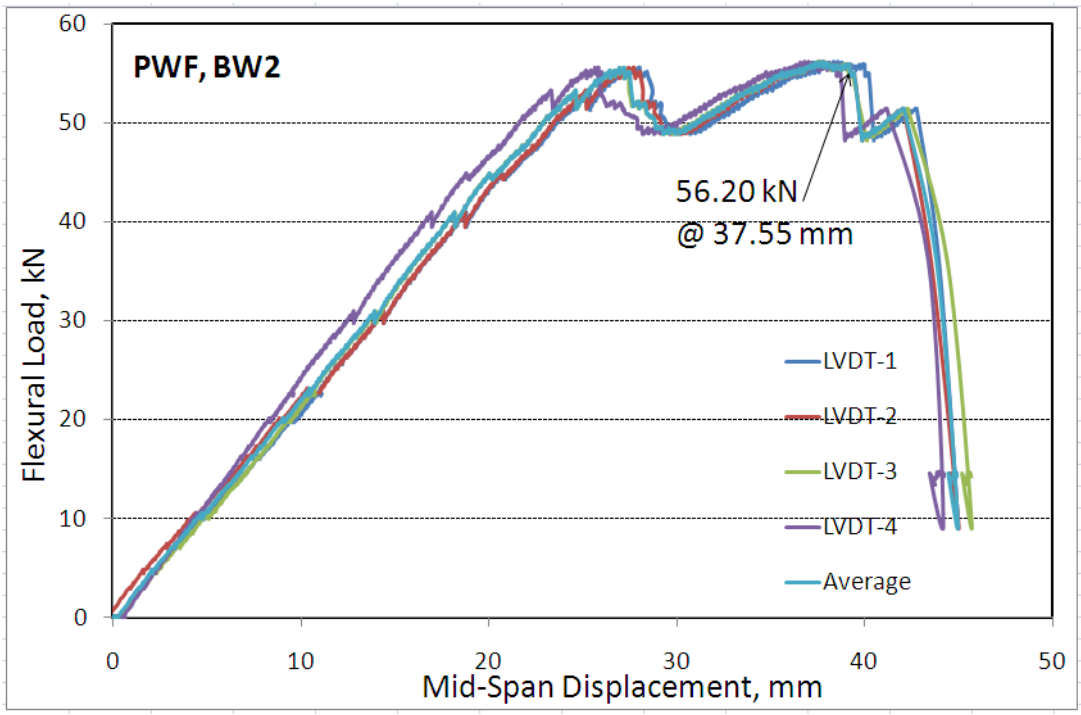

Figure 4.53. Flexural load-deflection curves for the 4 LVDTs for BW2, along with the average curve

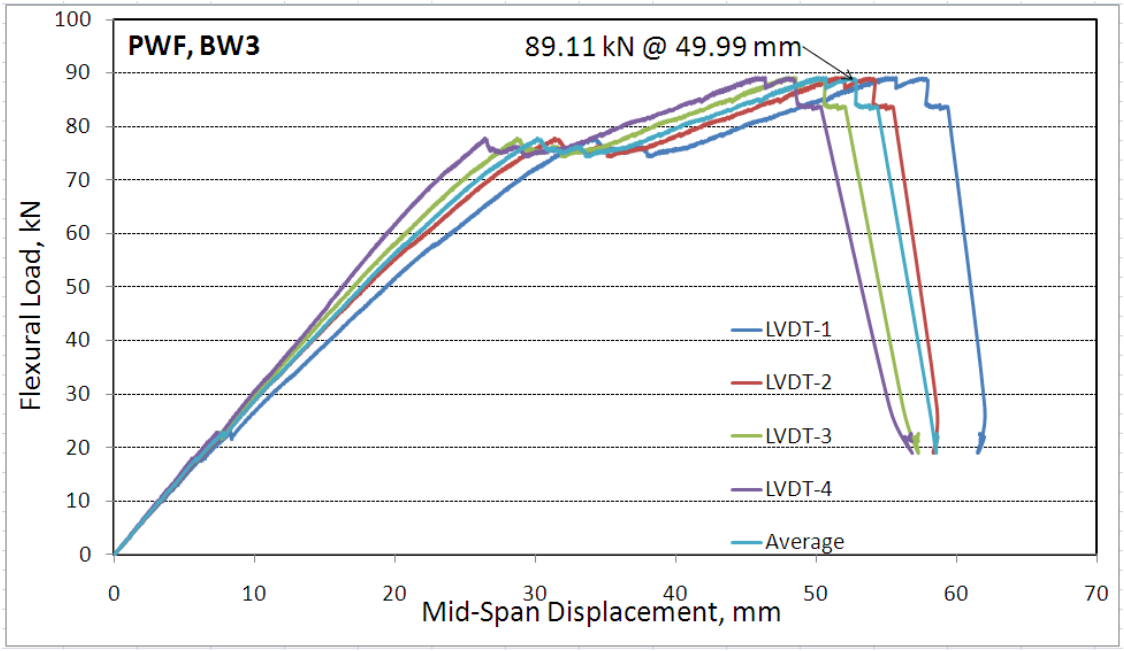

Figure 4.54. Flexural load-deflection curves for the 4 LVDTs for BW3, along with the average curve

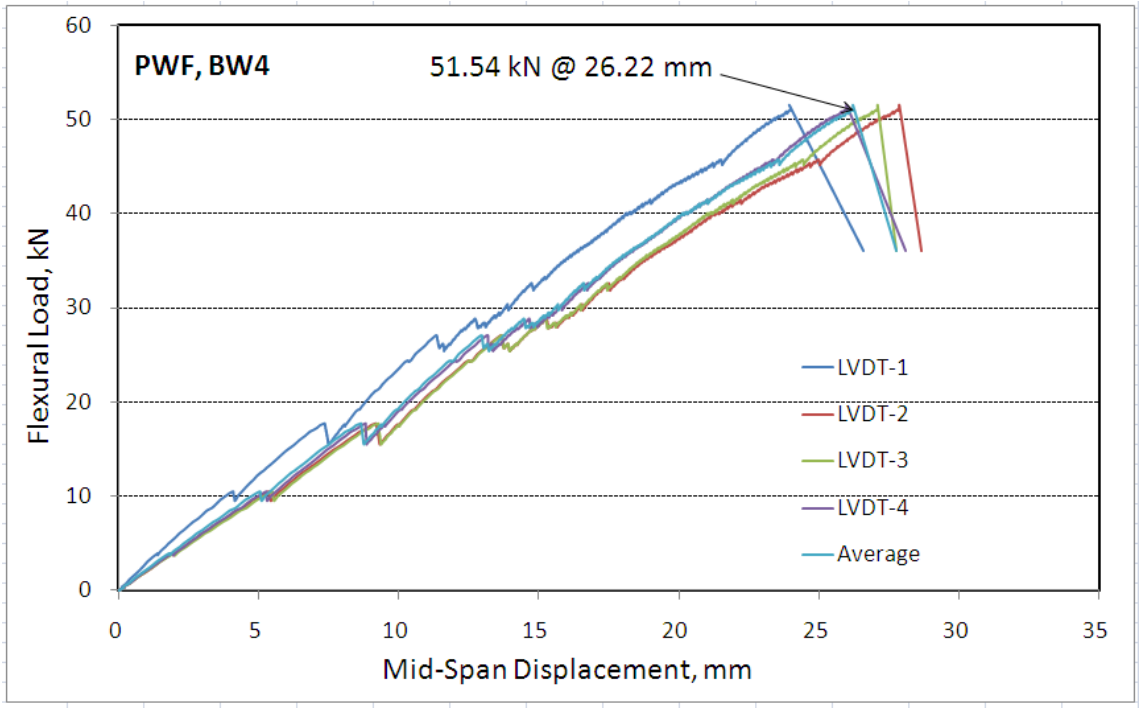

Figure 4.55. Flexural load-deflection curves for the 4 LVDTs for BW4, along with the average curve (Mohamed, 2009)

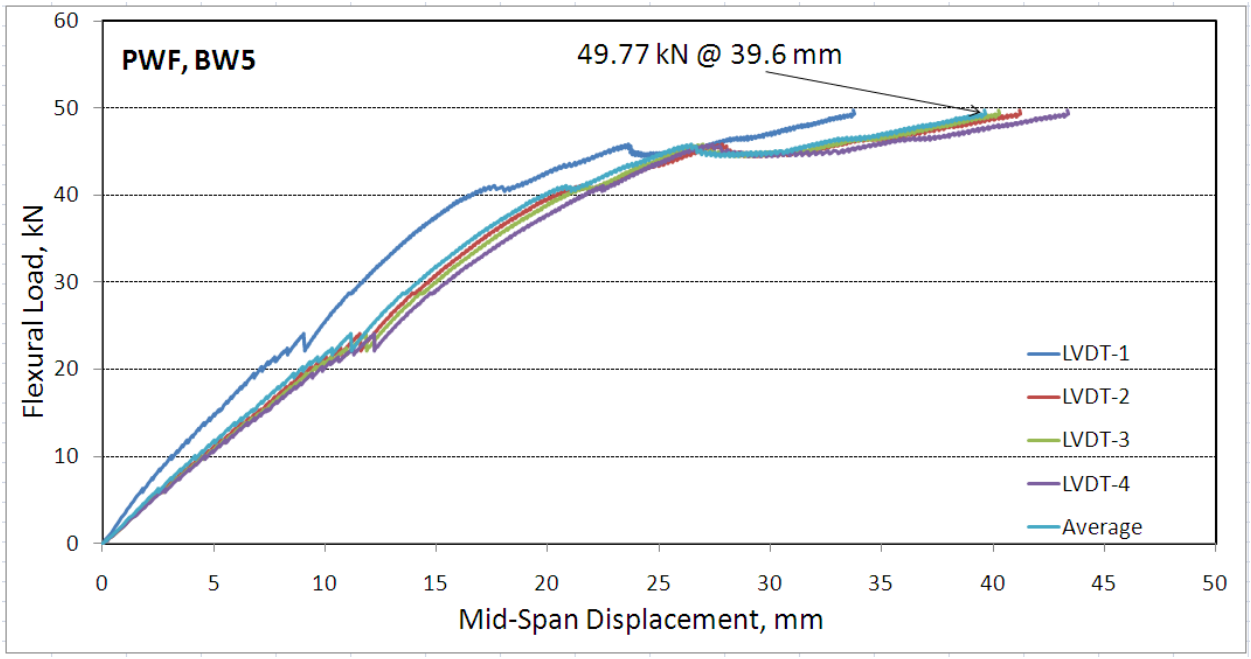

Figure 4.56. Flexural load-deflection curves for the 4 LVDTs for BW5, along with the average curve (Mohamed, 2009)

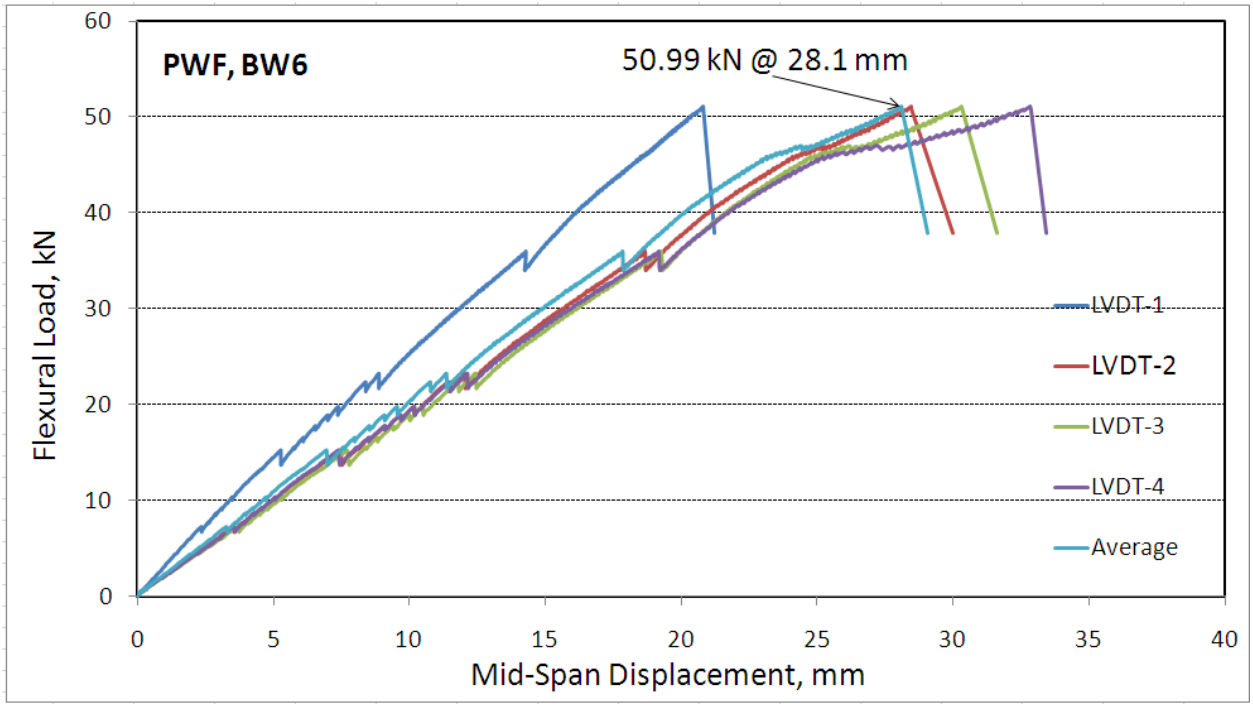

Figure 4.57. Flexural load-deflection curves for the 4 LVDTs for BW6, along with the average curve (Mohamed, 2009)

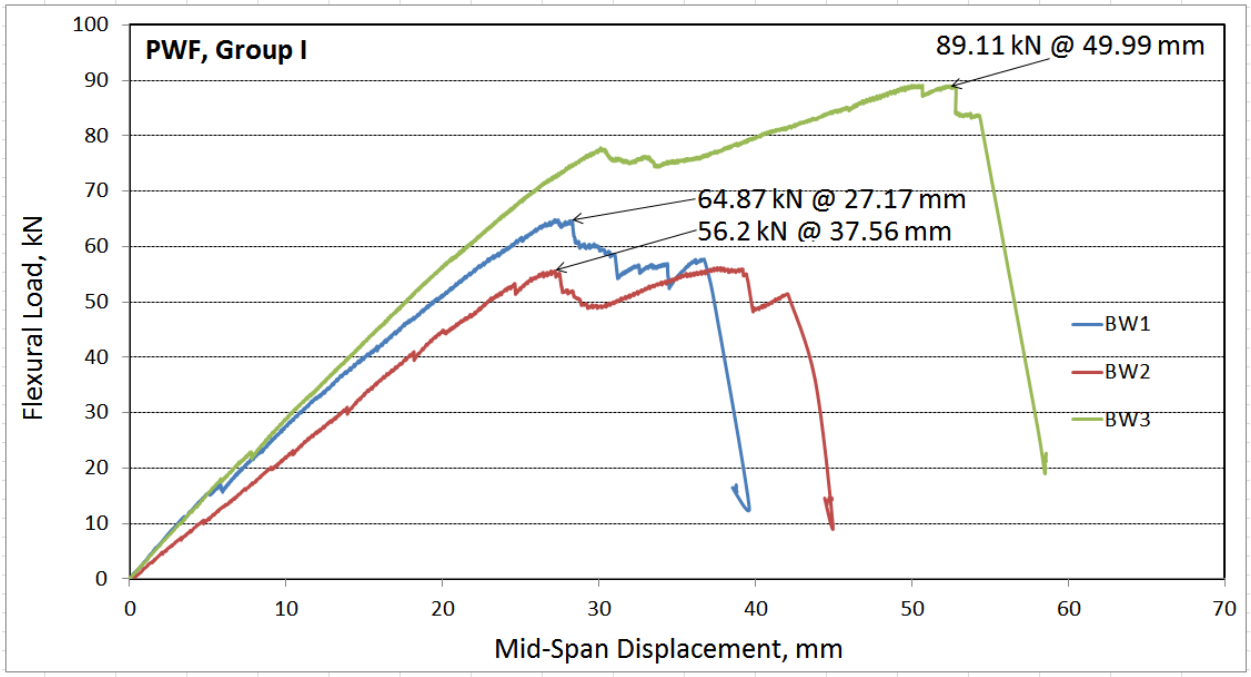

Figure 4.58. Former 4.52-4.54 for flexural load-deflection curves, first group

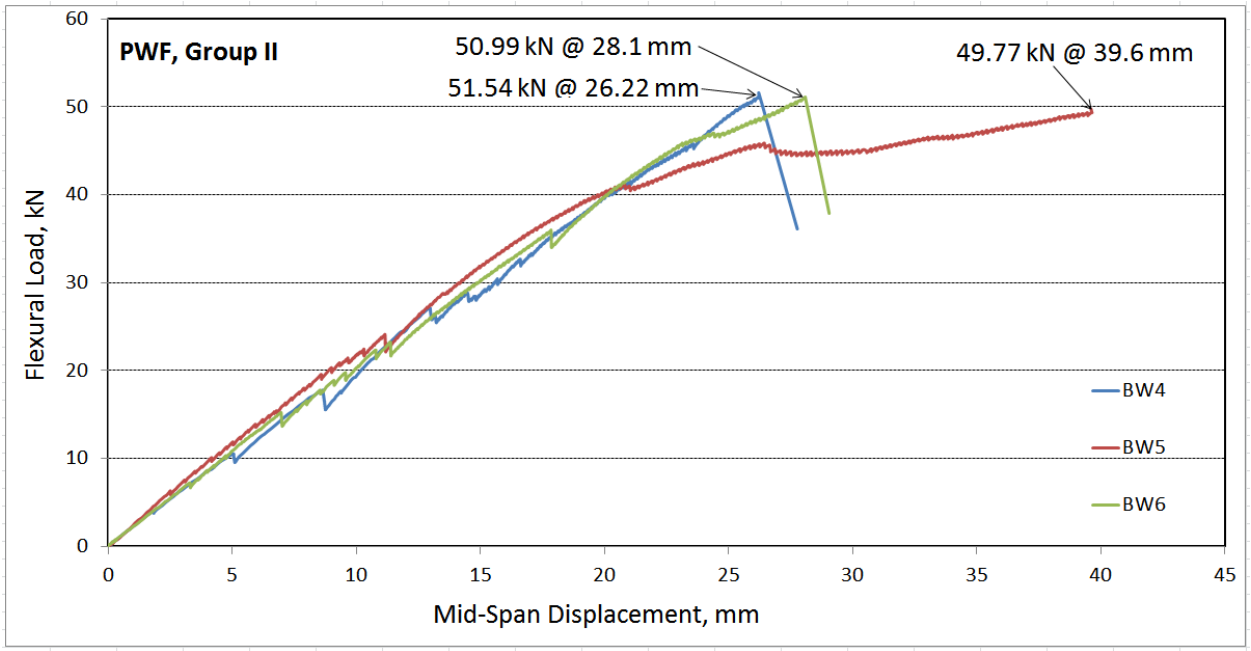

Figure 4.59. Former 4.55-4.57 for flexural load-deflection curves, second group

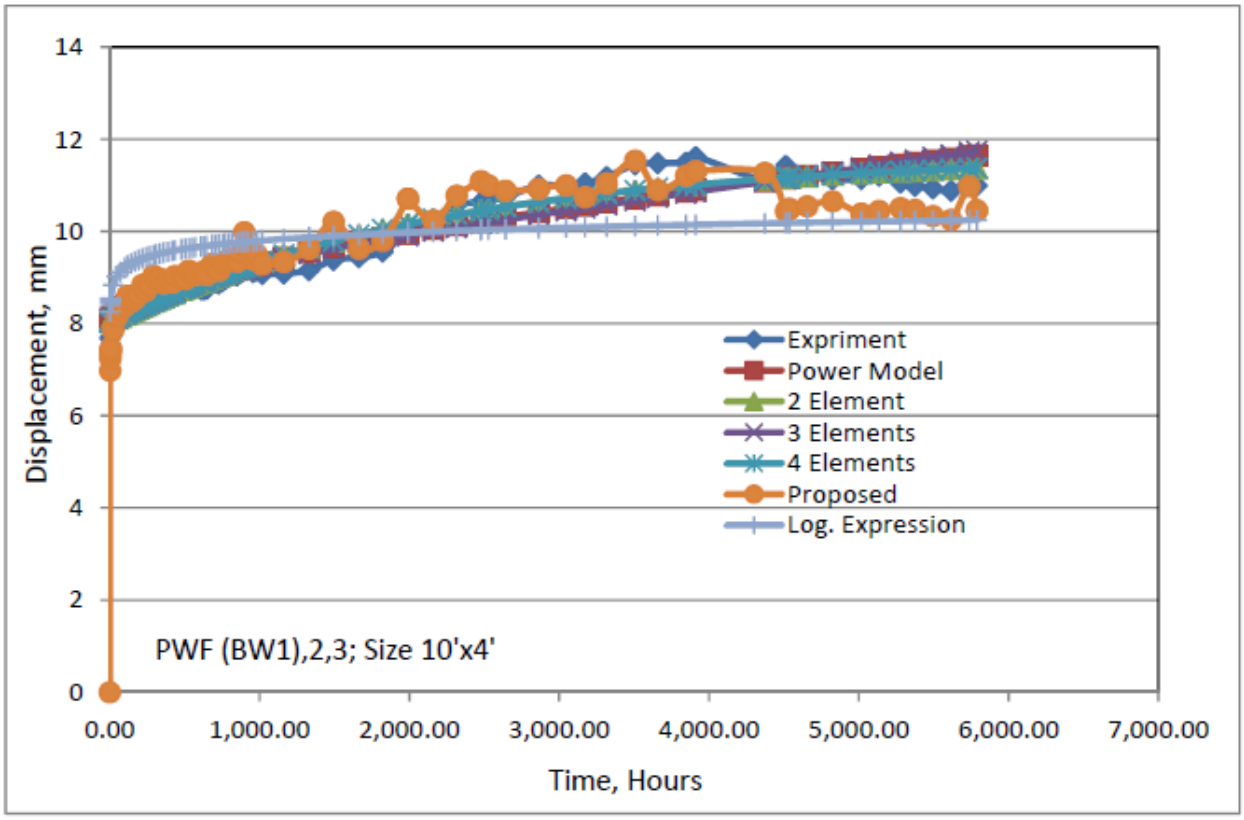

Figure 5.1. Correlation of Experimental Results with Common Creep Models for Tested Walls BW1, BW2, and BW3

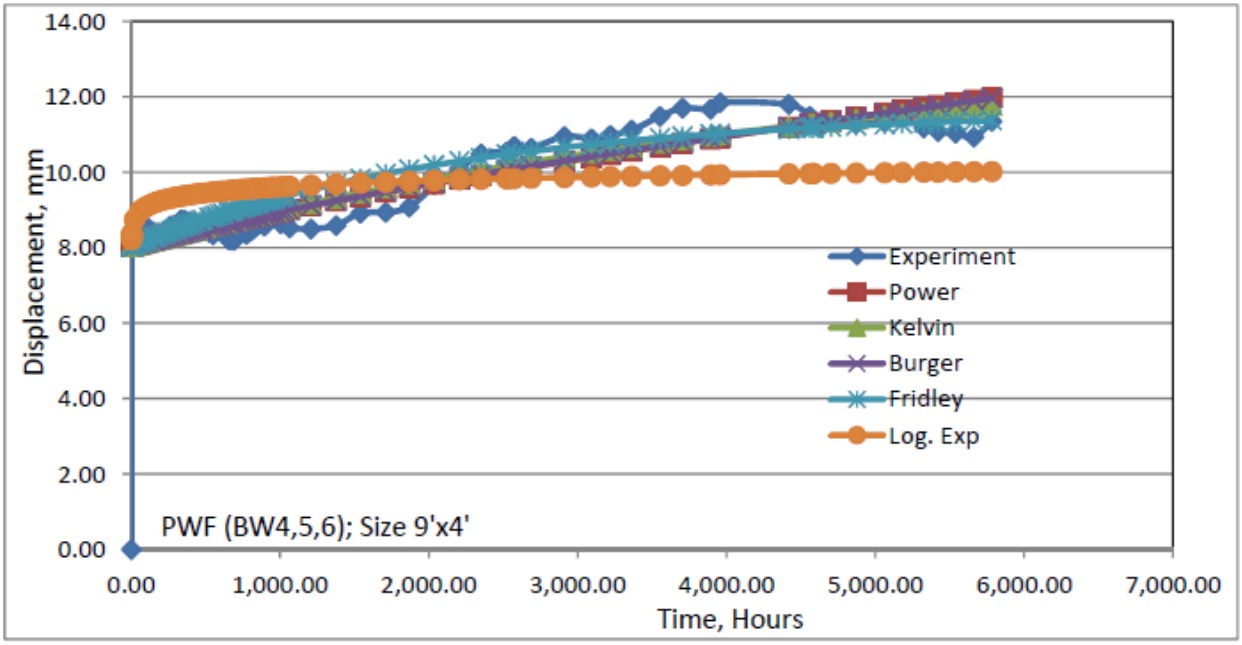

Figure 5.2 Correlation of Experimental Results with Common Creep Models for Tested Walls BW4, BW5, and BW6

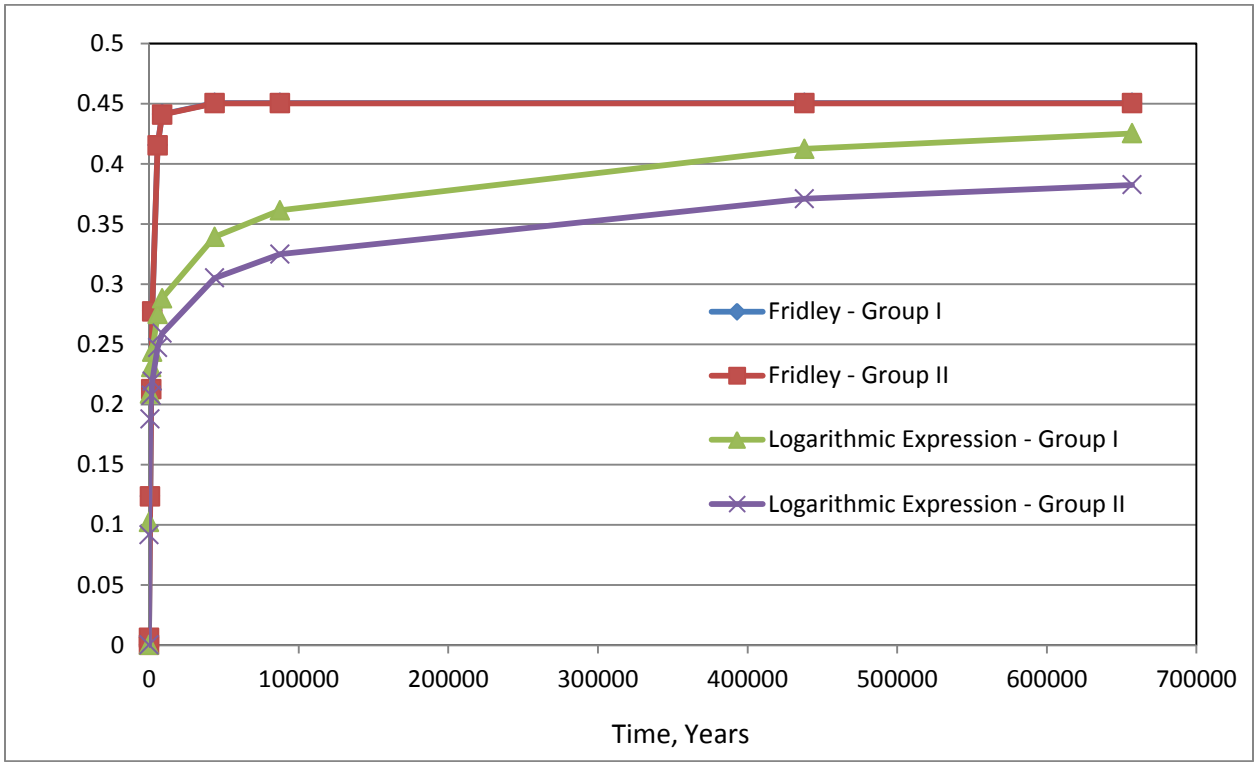

Figure 5.3. Comparison between Predicted Relative Creep using Logarithmic Expression and Fridley Model

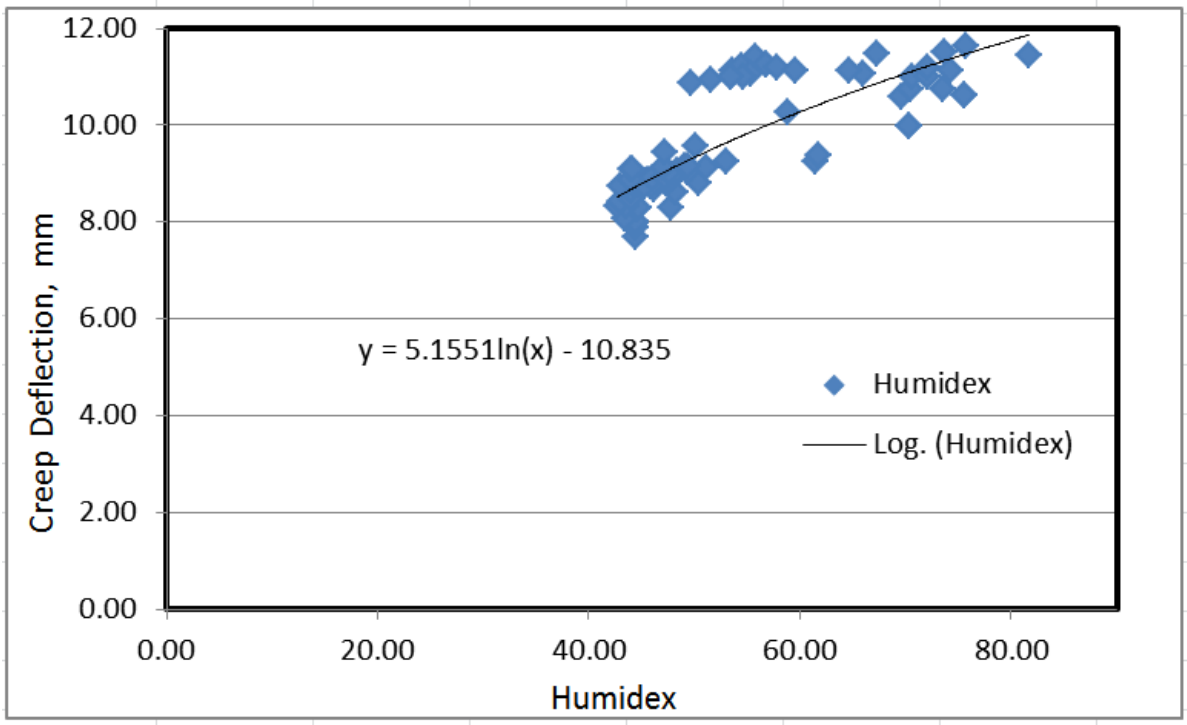

Figure 5.4. Effect of Humidex on Creep Displacement for Tested Panels BW1, BW2, and BW3

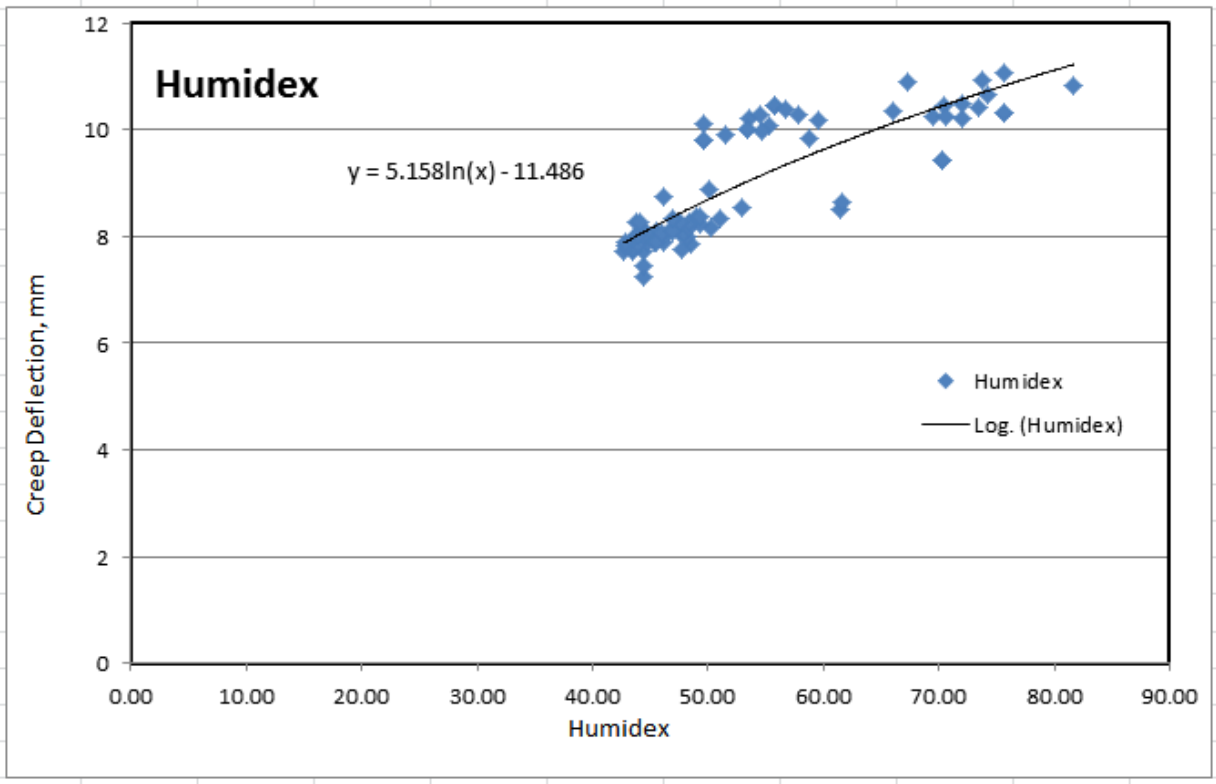

Figure 5.5. Effect of Humidex on Creep Displacement for Tested Panels BW4, BW5,and BW6

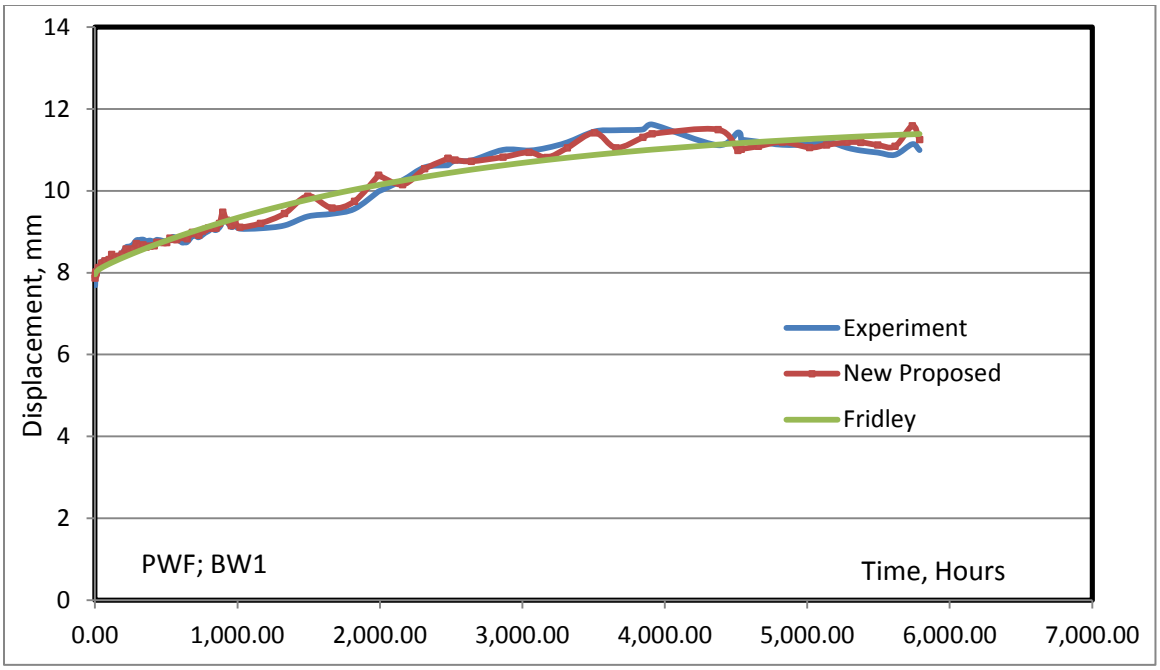

a. Comparison Between Experimental data for Group I, Fridley Model and The Proposed Model

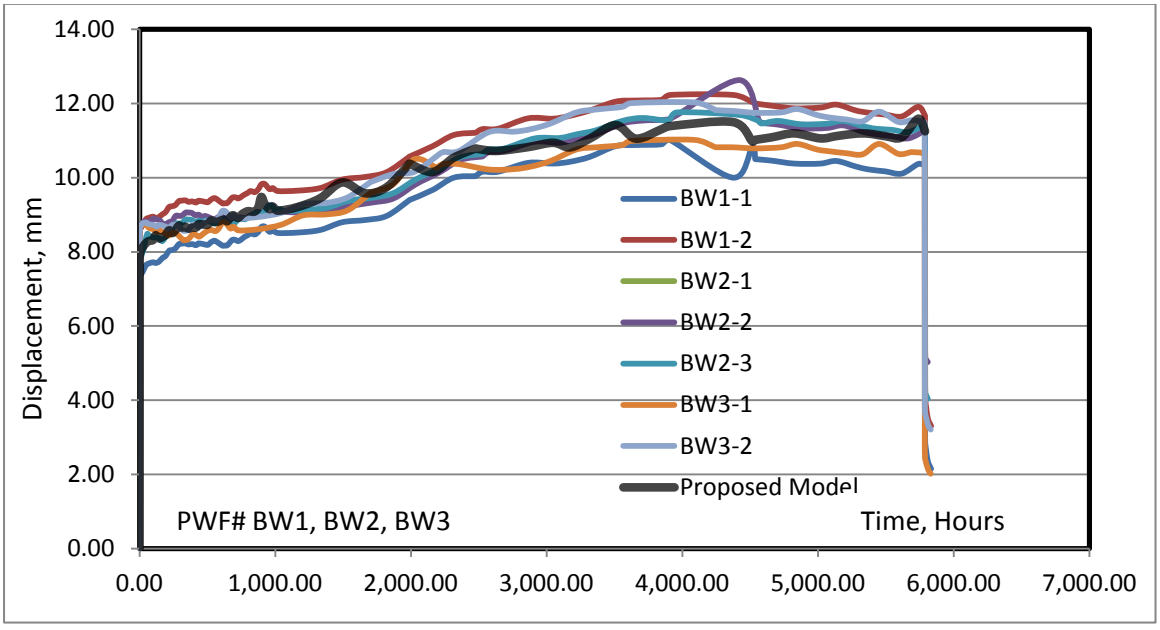

b. Plot of the Proposed Model with Experimental Data for Group I (in black line)

Figure 5.6. Proposed Creep Model for Group I

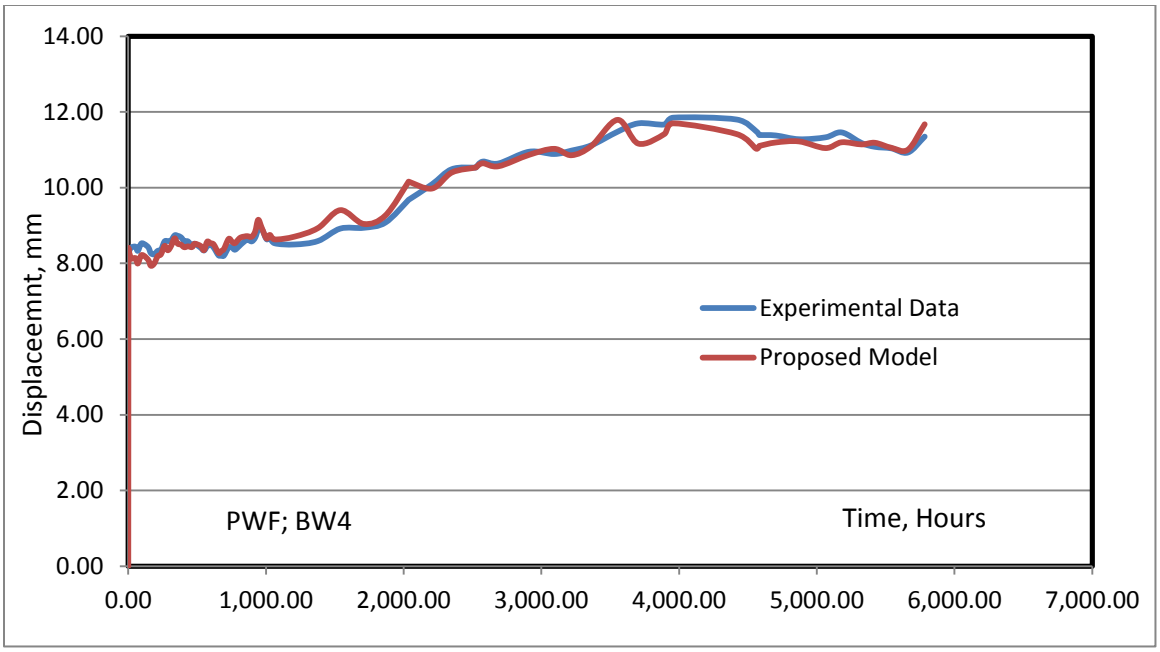

a. Comparison Between Experimental data for Group II, Fridley Model and The Proposed Model

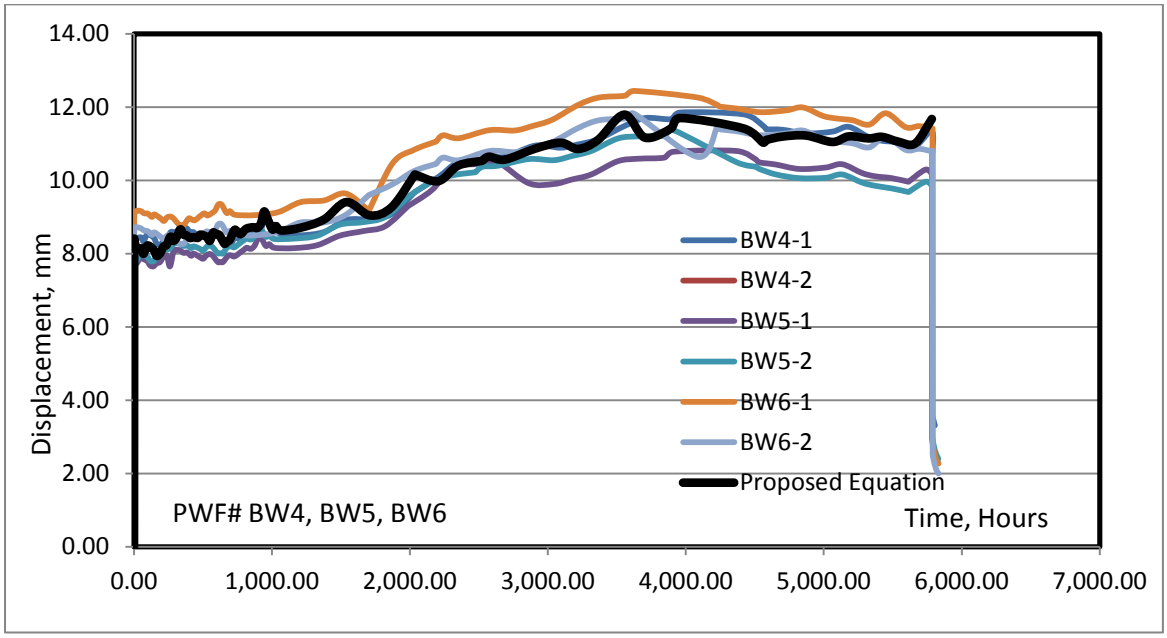

b. Plot of the Proposed Model with Experimental Data for Group II (in black line)

Figure 5.7. Proposed Creep Model for Group II

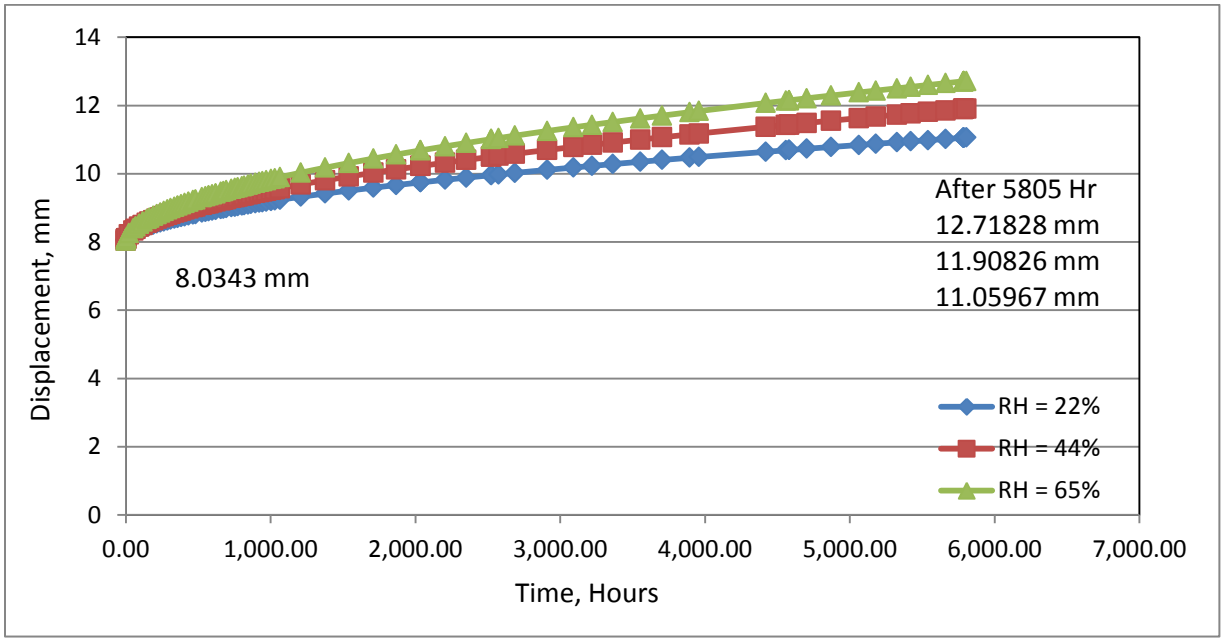

a. Effect of change in total deflection with change in relative humidifies at a 23.5°C ambient temperature for Group I

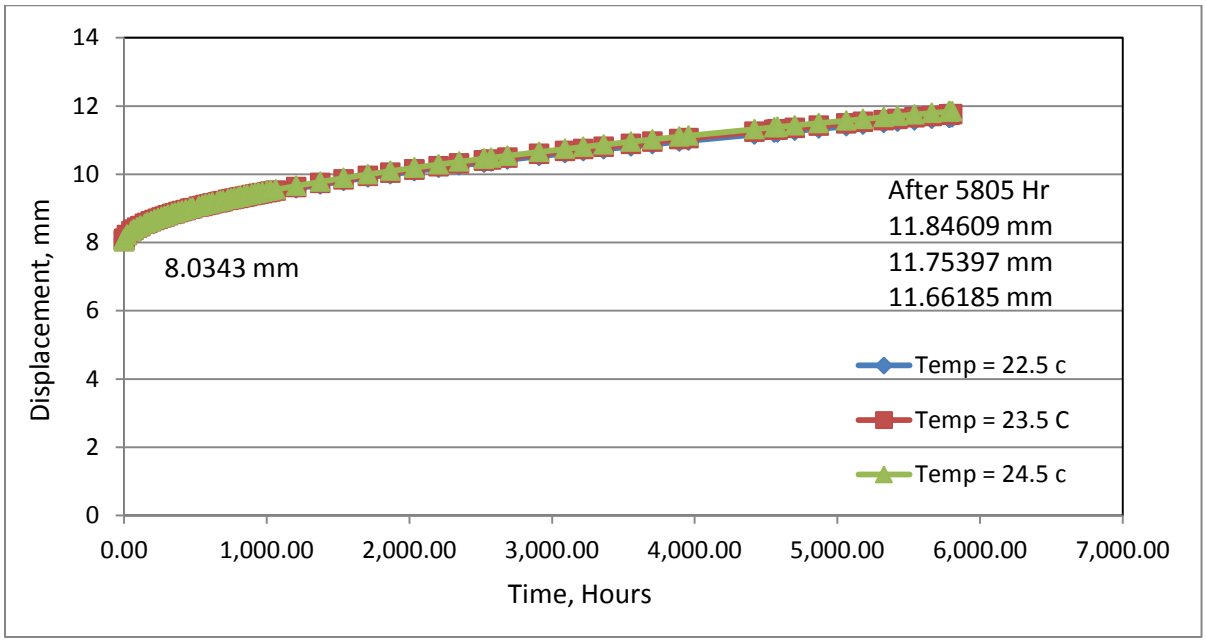

b. Effect of change in total deflection with change in ambient temperature at 40% Relative Humidity for Group I

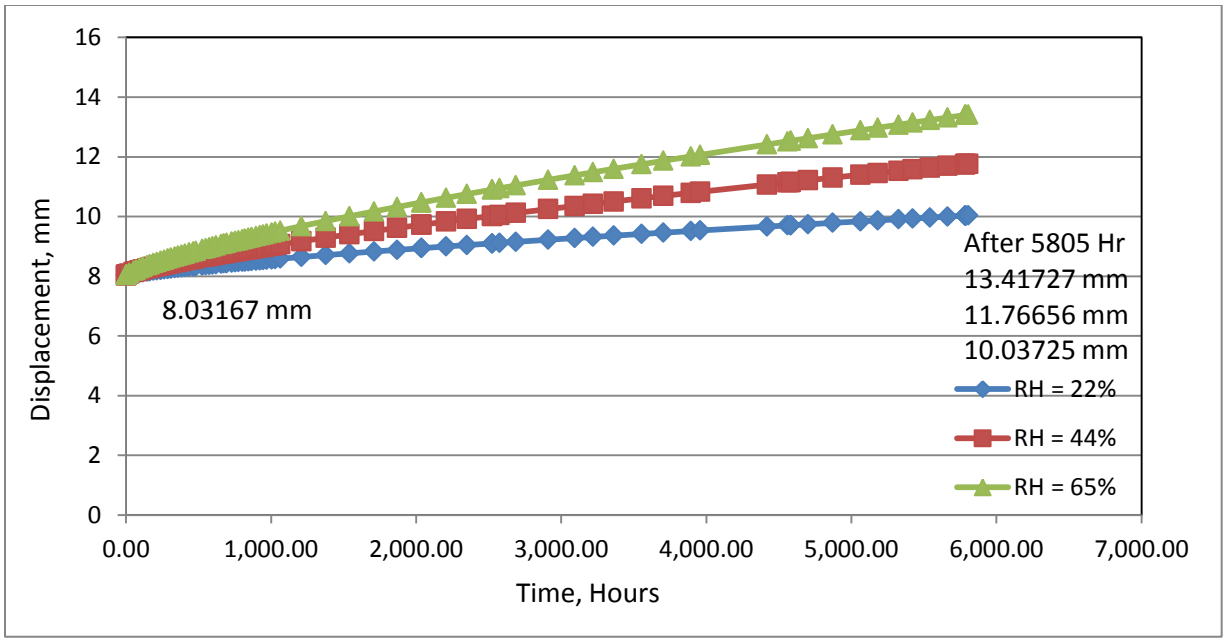

c. Effect of change in total deflection with change in relative humidifies at a 23.5°C ambient temperature for Group II

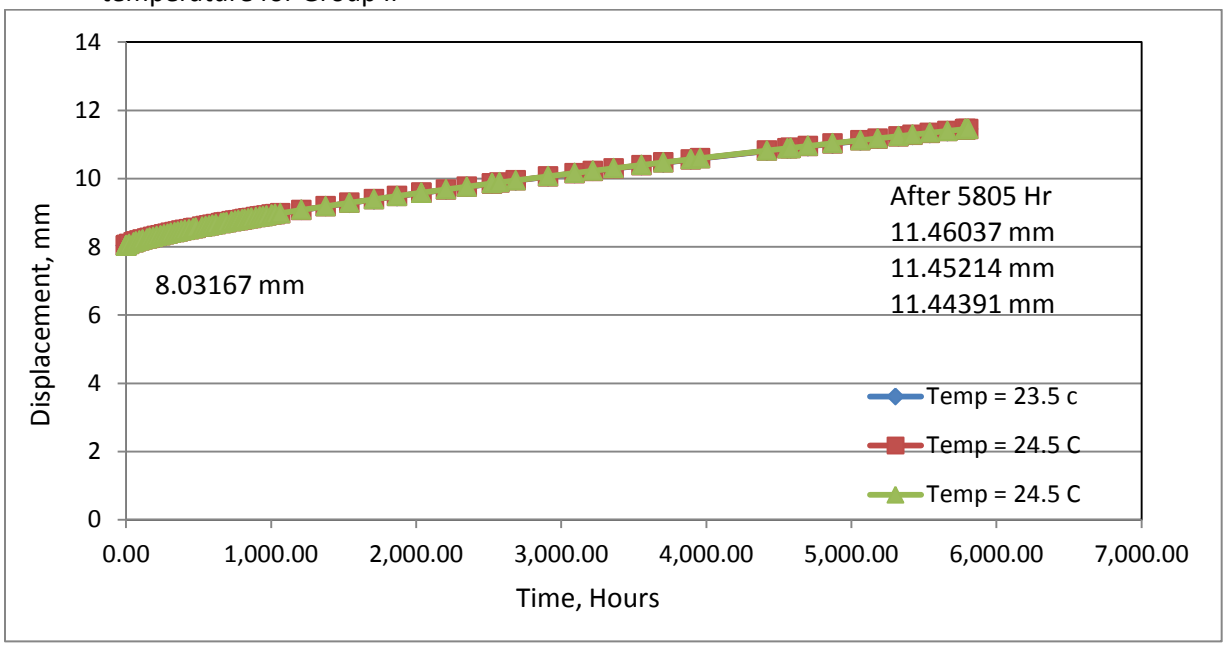

d. Effect of change in total deflection with change in ambient temperature at 40% Relative Humidity for Group II

Fig. 5.8. Change in creep deflection with the change in temperature and relative humidity based on the proposed creep model

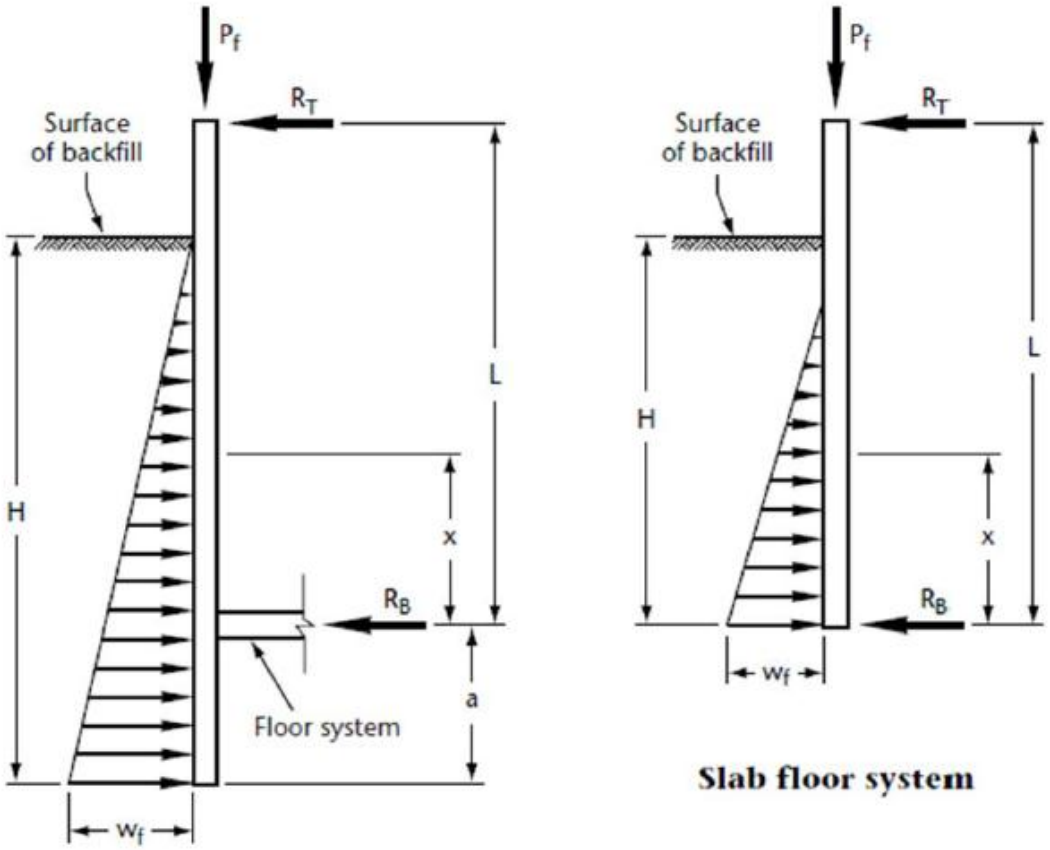

Legend:
L = *Stud length (mm)*
x = *Location of maximum moment (mm)*
H = *Height of backfill (mm)*

Figure 5.9. Schematic diagram of loading on the permanent wood foundation (CSA-O86.01)

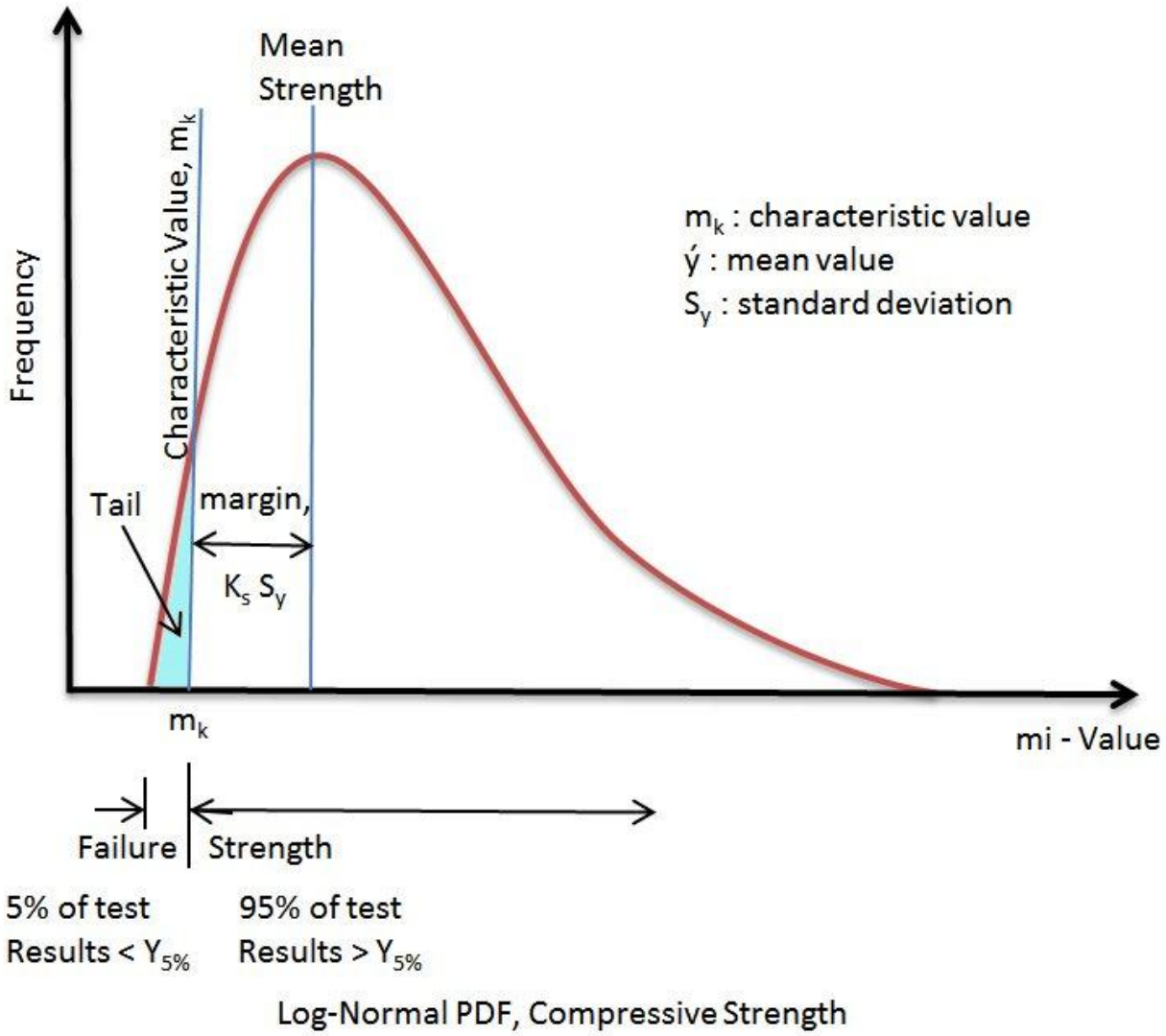

Log-Normal PDF, Compressive Strength

Where

ý = mean value

S_y = standard deviation

m_k = characteristic value

K_s = factor determined as $K_s = \frac{K}{\sqrt{n}}$ where k is the α-percentile in a non-central t-distribution with n-1 degrees of freedom

Figure 5.10. Characteristic Value obtained by Log-Normal Distribution